POLITECNICO DI TORINO

Master of Science in

Mechanical Engineering

Master Degree Thesis

Automotive laser welding process set-up by design of experiments for low carbon steels

Supervisor
Gianfranco Genta

Co-supervisors
Roberto Cagliero

Candidate
Di Paola Giovanna
258155

Academic year 2020/2021

To mum and dad,

who taught me to preserve and love freedom.

Abstract

The master thesis project elaborates results on laser welding of a drive clutch mounted on VT3 punch powertrain engine. The proposed research project consists in the development of a methodology to define the main influent parameters on a laser welding weld bead for a drive clutch.

The study will be conducted through a statistical data analysis in parallel to a deep metallographic analysis. In particular a Design of Experiments (DOE) experiment will be planned in order to define the most influent parameters and it will be intensified afterwards through a General Linear Model (GLM) analysis. At the same time, metallographic inspections by optical and stereoscopic microscope and Non-Destructive Testing (NDT) inspections by eddy current will be exploited to acquire information on thermally altered areas. The metallographic inspection will be useful to observe and extrapolate data on the weld bead geometry and defects which will be defined as output factors in DOE and GLM analysis. The presence of defects will be studied in relation to the material chemistry focusing the attention on different type of observed defects through the instruments mentioned above, SEM and profilometer microscope. Moreover, problems related to low carbon steels weldability will be discussing about the DD steel microscopic structure after the experimental welding process.

Based on metallographic observations and numerical statistical data, the developed method justifies the presence of defects in weld beads and makes considerations on the influence of working conditions on geometric weld beads parameters.

Contents

Automotive laser welding process set-up by design of experiments for low carbon steels

CHAPTER 1

Introduction

1.1 Fundamentals of laser welding

Welding technologies are critical to most relevant engineering applications. Generally, *welding* is defined as the most flexible and realistic joining method suitable to manufacturing process in every industrial field. *Laser* is a high-power density heat source.
A great evolution came between the 1800's and 1900's when the Russian scientist Nikolay Bernardos experienced the first tool for welding with an indirect arc. The tool was powered by an electric generator and based on an electrode which produced a current, an arc, between itself and the component to be welded. The use of metal arc welding method of coal electrode was called " Benardos way." Among the methods of arc welding the Benardos method was the first widely used and is today one of the most common. A patent for arc welding was given to Bernardos, which was named as *Elektrogefest* ('Electric Hephastud') [1] [2].

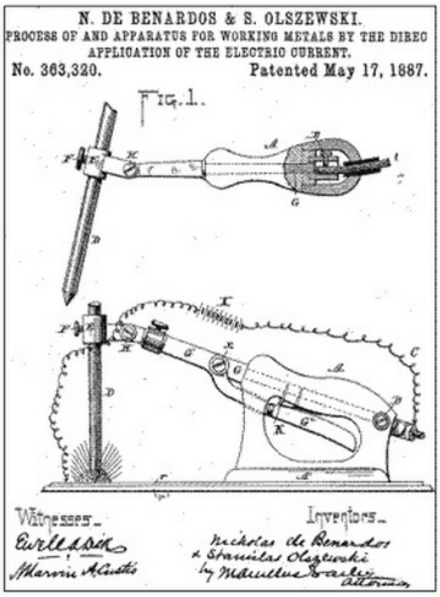

Figure 1: The patent for the arc welding named Elektrogefest granted to N. Bernardos

More than 50 years ago a laser beam was discovered and since then many lasers have been developed. Recently, diode lasers, disk lasers and fiber lasers are emerging and receiving considerable attention thanks to their high efficiency, high quality and high power. Studies show how laser processes are improving and are expected to be an indispensable technology for the twenty-first century [3].

'Laser welding' is a non-contact fusion welding process similar to the electron beam welding process, used to join metals through the use of a laser. It can be defined as a key joining technology characterized by small heat affected and fusion zones, as well as minimal or non-existent distortions. Nowadays, it's one of the highest power density source available in industrial sectors. As the following table shows, its heat source intensity is much higher than that of arc or plasma welding [4] [5].

Process	Heat source intensity ($W\,m^{-2}$)	Fusion zone profile
Flux-shielded arc welding	5×10^6–10^8	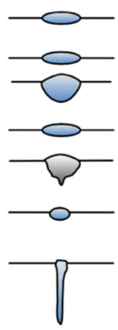
Gas-shielded arc welding	5×10^6–10^8	low high
Plasma	5×10^6–10^{10}	low high
Laser or electron beam	10^{10}–10^{12}	defocus focus

Table 1: Power densities of different welding processes

Laser welding technology is characterized by high speed, high power density, concentrated heat input and high production rate. It finds application in welding of thin sections thanks to some important features such as low energy input into the metal, large welding speed, the narrow bead produced and low heat affected zone [6].

1.2 Application of laser welding in automotive

The laser welding is largely used in production processes by robotization, automation and systematization in production lines. All of these properties make the advanced technology be applied in several industrial fields. In fact, among all the welding processes, its own versatility allows the joint of metals ranging from very thin sheets of about 0.01 mm to plates of about 50 mm of thickness guaranteeing high precision, high performance and high quality [3].

Laser welding is one of the newest techniques adopted in several number of industries. All the advantages listed above allow laser welding to be used in many applications. Some important fields in which laser welding is involved are aerospace, textiles, thin metal fabrication, windows and signs, bio-medical devices, food and metal packaging, electronics and automotive [7]. It finds a great application in automotive field. Automotive industries require rapid production but focusing at the same time on quality, safety and cost effectiveness. Quick production has a key role in automotive.
The use of lasers is introduced thanks to their ability to work with reflective metals without having their beam redirected back into the laser system itself. A particularly important benefit given the fact that reflective metals are common part of this sector. However, aluminum and copper do present difficulties to laser welding. This is mainly due to the fact that these material do not absorb laser light because of their high reflectivity. Because of that, it’s important to use processes which are able to create strong weld joints between metals of different nature. The main characteristic of laser welding is the ability to create a strong and long-lasting joint, which is also effective, safe and environmentally friendly. In particular, fiber laser welding is widely used for fuel injectors and air bag initiators welding. [8]
Moreover, remote lasers welding allows easier control of the weld size leading to an improvement in peel strength. Given the high ability to be applied in industrial technology, most of mechanical components required to be worked by welding methods.

Case of study

The case of study is focused on analyzing welding worked on a drive clutch. The specific drive clutch is mounted on a VT3 Punch Powertrain engine.

Figure 2: VT3 Punch Powertrain engine

The VT3 Punch Power train has already proven to be very successful, robust and cost-effective continuously variable transmission (CVT), which can be taken advantage of.
CVT helps to improve the fuel consumption of vehicles and perform very well on driving comfort, thanks also to its flexible design.
Unlike conventional automatic transmissions, continuously variable transmissions do not have any gears. A CVT uses two cone-shaped pulleys. One pulley is connected to the engine and the other is connected to the rest of the transmissions. A steel or composite belt connects the two pulleys [9]. The pulleys change widths depending on how much power the wheels need from the engine. As one pulley gets larger, the other gets smaller. This design allows a CVT-powered car to accelerate with strength and smoothness at the same time. A key benefit of the CVT is its ability to change its gear ratio continuously as the engine speed changes. This means the engine is always operating at its peak of efficiency.
A CVT gives drivers quicker acceleration than standard automatic transmissions. Because of their greater ability to control the engine speed range, CVTs have small impact on gas emissions. CVTs are also lighter weight than traditional automatic transmissions.
In addition, the VT3 shows high flexibility which allows to be integrated in a high number of applications. In particular, the smart clutch actuation system of the VT3 allows combination with engine start-stop functionality, finding effective application in mild hybrid or full hybrid vehicles. The VT3 is available in various torque variants, ranging from 150 to 220Nm.

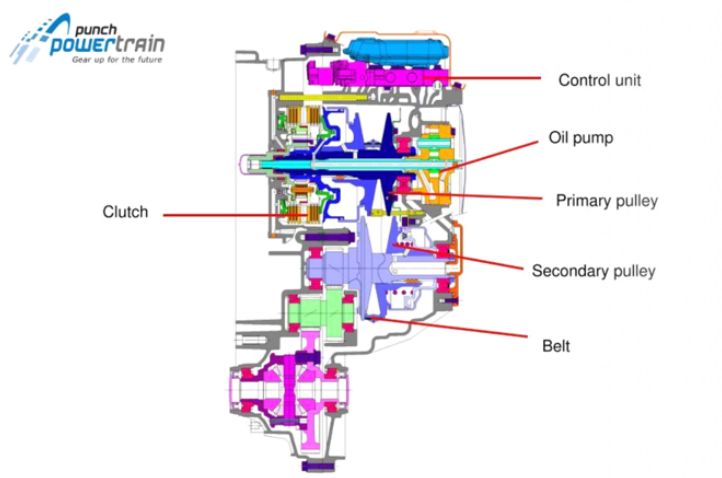

Figure 3: Schematic image VT3 Punch Powertrain

The clutch is a key element for the powertrain driving comfort during standing-start and gear-shifting operations. The introduction of automated manual transmission and dual-clutch transmission system use one or more clutches improving the driving comfort [10]. CVT clutch system is described by an automatic clutch that can change seamlessly through a continuous range of gear ratios. The drive clutch is an advanced form of centrifugal clutch and is mounted to the output shaft of the engine. The clutch has two faces: one is fixed and one can move in and out to engage the belt. A clutch must be designed to satisfy three basic requirements. First, the desired torque must be produced by an acceptable actuating force and clutch size, it means that the friction cannot be too low. Secondly, the energy dissipated during a clutch engagement must not produce destructively high temperatures, which would shorten the clutch life. Finally, the wear of the clutch must be low enough to give an acceptable life for the clutch. In automatic transmissions the input and output shafts have different angular velocities before the gear shift. This means that the clutch must stop this relative rotation and subsequently hold the shafts together. When this action, called engagement, takes place, there will be major stresses acting on the clutch faces.
Most multiple disc clutches, including those used in automatic transmissions, operate with lubrification. The oil provides local cooling around the asperity contact and this protection helps the clutch material to last longer. Certain properties of the clutch material, such as porosity and permeability, can help increase the durability of the clutch [11].

The clutch mounts two mechanical components: a tone wheel and hub to be joined by laser welding. The laser welding joins the tone wheel and the hub by producing a circular weld bead between them [12]. The clutch drive position on the VT3 powertrain is shown in the following image.

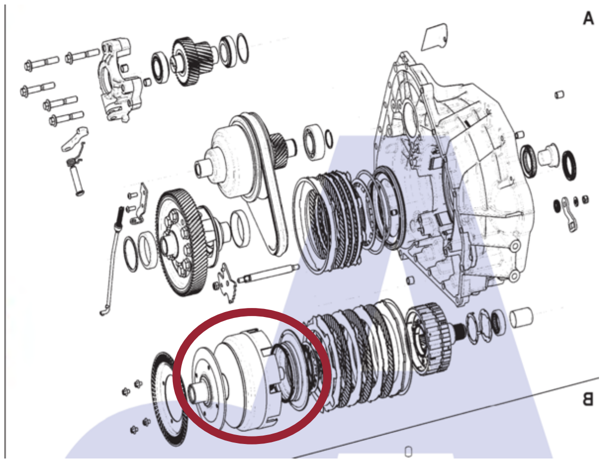

Figure 4: VT3 Punch Powertrain components

CHAPTER 2

Principles of laser welding and its characteristics

2.1 Laser welding process mechanism

The laser beam welding is one of the most used welding processes. In order to generate a laser weld, the main process technique is about focusing a beam of a laser light on a very fine spot. Thanks to the concentrated energy source due to high power density, the workpieces will be joined [7]. The general process arrangement is described by the following figure.

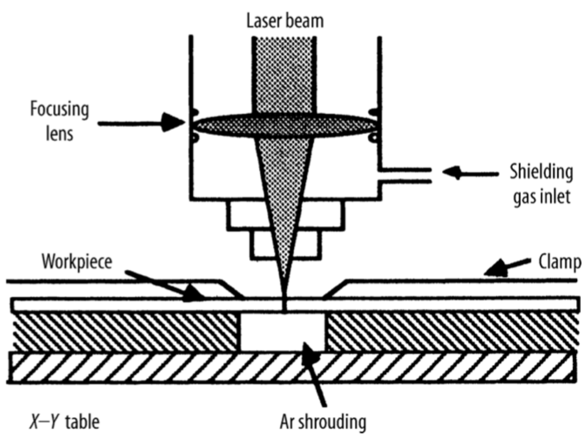

Figure 5: General laser welding arrangement

When the laser beam shot the workpiece surface, some energy is absorbed because of the interaction against free electrons in the metal and the interaction of electrons in metal lattice, imperfection and defects. The energy exchange, from laser beam energy to thermal energy, makes the workpiece temperature increases.
Then, depending on the laser irradiation time and the power density, two modes of welding are possible: conduction limited welding and deep penetration mode welding (keyhole). [3]

Conduction limited welding

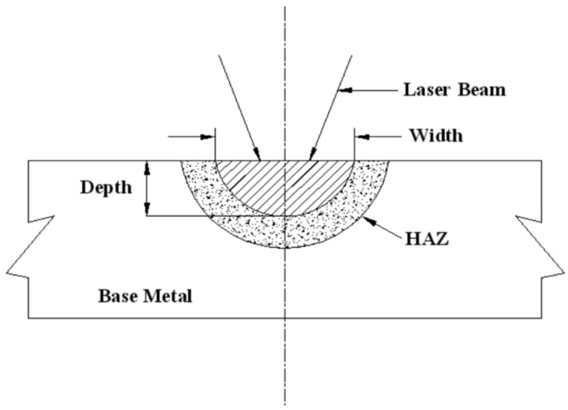

Figure 6: Conduction limited welding

Conduction limited welding take place at an irradiance level less than $10^6 \frac{W}{cm^2}$.

The process is possible when the absorbed energy is enough to melt the weld zone, but insufficient for vaporization phenomena or plasma formation. At the interaction between the laser beam and the metal surface, the generated heat is conducted through the metal melting the irradiated surface and the subsurface layers. As a consequence, the conduction limited welds are in liquid phase. The process keeps going without vaporization, in fact during the process the temperature raises but always below the boiling point. That's why conduction heat transfer mode occurs [5].

Conduction limited welding is chosen when a limited penetration in the thickness direction is desired, giving a low depth-to-width ratio [7].

Deep penetration welding (keyhole)

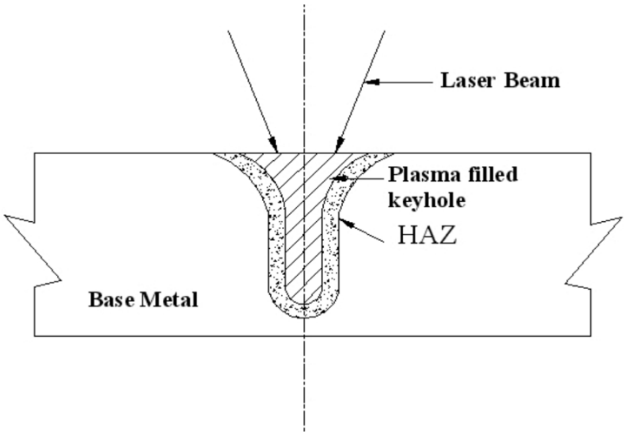

Figure 7: Deep penetration welding

Deep penetration mode laser welding takes place at an irradiance level in excess of $10^6 \frac{W}{cm^2}$. On the contrary to conduction limited welding, during the "keyhole" welding type process the substrate reaches the boiling point and the vaporization phenomena occurs. The result gives a high depth-to-width ratio [5].

When the laser beam is focused on the metal surface, the heat is transferred and an increase in temperature in the solid come about. The temperature rises above the melting point and the temperature around the irradiated area reaches the boiling point. During this action, the laser beam melts through the piece thickness and a narrow cylinder of liquid metal is produced. At this point the energy is sufficient to make vaporization phenomena happen. In this way a hole is usually formed by evaporation of the liquid and a column of metal vapor appears [3]. The vapor column surrounded by liquid metal is known as "keyhole" weld. The keyhole acts like an optical black body. In fact, the laser radiation is able to enter the hole but is subjected to several reflections before it can escape from the cavity [7]. That means some energy is partially absorbed by the surface while some is reflected towards a new point of interaction. This phenomena of absorption/interaction intensifies the overall amount of energy absorbed. As a result, the weld bead is much deeper than the one coming from the conduction laser welding [13].

2.2 Light and lasers

The word *laser* is an acronym, it stands for **L**ight **A**mplification **S**timulates by **E**mission of **R**adiation and describes the way in which the light is generated. Lasers produce a collimate and coherent beam. The difference between coherent and incoherent beam, is that coherent means that waves with same wavelength travel all in phase, while incoherent means radiations travel in all the direction from the source such as the sun light. Consequently, a focused and compact collimated beam acts with higher power density than the randomly radiated rays of the sun. Moreover, the one wavelength and the almost parallel waves allow the laser to focus on a small spot size with high precision [7].

2.2.1 Laser mechanism

In order to understand the laser usefulness, is necessary to describe how it works. First of all, is essential to define the active medium. An active medium is a collection of selected atoms, molecules or ions which can be in gas, liquid or solid status. Lasers are optical amplifiers and works by exciting an active medium placed between two mirrors. When they get excited, a pumping action take place emitting radiation as light waves. More accurately photons should be mentioned instead of light waves, because photon carries a defined amount of energy in relation to its wavelength. The pumping action of liquids and solids is achieved by heating them with light coming from a flash lamp while the pumping action of gases is due to electrical discharge. When the active medium is pumped, they absorb energy by holding it for a short and random lifetime. Then, spontaneous emission come out by releasing photons in all the direction. Some of them travels along the optical laser axis, while the others simply get lost from the system. During the release some photons can hit on other energized atoms leading to the emission of a photon prematurely. This action is called stimulated emission. Those photons which follow the optical laser axis, keep going along an extended path due to the optical feedback provided by the mirrors. This action amplifies photon generation by stimulated emission achieving the power level desired but also provide the collimate and coherent beam which make lasers so useful [7].

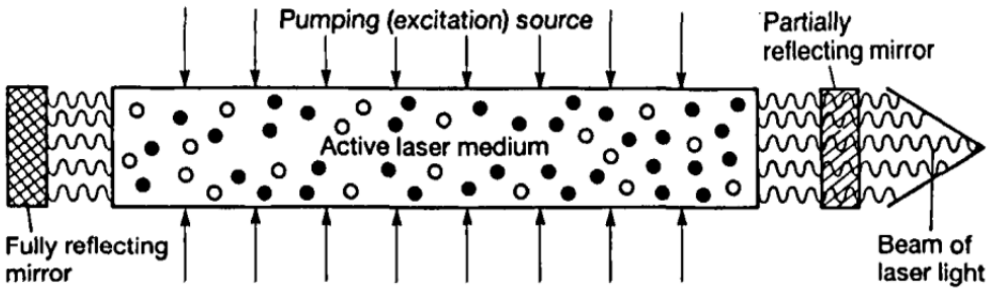

Figure 8: Basic elements of laser

2.2.2 Type of lasers

Lasers are classified depending on the state and properties of the active medium. Typical lasers that are commercially available for material processing are: gas lasers, solid state lasers, semiconductor lasers and fiber lasers. While the former is industrially available from long time, the latter are emerging recently. Surely, what's make difference between lasers is the laser wavelength [5].

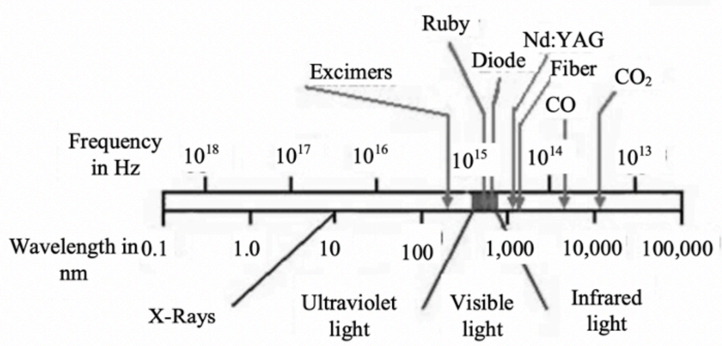

Figure 9: Electromagnetic spectrum of lasers

Gas laser

Gas laser is the earliest industrial laser type. They distinguish from others thanks to high voltage and low current power required. They have been studying for long time and so well developed. In fact, gas discharged allows exciting gas media in formable laser cavities, in which gas adopts limited shapes. Moreover, only gas media have the possibility to move fast through the laser device and heat removal can be easily achieved. [14]
Two types of gas lasers are available: the transverse flow laser and the axial flow laser. The gas lasers can reach about 40 kW, but the laser generated from CO2 cannot be transferred via fiber optic cable (FOC), which implies that welding can be done only close to the laser source. [5]

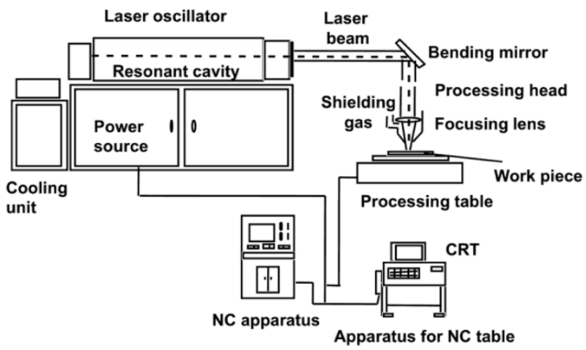

Figure 10: Gas lasers arrangement

Solid state laser

Nd:YAG laser is a solid-state laser source. It's named from the laser emitted from yttrium aluminum garnet rod. The light pumping comes from arc lamps, flash lamps as well as diode lasers by optical excitation. Usually, welding is performed by flexible fiber transmission optical system or using direct optical transmission. [15] Flexible fiber deliver is widely used thanks to low transmission loss.
A great improvement could be applied by substituting the pumping lamps with diode lasers. The advantage of using diode laser is that it reduces the effect of thermal gradients in the laser a FOC and integrated into production systems.

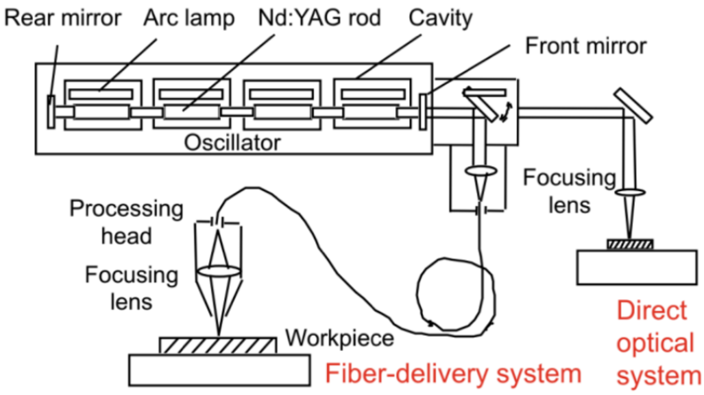

Figure 11: YAG lasers schematic arrangement

Disk lasers have been developed in order to overcome some problems. In case of the traditional Nd:YAG, some phenomena emerge such as thermal lensing[1] which leads to a reduction in laser beam efficiency, quality and affects the power density in the focused laser beam [3]. Instead of that, disk lasers introduce a very thin crystal disk used as a lasing medium. The disk is mounted on the heat sink, it's usually of about few hundred microns in thickness and it's coated by a reflective surface. The very small thickness by comparison with the greater diameter of the laser light, allows axial cooling being in contact. This axial temperature profile reduces thermal lensing to a minimum [15].

[1] "Thermal lensing (TL) is one example of a photothermal phenomenon. When an excitation laser is focused into a non-fluorescent sample in a microchannel, the sample absorbs the excitation laser and releases the light energy as heat following non-radiative relaxation. The heat generation induces a temperature distribution which is similar to a Gaussian profile due to the Gaussian intensity distribution of the excitation laser and heat diffusion. Generally, a temperature increase in a liquid decreases the refractive index, and a refractive index distribution working as a concave lens is formed around the focus. This concave lens is a thermally-induced lens and the phenomenon is known as thermal lensing" [44].

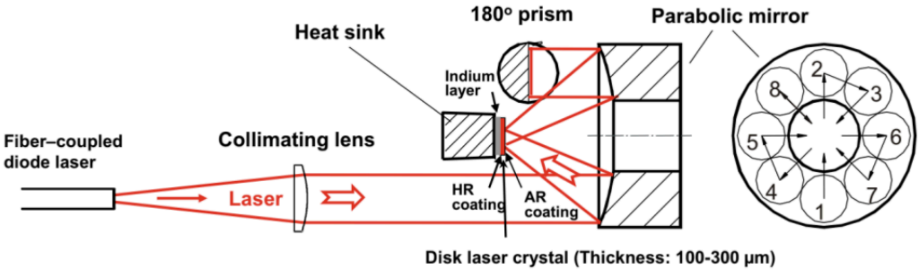

Figure 12: Disk lasers emission mechanism

Diode lasers

The main characteristic of a diode laser is to have the active medium as a semiconductor, that's explain why it is also named as semiconductor laser. The photons move forward and backward by the mirror and the laser radiates due to amplification by stimulated emission. The most popular diode lasers are powered by an injected electrical current and are covered by a thin layer of crystal wafer. The crystal produces an p-n junction or diode. [5]

The main advantages of diode lasers are smallness, compactness and lightweight. Moreover, they operate in high efficiency, high quality and are able to modulate the power due to various current. An improvement regards the production of a deep penetration in steels and aluminum alloys. [15]

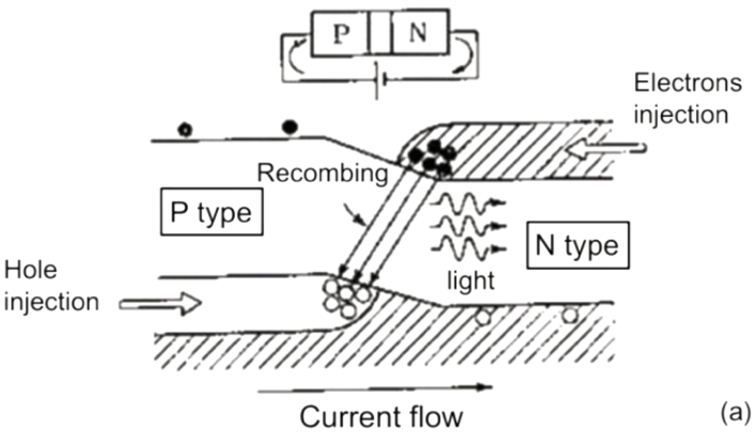

Figure 13: Diode laser arrangement

Fiber lasers

Over the past years fiber lasers have been developed overcoming gas lasers and semiconductor in terms of quality and efficiency. In case of fiber lasers, the active gain medium is an optical fiber characterized by elements such as erbium, ytterbium, dysprosium etc. The main advantage of those elements consists in providing light amplification while avoiding lasing phenomena as well as disk lasers. In fact, lasers and disk lasers are the most recent and promising technology in welding operations. Both are able to reach power values ranging from 16 kW to 100 kW operating with high efficiency [15].
The easiness of using fiber lasers regard its laser generation inside the fiber, which implies no need of sensitive optics applications in the delivery of the beam. Surely, the success of fiber lasers come from some advantages such as high beam quality, power density and efficiency but also their smallness and lightweight. The good flexibility and the high production rate lead to laser welding robotization [5].

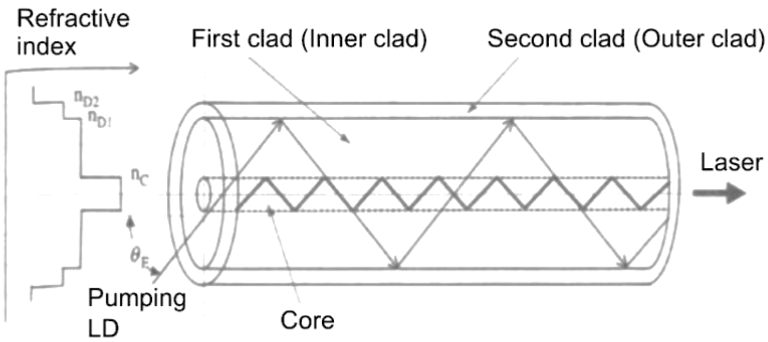

Figure 14: LD pumping for fiber lasers

The main features of the listed types of laser are summarized in the following table [3]:

Types of laser	Laser characteristics
CO_2 laser	Wavelength: 10.6 μm; far-infrared ray Laser media: CO_2-N_2-He mixed gas (gas) Average power [CW]: 50 kW (Maximum) (Normal): 1–15 kW
Lamp-pumped YAG laser	Wavelength: 1.06 μm; near-infrared ray Laser media: Nd^{3+}:$Y_3Al_5O_{12}$ garnet (solid) Average power [CW]: 10 kW (cascade-type max & fiber-coupling max) (Normal): 50 W–7 kW (Efficiency: 1–4%)
Laser diode (LD)	Wavelength: 0.8–1.1 μm; near-infrared ray Laser media: InGaAsP, etc. (solid) Average power [CW]: 10 kW (stack-type max.), 15 kW (fiber-delivery max.) Merits: Compact, and high efficiency (20–60%)
LD-pumped solid-state laser	Wavelength: about 1 μm; near-infrared ray Laser media: Nd^{3+}:$Y_3Al_5O_{12}$ garnet (solid), etc. Average power [CW]: 13.5 kW (fiber-coupling max.) [PW]: 6 kW (slab-type max.)
Disk laser	Wavelength: 1.03 μm; near-infrared ray Laser media: Yb^{3+}:YAG or YVO_4 (solid), etc. Average power [CW]: 16 kW (cascade-type Max.) Merits: Fiber delivery, high brightness, high efficiency (15–25%)
Fiber laser	Wavelength: 1.07 μm; near-infrared ray Laser media: Yb^{3+}:SiO_2 (solid), etc. Average power [CW]: 100 kW (fiber-coupling max.) Merits: Fiber delivery, high brightness, high efficiency (20–30%)

Table 2: Principal features of different types of laser

2.2.3 Advantages and disadvantages of laser welding

Advantages

Some main characteristics of laser welding are listed as follows.

Characteristic	Comment
High energy density – "keyhole" type weld	Less distortion
High processing speed	Cost-effective (if fully employed)
Rapid start/stop	Unlike arc processes
Welds at atmospheric pressure	Unlike electron beam welding
No X-rays generated	Unlike electron beam
No filler required (autogenous weld)	No flux cleaning
Narrow weld	Less distortion
Relatively little HAZ	Can weld near heat-sensitive materials
Very accurate welding possible	Can weld thin to thick materials
Good weld bead profile	No clean-up necessary
No beam wander in magnetic field	Unlike electron beam
Little or no contamination	Depends only on gas shrouding
Relatively little evaporation loss of volatile components	Advantages with Mg and Li alloys
Difficult materials can sometimes be welded	General advantage
Relatively easy to automate	General feature of laser processing
Laser can be time-shared	General feature of laser processing

Table 3: Main features of laser welding

Laser welding offers great benefits. First of all, it works with very high speed and a total input heat definitely lower than the one achieved from arc welding. Although the possibility of joining different materials the product will be worked with high precision and with low residual stresses as well. Added to this, the capability to make very deep and narrow penetration into materials produce a very low workpiece distortion. A big benefit of laser welding is the small impact on the heat affected zone (HAZ) decreasing distortion and possible deformations. Furthermore, the laser beam can be manipulated by robotization operating easily and quickly raising so the production rate [15].

It could be useful to compare also the laser welding features with those that belong to other technologies. The following Table 4 checks point of merits and disadvantages of each welding process [3].

Quality	Laser	Electron beam	TIG	Resistance	Ultrasonic
Rate	✓	✓	×	✓	×
Low heat input	✓	✓	×	✓	✓
Narrow HAZ	✓	✓	×		✓
Weld bead appearance	✓	✓	×		✓
Simple fixturing	✓	×	×		
Equipment reliability	✓		✓	✓	
Deep penetration	×	✓		×	
Welding in air	✓	×		✓	
Weld magnetic materials	✓	×	✓	✓	✓
Weld reflective material	×	✓	✓	✓	✓
Weld heat-sensitive material	✓	✓	×	×	✓
Joint access	✓			×	×
Environment, noise, fume	✓	✓	×	×	×
Equipment costs	×	×	✓		
Operating costs	–	–	–	–	–

✓ point of merit, × point of disadvantage

Table 4: Main differences between welding technologies

In addition, it's possible to have an overall view by comparing laser welding with other technologies looking at the "joining efficiency" values. It's possible to evaluate the energy used for joining and the amount of energy lost in all the surrounding area. The joining efficiency is defined as Vt/P, the reciprocal of the specific energy, where V is the traverse speed (mm s^{-1}), t is the thickness welded (mm) and P is the incident power (kW) [3].

An evaluation of the efficiency value explains that the higher the joining efficiency the lower the energy spent to heat unnecessary areas, increasing distortion and affecting HAZ. Some values are given by the table:

Process	Approximate joining efficiency ($mm^2\ kJ^{-1}$)
Oxyacetylene flame	0.2–0.5
Manual metal arc	2–3
TIG	0.8–2
Submerged arc welding	4–10
High-frequency resistance welding	65–100
Electron beam	20–30
Laser	15–25

TIG tungsten–inert gas

Table 5: Joining efficiency of different types of welding

Disadvantages

There is no doubt that laser welding equipment require high cost. In keyhole welding, vaporization process take place as it has been explained. Some materials need a ventilation system in order to remove hazardous gas or products coming from vaporization of polymers. The high-power density is a good benefit of laser welding, but on the other hand it implies possible vaporization of volatile alloys [16].
Some materials cannot be easily welded such as aluminum, due to its high reflectivity. Moreover, although the laser welding benefits of high flexibility, the joining of different parts and geometries is limited, and the equipment lacks mobility [15].

2.3 Power density

Power density is defined as power (W) per unit area (m^2) and it's also known as irradiance. It has large application in laser cutting and welding because the depth of laser penetration must be considered apart from a simply encountering with the surface [17].

$$I(r,z) = \frac{P}{\pi r_z^2} \tag{1}$$

$$r_z^2 = r_0^2 \left[1 + \left(\frac{\lambda D_f}{\pi r_0^2}\right)^2\right] \tag{2}$$

I(r,z) is the power density on the surface of the workpiece, P is the power, r_z is spot size, r_0 is focus size, D_f is focal position and λ is the wavelength of laser.

The equation shows the power density is directly proportional to the emitted power and inversely proportional to the spot area. The spot area is the laser beam projected area on the workpiece surface. The focus size is strongly related to the focus distance from the workpiece. The higher the focus distance, the lower the spot radius. Moreover, the focused spot size is determined by the laser beam diameter, the focal length of the focusing optic used, the beam mode and the beam divergence angle.

Laser beam welding has high power density resulting in small heat-affected zones and high heating and cooling rates. The spot size of the laser can vary between 0.2 mm and 13 mm, though only smaller sizes are used for welding. The depth of penetration is proportional to the amount of power supplied and also depends on the location of the focal point: penetration is maximized when the focal point is slightly below the surface of the workpiece.
The depth of penetration during laser welding is directly related to power density of the beam. This is a function of beam power and diameter of the focused spot. The general observation is that for a given thickness a minimum threshold power is required for laser welding. An increase in power densitiy rises the amount of penetration almost linearly [18].

2.4 Effect of main welding process parameters

Different parameters can affect the weld bead during the operation process. Power, speed, joint configurations, wavelength, focus are all key elements for the final product.

Power

The welding process could be executed by continuous or pulsed power.
The main problem regarding welding by continuous power are lack of penetration and inverse "dropout". Penetration is strongly connected with power level, more precisely penetration is inversely proportional to power. On the other hand, the use of pulsed power introduces two more variables: pulse repetition frequency and percentage overlap. Anyway, penetration keeps being dependent from power, but independent from speed. The big and marked advantage of pulsed power is that the higher the power by pulsing or modulating the beam, the greater the penetration. Moreover, high peak power also means better welding of reflective material and greater tolerance to focal position.
By comparing pulsed and continuous power, the former has better control during operation and can also reduce porosity. Furthermore "pulsing" means less energy, so a low amount of energy in the workpiece lead to a reduced distortion [6].

Speed

Speed is one of the most influencing parameters. Speed changes affect the weld bead shape and the weld pool. In fact, at slow speeds the pool is large and wide leading to a possible dropout as the figure d shows. On the other hand, at high speed, the quick flow has no time to uniform itself in the keyhole wake showing a frozen part in the middle and undercuts on both sides as shown in the figure b [6].

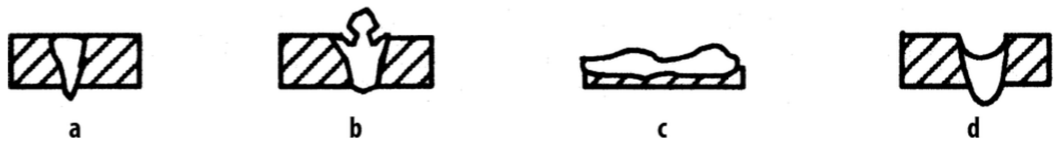

Figure 15: Weld shapes varying with speed: a) normal; b) undercut; c) humping ; d) dropout

Joint configurations

Keyhole laser beam prefers joint which helps absorption and keyhole formation. Several types of joint can be worked, but two are considered the most difficult: butt joint between two solid round bars and the T configuration in round pipe joint.

The "T" weld geometry allows the thermal load reduction on the T side of the keyhole due to the following process: as the keyhole penetrates into the workpiece it acts by turning upwards leading to full penetration around the T base. This is an important point due to the fact that If the weld is not fully penetrated cracks could occur. A way to overcome the problem is increasing the used power or welding slowly. Instead, in the butt joint between two solid round bar the welding speed decrease as the weld keyhole get closer to the center of the bar. This induces to an increase of the amount of heat produced at the center of the joint and hence possible porosity or material expulsion [6] [7].

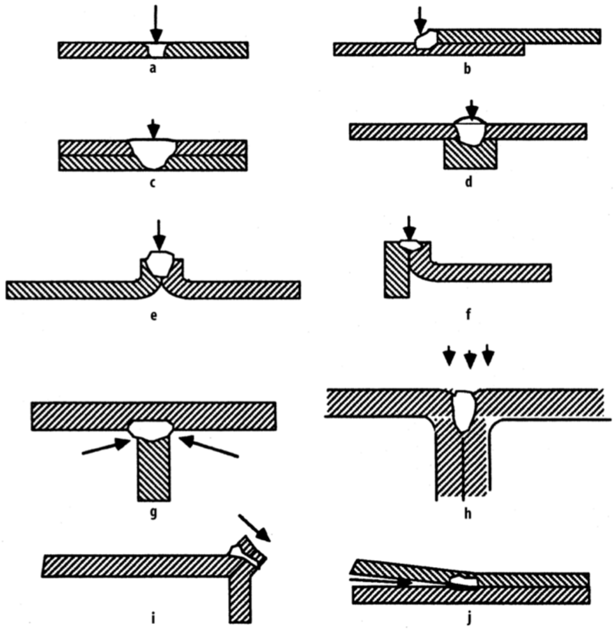

Figure 16: Joint configurations

Wavelength

Welding with long or short wavelengths lead to different results. It's important to underline that a shorter wavelength lead to less absorption and hence cooler plasma. The produced plasma can significantly affect the absorption because of the hot gases emitted from the keyhole and it will produce some effects. In fact, plasma is full of electrons and electrons could absorb photons. Then, plasma blocks the beam. Also, hot plasma affects density changes and so changes in the refractive index which could disperse the beam. All of these elements depend on the amount of plasma absorption. It's essential to show the connection between absorption and wavelength by Raizer equation [19]:

$$\alpha \approx n^2 \lambda^2 T^{\frac{3}{2}} \tag{3}$$

Where α is the absorption coefficient, n is the gas density , λ is the wavelength and T is the absolute temperature of the plasma [6].

Focus

Focal position is the distance between the laser focus and the workpiece surface. Focal position affects the power density by changing the spot size. It has a great impact on welding mode, depth and width of the molten pool. In fact, the molten pool depth decreases as the width increases due to change in power density [20].

The positive defocus lead to a conduction weld very stable melt pool while negative defocus lead to a deep penetration with possible porosity in the keyhole. The porosity forms as much as laser beam moves away from the molten zone, the vapor cavity collapses leaving voids. On the other hand, the negative defocus distance is more natural and enhance the focus efficiency. The laser beam being convergent drills deeper into the material approaching to the focal plane which increases its intensity [21].

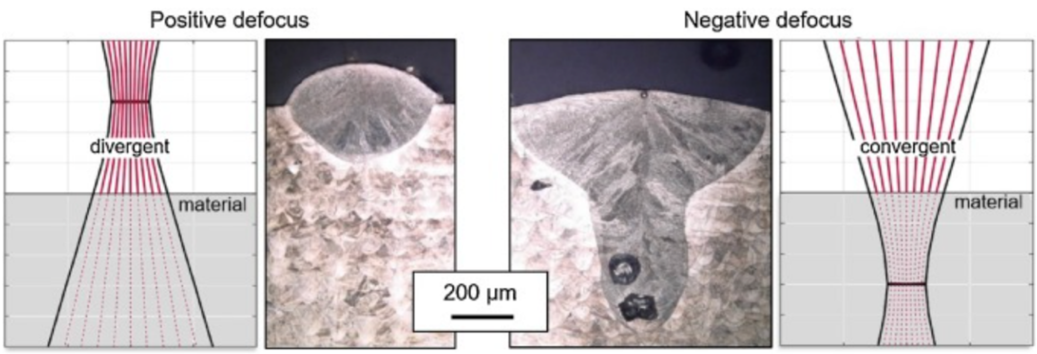

Figure 17: Positive e negative defocus

A new technique is recently introduced named as wobbling welding. Focus wobbling is characterized by a periodical change of the focal distance during the welding process.
The wobbling technique begins to play an important role in laser welding because it allows to programmatically change the width and other characteristics of the weld and allows to make large welds even with a small spot size. In this technology, a periodic repetition of the primitive curve is added to the welding speed. Nowadays, a number of primitive curves have been experimentally tested, such as a line, circle, eight or infinity [22].
Wobbling has an effect on the beam, in particular it increases its diameter. It allows to work at high efficiency reaching a deep keyhole welding. The wobble welding is equipped with a rotating lens weaving which means moving the beam with internal mirrors. In this way the focal spot gets no longer static and it can be dynamically adjusted by changing the shape,

amplitude and frequency of various patterns. This allows the laser beam to circle within a defined radius. The result is less material deposited and the amount of input heat is reduced [23].

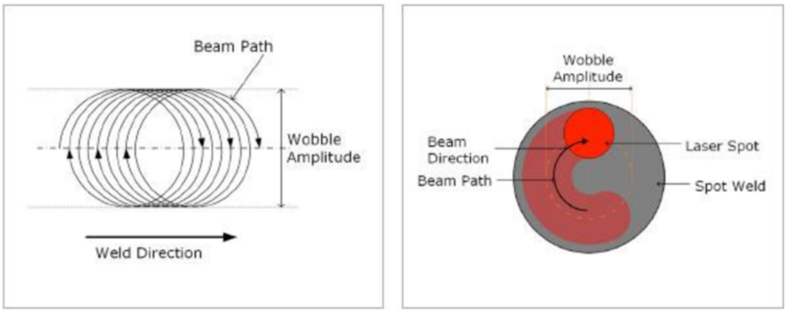

Figure 18: Wobbling technique

2.5 Weld bead defects

Defects in weld bead could be described as irregularities due to the use of incorrect welding parameters, wrong weld procedure or material issues. Defects in welding can occur at any stage of the welding process and they can easily be detected in terms of geometric imperfection.
Defects can appear on the workpiece surface or inside the material, named as external and internal defects. External defects are incorrect profile, crater, cracks, spatter or porosity, distortion, incomplete filled groove. Internal defects are internal porosity, incomplete fusion, lack of fusion.
Some of them are less critical than others and they can be considered acceptable into defined limits, typically imposed by costumer requests. Most of defects depend on improper welding procedure, wrong operator actions or material characteristics.

In laser welding the most typical defects are cracks, porosity, undercut, incomplete fusion, overlap and spatter. All of them are shown in the figure below.

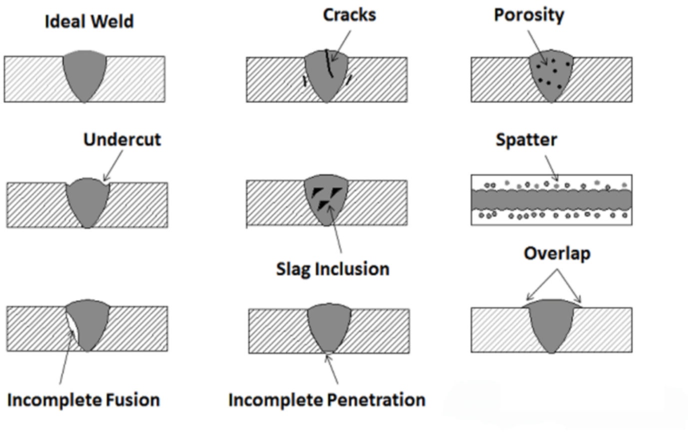

Figure 19: Type of defects

Cracks

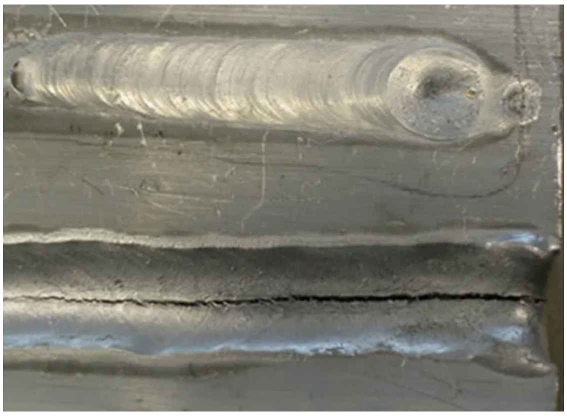

Figure 20: Crack in welding

Cracks can be of micro or macro size and can appear in the weld metal, base metal or metal boundary. Every crack is considered a defect and it could show up when load go over the maximum tensile strength admissible of the material. Cracks could occur due to poor ductility of the base material, fast cooling rate or high carbon contents. Cracks appear because of the presence of residual stresses or metal expansion and contraction due to the rigidity of the joint. Cracks can be divided in hot cracks and cold cracks.

Hot cracking

The phenomenon takes place just after the welding process usually into the weld. The cause could be the presence of Sulphur or not homogeneous cooling within the weld. Cracks are often located along the axis of the joint.

Cold crack

On the contrary cold cracks do not appear soon but within a few days from welding. It is usually induced by hydrogen absorbed into the weld or by metal contamination. Hydrogen may be absorbed due to the presence of moisture seeping into an electrode [24].

Microfissure

Microfissure could show up later in a future weld scenario. Factors that can affect its outcome are metal fatigue and stresses in the heat affected zone. Heat treatments could minimize the risk.

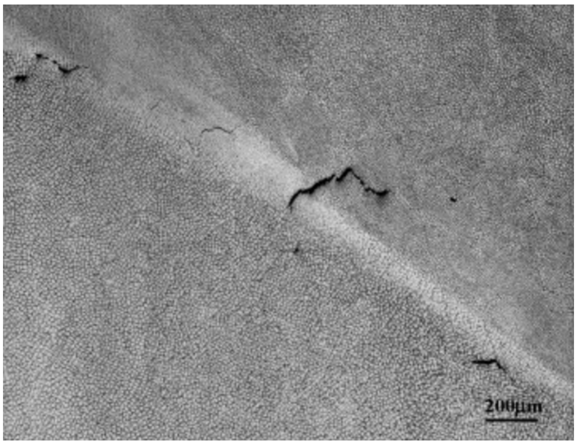

Figure 21: Microfissure in welding

Crater crack

Crater crack develops when a welder accidentally leaves a crater behind when welding stops. Usually, the welding procedure involves welding over the end or on the top of the joint to prevent a crater.

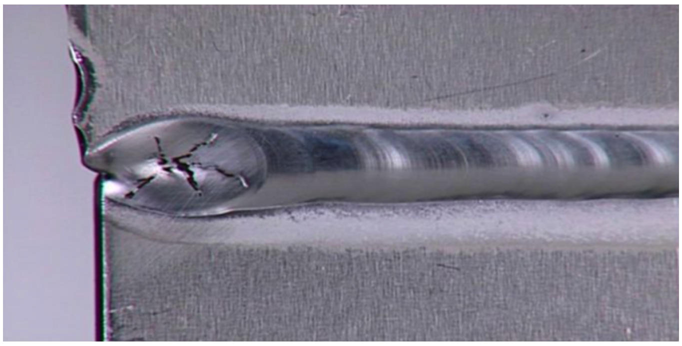

Figure 22: Crater crack in welding

Porosity

Porosity is one of the most common defect during welding. Porosity usually emerges when gases get entrapped in the solid metal or from causes such as contamination or inadequate shielding. However, in laser welds, porosity can also result from laser keyhole instability and collapse. Porosity could be avoided by cleaning the surface from rust, oil and grease. Even if porosity is not considered as cause of fatigue, it reduces the strength of the material due to localized concentration of stress.
Oxygen and hydrogen are the worst enemy of welders. Surface oxidation leads to corrosion and it has to be removed just before starting the welding process. Hydrogen instead, makes one more phenomenon appears, it is called hydrogen embrittlement. Hydrogen gets inside the material and being the smallest atom existing, it gets trapped in the crystal boundaries creating bubbles.

Figure 23: Porosity in welding

Undercut

Undercutting is one of the most sever defect during welding. It shows unfilled groove along both side of the weld bead. The causes are usually associated to an incorrect electrode angle, weaving technique, travel speed or excessive current. It could be avoided by paying more attention about details during welding process. Accurate heat input helps to prevent undercutting as well as working at medium speed. Welding too quickly bring the base metal becoming molten metal and it cannot return to its original shape.

Figure 24: Undercut in welding

Incomplete fusion

Incomplete root fusion is when the weld fails to fuse one side of the joint in the root. Incomplete fusion is an internal planar discontinuity in which fusion did not occur between the weld metal and fusion faces. Actually, the lack of fusion can happen at any location leading to higher danger and difficulty in their detection. Lack of fusion happens when the base material or the deposited weld metal does not reach its melting temperature during the welding process. It is usually located along the fillet weld and can be caused by an incorrect welding angle [25].

Figure 25: Incomplete fusion in welding

Incomplete penetration

Incomplete root penetration occurs when both sides root region of the joint are unfused. Incomplete penetration means that the weld depth is not up to the desired level or root faces have not reached the melting point in a groove joint. It often occurs when weld metal does not create bond with the base metal without reaching the desired depth and as a consequence, it does not extend through all the joint thickness. This phenomenon usually depends on root and groove design, when their shape or dimensions exceed the standard. Causes can be a too narrow root or too large root, a too small opening root as well. To prevent incomplete penetration a good joint should be designed to ensure the correct welding procedure [24].

Figure 26: Incomplete penetration in welding

Overlap

Overlap is the opposite extreme of undercutting. Here, the weld metal flows across the base metal at the toe without producing any fusion between the two. This may be caused by insufficient heat to melt the base metal, and/or improper manipulation of the electrode. The excess of weld metal beyond the weld root is caused by poor welding technique. The overlap could be repaired by grinding off the excess metal.

Figure 27: Overlap in welding

Spatter

During welding process spatter phenomena could occur. It consists in metal droplet which drop out of the weld bead on the surrounding surface. Spatter involves the ejection of melt from the weld pool as a result of high levels of acceleration in directions approximately perpendicular to the weld liquid surface. Of course, irregular weld surface can also drive to spatter phenomena as well as the combination between rotation movement and gas and laser emission on the metal. It can be surely minimized by improving the welding conditions and it can be admissible If satisfy the customer requests.

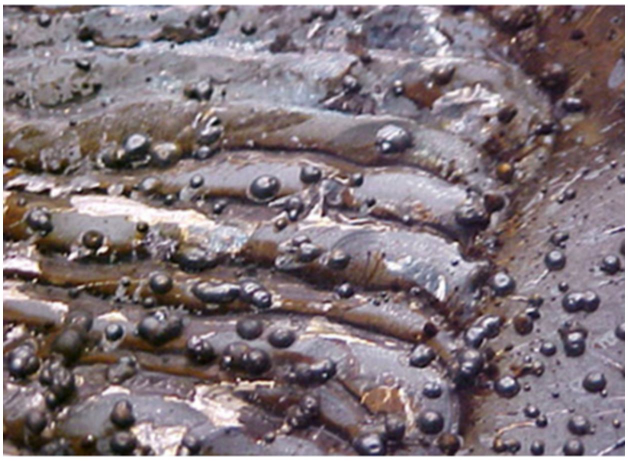

Figure 28: Spatter in welding

Distortion

Because metal expands when heated and then shrinks after cooling, the two sides of a joint may shift position during welding. Because of contraction or expansion of the heated material, not uniform stresses are imposed on the material. When weld pool is formed compressive stresses are produced due to thermal expansion of the HAZ. Then cooling occurs, leading to a contraction of the weld metal generating stresses. When the produced stresses exceed the yield strength of the material, plastic deformation takes place. Plastic deformation means permanent modification in component size and distorts the structure. Of course, the shape and rate of distortion depends on several factor: material type, geometry, weld design, heat input. For example, stainless steel is significantly prone to deformation.
Distortion can occur in different ways: transverse, longitudinal, angular, buckling, twisting, bowing and dishing [26].

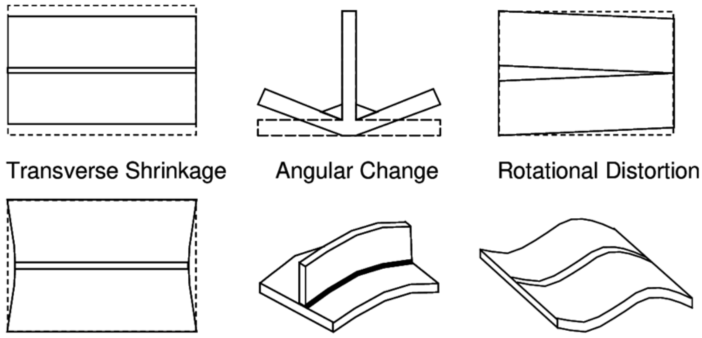

Figure 29: Distortion in welding

Humping effect

The humping phenomena is generally understood as the formation of drop like piles on the top of a weld bead that alternates with the appearance of undercut between the individual humps. It occurs during seam welding at speed rates above a certain value and is likewise observed in electron beam, arc and laser beam welding [27]. It can also depend on power level, material thickness, focal diameter. Hump can affect the weld bead by deteriorating weld morphology. Associated to this, the undercut added at the humping phenomena, reduces the effective cross-sectional area of the joint decreasing the ability of the joint to tolerate dynamic loads.

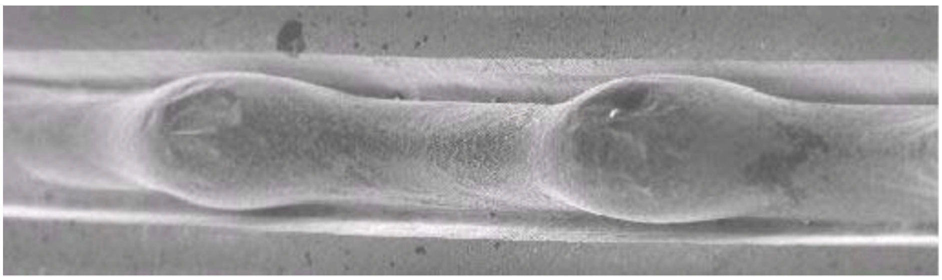

Figure 30: Humping in welding

2.6 Application of materials in laser welding

The main problem related to material in laser welding applications is poor absorption due to its reflective properties, porosity formation , crack sensitivity and HAZ embrittlement. Crack formation is due to the shrinkage stress before the weld has fully solidified while porosity often results in materials subjected to volatilization. When lasers hit the workpieces surface some laser energy is absorbed and an amount is reflected. The absorbed laser energy into the material increases its temperature. This process could lead to different results depending on material properties. If the material has a high reflectivity, then the energy absorbed will be low like in aluminum or copper. Moreover, if the material has high thermal diffusivity, then the thermal energy will be easily conduct through the workpiece bringing to a greater depth of welding. To sum up, the lower the thermal diffusivity the more likely the material to absorb energy and the higher thermal conductivity, the larger penetration [15] [3].
The absorptivity may depend on the kind of materials, surface condition, surface temperature and laser wavelength as described in the table below.

Material	300–600 nm	1.06 μm	10.6 μm
Aluminium, smooth		0.06–0.2	0.03–0.06
rough		0.2–0.4	0.1–0.4
Copper, polished	0.05	0.04	0.01–0.03
rough	0.05	0.1–0.3	0.05–0.10
oxidized	0.85	0.5	
Gold		0.02–0.04	0.01–0.02
Iron, polished	0.37–0.40	0.25–0.32	0.12
Molybdenum, polished	0.4–0.5	0.25–0.35	0.05–0.15
Nickel	0.5	0.15–0.35	0.05–0.15
Platinum		0.25–0.30	0.03–0.08
Silver		0.03	0.02–0.10
Tungsten	0.5	0.35	0.03–0.3
Carbon (graphite)	0.75	0.8–0.9	0.7–0.9
Alumina (Al_2O_3)		0.05–0.1	0.90–0.99
Magnesia (MgO)		0.2	0.93–0.98
Silica (SiO_2)	Transparent	Transparent	0.9
Zirconia (ZrO_2)		0.1–0.2	0.85–0.98
Silicon carbide (SiC)	0.8–0.9	0.85–0.95	0.8–0.9
Silicon nitride (Si_3N_4)	0.6–0.7	0.6–0.8	0.9

Table 6: Absorptivity of materials in welding

The absorptivity normally increases with temperature. During laser welding, formation of molten pools enhances the absorption of laser energy. Aluminum and copper show low absorptivity, so high reflectivity, that's the reason why both materials are considered hard to be welded by lasers.

The problem described shows more difficulties during joining dissimilar materials. For example, steel and copper have different thermal conductivity and this affects the absorption of laser light. Copper has high thermal diffusivity which transfer away the absorbed energy and most of it will be lost. There is also a great tendency to form metastable solid solutions. Austenitic stainless steel is a good candidates for laser welding being a single-phase ductile material with high ductility and good corrosion resistance. Although austenitic stainless steel undergoes to chromium precipitation at grain boundaries when temperature reach very high values, it welds easily [5].

2.6.1 DD steels characteristics

Hot rolling process requires as a first stage heating the material in the hot deformation region in order to increase workability and reduce the flow stress. Then, the material goes through plastic deformation in successive rolling passes in roughing and finishing mills. As a consequence, the desired dimension and shape is achieved [28].

Depending on actual width, strip can be classified as

- hot rolled wide strip if its width is greater than or equal to 600 mm.
- hot rolled slit wide strip if its width is less than 600 mm.

Hot rolled products should be delivered with their surface as rolled and they are classified into 4 grades: DD11, DD12, DD13 and DD14. Differences are defined by their chemical composition , mechanical and forming characteristic. Moreover, hot rolled steel is typically cheaper than cold rolled steel due to the fact that it is often manufactured without any delays in the process, and therefore the reheating of the steel is not required. [29]

Mechanical properties of DD steels are defined in the following table:

Steel name	Steel number	Method of deoxidation	Ladle analysis chemical composition [b]				Mechanical properties [c]							Validity
							R_{eL} [d]		R_m	Minimum elongation after fracture				
										L_0 = 80 mm			$L_0 = 5{,}65\sqrt{S_0}$	
			C	Mn	P	S	1,0 mm ≤ e < 2 mm	2 mm ≤ e ≤ 11 mm		1,0 mm ≤ e < 1,5 mm	1,5 mm ≤ e < 2 mm	2 mm ≤ e < 3 mm	3 mm ≤ e ≤ 11 mm	
			max. %	max. %	max. %	max. %	MPa	MPa	max. MPa	%	%	%	%	months
DD11	1.0332	At the discretion of the manufacturer	0,12	0,60	0,045	0,045	170 to 360	170 to 340	440	22	23	24	28	–
DD12	1.0398	Fully killed	0,10	0,45	0,035	0,035	170 to 340	170 to 320	420	24	25	26	30	6
DD13	1.0335	Fully killed	0,08	0,40	0,030	0,030	170 to 330	170 to 310	400	27	28	29	33	6
DD14	1.0389	Fully killed	0,08	0,35	0,025	0,025	170 to 310	170 to 290	380	30	31	32	36	6

NOTE 1 MPa = 1 N/mm^2.

a The mechanical characteristics relate only to hot rolled non-descaled or chemically descaled and oiled products, skin-passed or not.

b Unless otherwise agreed at the time of enquiry and order, nitrogen-fixing elements such as titanium and boron may be added at the discretion of the manufacturer.

c As long as the width of the product permits, the test pieces for the tensile tests shall be taken transverse to the direction of rolling.

d $R_{p0,2}$ shall be used instead of R_{eL} if the product does not exhibit any yield phenomenon.

e It is recommended that products in grade DD11 should be formed within 6 weeks from the time of their availability.

Figure 31: EN 1011-2018

These steels are also defined as soft steel because of their excellent formability, in fact they can be also used for deep drawing and bending. DD13 is the main material tested in the case of study.

2.6.2 Influence of steel chemical composition on laser welding

The high intensity laser beam melts and partially evaporates the welded material during the process. Achieving a high temperature gradient during the heating and cooling time leads to development of high thermal stresses in the welding zone. Once the cooling time is over, residual stresses are then generated in the welding zone. This, in turn, affects the mechanical performance of the resulting welds. Consequently, the analysis of the development of thermal stress and the formation of residual stresses in the welding zone becomes essential. In addition to residual stress measurements by diffractometry, metallographic inspection becomes strongly important in determining the extent of the thermally altered zone (HAZ) and identifying the microstructure. For example, the quantities of bainitic ferrite and martensite can also increase in steels with a low carbon content, it depends on various process parameters (e.g., welding speed, shielding gas, laser power).
The best mechanical characteristics in the HAZ zone has to be associated with microstructures made up of mixtures of bainitic ferrite (BF) and low carbon martensite (M)

with low amounts of ferrite (F). The percentage of martensite increases as much as the carbon content of the steel and the welding speed increase at the same time. The effect of martensite on the hardness and tensile strength of laser welding is highly important. The use of CCT diagrams to estimate the temperature and the microstructural composition of very low carbon steels during the welding process is essential. CCT diagram related to the investigated DD13 steel is shown below:

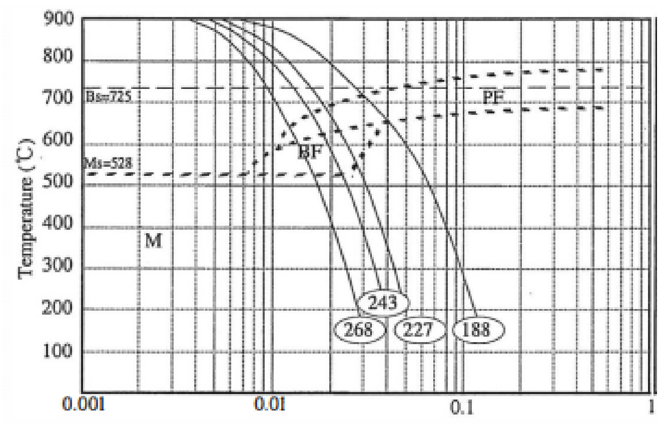

Figure 32: DD13 CCT diagram

DD13 steels are considered to be easily weldable due to their low alloying element content. However, these materials can still show the following defects: porosity, cracking during solidification, cracking due to the presence of hydrogen, cracking due to coarse grains.

Porosity is formed by the entrapment of gas pockets in the solidifying melt bath. The gas can come from poor shielding, surface contaminants such as rust or grease. A particularly serious form of porosity is represented by "wormholes", caused by the coarse contamination of the surface. The presence of manganese and silicon in steel is useful because they act as deoxidizers, which interact with the air trapped in the melt bath in order to form slag. To achieve porosity-free welds, the joint area must be cleaned and degreased prior to welding.

Solidification cracks occur longitudinally to the weld bead. That's due to the fact that the weld bead has insufficient mechanical strength to withstand the contraction stresses of the surrounding metal. Sulfur, phosphorus and carbon increase the risk of cracking of the weld metal, especially during thick sheet metal welding. During welding of high sulfur steels, weld beads are more susceptible to solidification cracking. The EN 1011-6:2018 defines the amount of the most influent sulfur elements related to a carbon percentage in order to guarantee a good weldability. The argument will be discussed in deep in section 4.5.1. In the case of a weld with a large depth-to-width ratio, the center of the weld (i.e., the last part

to solidify) will have a high concentration of impurities which increase the risk of cracking. Solidification cracking can be avoided with careful attention to the choice of welding parameters. The weld parameters must produce an adequate depth-to-width ratio in butt welds or the throat thickness in fillet welds. High weld speeds also increase the risk of solidification cracks as the amount of segregation and weld stresses will increase.
It is necessary to add that the costumer request defines the weld bead geometry more suitable to the component operating conditions. [30]

A feature of high carbon and low alloy steels is that HAZ immediately adjacent to the weld hardens during welding with a consequent risk of cold cracking. Although the risk of hydrogen cracking is determined by the level of hydrogen produced by the welding process, this susceptibility will also depend on several other factors: material composition (carbon equivalent), bead thickness, laser energy input. After all, the composition and the cooling rate of the steel determine the hardness of HAZ. The chemical composition determines the hardenability of the material, and the higher the carbon and alloy content of the material, the higher the hardness of the HAZ. Sometimes, HAZ cracking is prevented by heating the material. The use of a preheating reduces the cooling rate, promotes the removal of hydrogen and reduces the HAZ hardness, thus avoiding the formation of a structure sensitive to crack. If the material is allowed to cool too quickly, cracking can occur up to several hours after welding, often referred to as "delayed hydrogen cracking". After welding, therefore, it is sometimes useful to keep the heating for a given period (waiting time), depending on the thickness of the steel, to allow the hydrogen to diffuse from the weld area. In conclusion, the risk of HAZ cracking is reduced by using a low hydrogen process (such as laser welding) and by reducing the level of surface contamination.

Cracking due to coarse grains is typical of the HAZ of thick section components, usually with a thickness greater than 50 mm. The most likely cause of rupture is HAZ embrittlement during high temperature treatment or stress relieving heat treatment. Since a coarse-grained HAZ is more prone to cracking, low-energy welding procedures reduce the risk. Although such cracking occurs in sensitive materials (high-alloy steels, AHSS steels), high stresses during welding must be avoided and local stress concentration points eliminated. Preheating (which, in the case of DD and C40 steels occurs at about 250-300 ° C due to the thickness of the case) would significantly increase the cycle times. The choice of the parameters for the laser welding cycle must therefore be suitable to guarantee the tightness of the weld, the mechanical strength of the weld and low cycle times. The use of steels with a low content of alloying elements is to be preferred in order to avoid harmful preheating and / or stress relieving heat treatment cycles [31] [32].

The most commonly used parameter to correlate the weldability of steels with their composition is the so-called carbon equivalent (CE). Carbon equivalent is used to understand how different alloying elements affect the hardness of the steel being welded. This is therefore directly related to hydrogen-induced cold cracking, which is the most common weld defect for steel. Higher concentrations of carbon and other alloying elements such as manganese, chromium, silicon, molybdenum, vanadium, copper and nickel tend to increase hardness and reduce weldability. There are two commonly used formulas to calculate the equivalent carbon content. The first comes from the American Welding Society (AWS) and is recommended for structural steels, while the other formula was proposed by the International Institute of Welding (IIW).

$$CE = \%C + \left(\frac{\%Mn + \%Si}{6}\right) + \left(\frac{\%Cr + \%Mo + \%V}{5}\right) + \left(\frac{\%Cu + \%Ni}{15}\right) \qquad (4)$$

$$CE = \%C + \left(\frac{\%Mn}{6}\right) + \left(\frac{\%Cr + \%Mo + \%V}{5}\right) + \left(\frac{\%Cu + \%Ni}{15}\right) \qquad (5)$$

The AWS states that for a carbon equivalent content greater than 0.40% there is a potential risk of cracking in the heat affected zone (HAZ) on flame cut edges and welds.
For the second equation the weldability based on a range of CE values can be defined as follows:

Carbon equivalent (CE)	Weldability
Up to 0,35	Excellent
0,36 – 0,40	Very good
0,41 – 0,45	Good
0,46 – 0,50	Fair
Over 0,50	Poor

Table 7: Weldability classification

CHAPTER 3

Methods and Materials

3.1 IPG Photonics fiber laser source

The IPG laser welding used in this research study is YLS-5000. It is a laser with wavelength 1.07 μm, Power 5 kW, Output Power 5 kW and with fiber parameters of about 50, 100, 200 μm.

Figure 33:IPG YLS-5000

The IPG YLS-5000 is implemented on a process line. The welding process line starts with a washing machine where the workpieces to be welded passe through in order to eliminate any form of contamination. Once they are polished, a robot arm takes both components and places them to the laser cabin entrance. Then, they move in and the welding process takes place in a safety cabin.
The process line is composed by two more stations: a turning station and a non-destructive testing (NDT) station with eddy current inspection method.

3.2 *Design and Analysis of Experiments*

3.2.1 Design of experiments (DOE)

Statistical experimental design, or design of experiments (DoE) is the methodology of how to conduct and plan experiments in order to extract the maximum amount of information in the fewest number of runs. The first example of DoE dates back to 1923, with a publication by the statistician Ronald Fisher.

DOE, is used in many industrial sectors, for instance, in the development and optimization of manufacturing processes. Typical examples are application on the production in the electronics industry, the manufacturing of engines in the car industry, and the synthesis of compounds in the pharmaceutical industry. Another main type of DOE-application is the optimization of analytical instruments. Usually, however, an experimenter does not jump directly into an optimization problem, but an initial screening is necessary in order to pay attention on the most fruitful part of the experiment. Especially in manufacturing field there is a high interest in exploring relationship between the key input variables, called factors and the output performance, or quality features. Areas where DOE is used in industrial research, development and production:

- optimization of manufacturing processes
- optimization of analytical instruments
- screening and identification of important factors robustness testing of methods
- robustness testing of products
- formulation experiments

Consider a generical welding process, by applying DOE is possible to evaluate which input factors are more significant on the interested outputs. Moreover, through experiments, it is also possible to predict the output by varying several key input welding factors.
The steps for designing an experiment are:

1. Recognition of/statement of the problem: it can be very helpful in terms of process understanding.
2. Choice of factors and levels: it derives from process knowledge, based on practical experience and theoretical understanding; usually in a first step the number of factors is kept low.

3. Selection of the response variable: the experimenter should know in advanced which variables could be more affected by the factors, giving useful information about the process. Sometimes multiple responses are considered.
4. Choice of experimental design: selection number of replicates and run order for experimental trials, eventual introduction of blocking or other randomization restrictions.
5. Performing the experiment: at this stage is important to take care of experimental procedures, because eventual errors could affect negatively the experimental validity.
6. Data Analysis

Of course, in order to apply the steps in the correct way is necessary to understand well the process. A process is transformation of input into outputs. In manufacturing, inputs are factors or process variables while outputs are performing or quality elements. During the experiments, input variables can be changed in order to observe their effects on the output process [33].

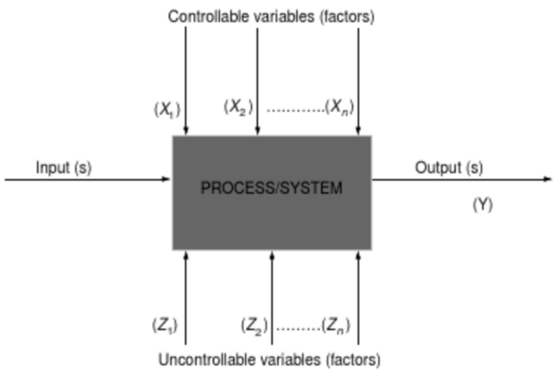

Figure 34: General model of a process or system

During any experiments there are some variables that can be controlled, and others called uncontrollable which determine the process variability. For this reason, is important to well defined controllable factors in order to minimize the effects of uncontrollable variables and makes the process solid.
In manufacturing two types of variables can be integrated: qualitative or quantitative factors. For quantitative factors a range of setting has to be decided, while qualitative factors require more levels.

Basic principles of DOE

Design of experiment is defined by three important subdivisions: planning, designing and analyzing the experiment so that valid conclusions can be drawn. The method to be implemented has to be chosen for developing a successful process.

To have an efficient experimental process three important principles should be applied: randomization, replication and blocking. These three principles help to increase the results validity and improve its truthfulness [34].

- Randomization is one of the method which reduce the effect of experimental bias. It makes the experiment more real, since the world is non-stationary. Randomization can ensure that all levels have an equal chance of being affected by noise factors.
- Replication means repetitions of an entire experiment or of a specific part of it, under more than one condition. The method helps to obtain an estimate of experimental error and a more precise factor/interaction effect.
- Blocking has the aim of avoiding the process being affected by unwanted parameters such noise and systematic factors. The idea is to arrange the experiments into blocks or group which correspond to homogeneous experimental conditions.

Empirical model

It is reasonable to assume that the outcome of an experiment is dependent on the experimental conditions. This means that response y , can be defined as a function based of the experimental variables x_i. In addition, a contribution due to experimental error has also to be considered. Design selection also involves thinking about and selecting a tentative empirical model to describe the results. The model is expressed by an equation which makes in relation the response and the important design factors. In many cases, a low-order polynomial model is more suitable.

A first-order model in two variables is

$$y = \beta_0 + \beta_1 x_1 + \beta_2 x_2 + \varepsilon \tag{6}$$

where y is the response, the x_i s are the design factors, the β's are unknown parameters that will be estimated from the data in the experiment while ε is the random experimental error term. The first-order model is also sometimes called as main effects model, in particular they are widely applied in screening or characterization experiments. An extension of the first-order model is to add an interaction term

$$y = \beta_0 + \beta_1 x_1 + \beta_2 x_2 + \beta_{12} x_1 x_2 + \varepsilon \tag{7}$$

where the cross-product term $x_1 x_2$ represents the two-factor interaction term. When more than two factors are necessary, higher-order interactions can be included in experiments by using the second-order model

$$y = \beta_0 + \beta_1 x_1 + \beta_2 x_2 + \beta_{12} x_1 x_2 + \beta_{11} x_{11}^2 + \beta_{22} x_2^2 + \varepsilon \tag{8}$$

Higher-order models are often used in optimization of experiments.
The minimum number of experiments required in the three cases is: 3 (linear model), 4 (interaction model), 6 (quadratic). [35]

Factorial design

As a general definition, a factorial design consists of two or more factors at which a 'value' or a 'level' is associated. When the experiment is set on all possible combinations of the levels and so relative factors, the design is defined as "full factorial". On the contrary, a "fractional factorial" design consists of a chosen part or fraction of the experimental runs of a full factorial design. The risk of applying a full factorial design is its redundant which could give no useful information about the system. Usually, a factorial experiment is the strategy to dealing with several factors in which they vary together instead of one at time.

General full factorial design

It is widely accepted that most manufacturing companies plan full or fractional design at two or three levels. In general, factorial designs are the most efficient for this type of experiment. By a factorial design, each complete trial or replicate of the experiment in all possible combinations of the levels of the factors are investigated. For example, if there are a levels of factor A and b levels of factor B, each replicate contains all ab treatment combinations. When factors are arranged in a factorial design, they are often said to be crossed.
A factorial design can be either full or fractional. The effect of a factor is defined to be the change in response produced by a change in the level of the factor. This is frequently called a main effect because it refers to the primary factors of interest in the experiment.
The experimental design points in a full factorial design, which are also named as factorial points, are the vertices of a hyper cube in the n-dimensional design space defined by the minimum and the maximum values of each of the factors. For example, by applying a full factorial design on three factors having four levels of each factor a total 4^3 (64) numbers of experiments have to be carried out. If there are *n* replicates of complete experiments, then there will be *n* times of the single replication experiments to be run. In the experimentation, it must have at least two replicates to determine a sum of squares due to error if all possible interactions are included in the model.

If all factors in the experiment are fixed, it is possible to formulate and test hypotheses about the main effects and interactions using the ANOVA. For a fixed effects model, test statistics for each main effect and interaction may be constructed by dividing the corresponding mean square for the effect or interaction by the mean square error. The number of degrees of freedom for any main effect is the number of levels of the factor minus one, and the number of degrees of freedom for an interaction is the product of the number of degrees of freedom associated with the individual components of the interaction.

3.2.2 General linear model (GLM)

A generalized linear model is basically a regression model where the response variable can have any distribution that is a member of the exponential family. The relationship between the response means and the linear predictor $x'\beta$ is determined by a link function.

$$g(\mu) = \mathbf{x}'\boldsymbol{\beta} \tag{9}$$

Many choices of link function are possible, but it must always be monotonic and differentiable. In addition to this, in a generalized linear model, the variance of the response variable does not have to be a constant, but it can be a function of the mean. In order to use a generalized linear model in an experiment, the experimenter must specify a response distribution and a link function. Then the model fitting or parameter estimation is executed by applying the maximum likelihood method, which is an iterative version of weighted least squares for the exponential family while it is standards least squares for ordinary linear regression or experimental design models with a normal response variable.
GLM is suitable for studying unbalanced factorial design.

Unbalanced factorial designs

Unbalanced factorial designs occur for various reasons. For example, the experimenter has designed a balanced experiment initially, but because of unforeseen problems at the setting step, resulting in the loss of some observations, it ends with unbalanced data. On the other hand, some unbalanced experiments are deliberately designed. Sometimes certain treatment combinations may be more expensive or more difficult to run than others, so fewer observations may be taken. Alternatively, some points may be of greater interest to the experimenter because they represent unexplored conditions, and so more replications take place. Because of the variance techniques is not applied, the orthogonality property of main effects and interactions are not present in unbalanced data respect to balanced plan. Consequently, the analysis of unbalanced factorials is much more difficult than that for balanced designs [36].

3.2.3 Case of study

DOE

Design of Experiments is applied to develop the case of study. DOE is set on Minitab, a statistics package developed at the Pennsylvania State University. Statistical analysis software such as Minitab automates calculations and generates plots and trend, allowing the user to focus more on the analysis of data and the interpretation of results.

A first General Full Factorial Design is implemented being the most suitable to comply with the study requests and avoiding levels constrains. The aim of the study is understanding which welding process parameter is the most significant on the weld bead geometry and on its own defects.

Objective 1: Determination of the main affective parameters

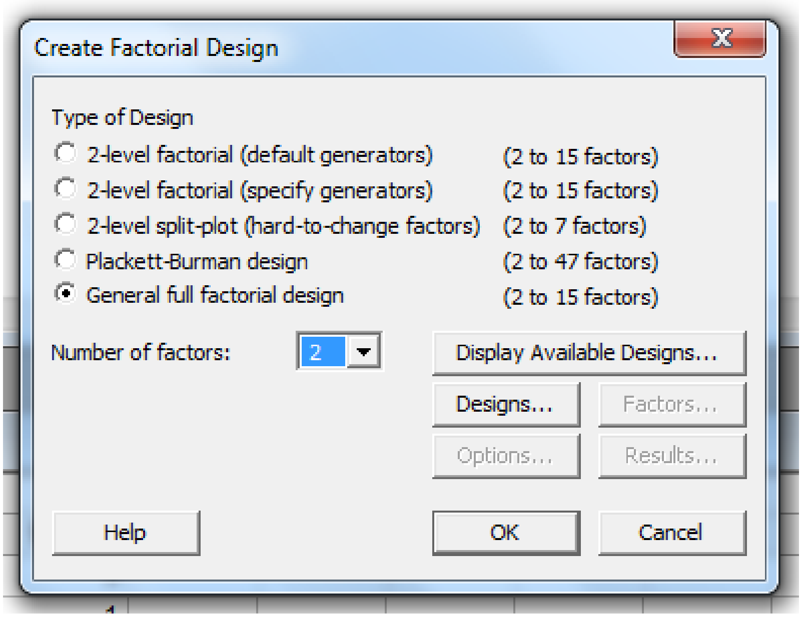

Figure 35: Minitab - General full factorial design

The general full factor design is set on two number of factors. Talking with specialists on the welding process line installed at AGLA Power Transmission , power and focus turn out to be the most influent factors from previous testes and they are the two chosen factors for the case of study. To determine the effect of process parameter and its interaction, a design matrix is designed.

Objective 2: *Levels and factors definition*

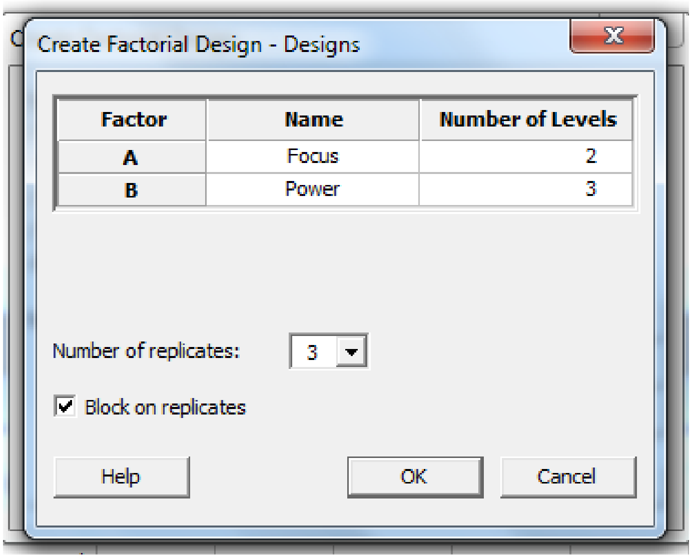

Figure 36: Minitab - Factors and levels definition

For both factors, a number of levels is associated. The number of levels is set at 2 for *focus* variable and at 3 for *power* . Then the matrix design is filled.

The corresponding values are defined in mm for focus and in $\frac{W}{mm^2}$ for Power which is expressed in parameterized values.

Factors	Name	N of levels	Level 1	Level 2	Level 3
A	Focus	2	-16	-12	
B	Power	3	13086	15031	16623

Table 8: Test 1 set-up by DOE

Each trial condition is replicated three times in order to obtain a higher accurate estimation of experimental error. Block on replicates is checked.

Objective 3: *Minitab Outputs*

Results for: Worksheet 20

Multilevel Factorial Design

```
Factors:       2     Replicates:     3
Base runs:     6     Total runs:    18
Base blocks:   1     Total blocks:   3

Number of levels: 2; 3
```

Figure 37: Minitab - Outputs

Once the input factors are unloaded, Minitab gives as output the number of blocks and runs. The number of total run to execute are 18 while the number of blocks is 3. All the tests have to be developed in the right order illustrated from Minitab output, following step by step the model matrix. Then a Test 1 is conducted by producing 18 workpieces.

GLM

The necessity of extending the experimental plan by making more tests implies the necessity to apply General linear model in order to have a statistical analysis on new more data. GLM is able to study an unbalanced plan, joining the DOE set with all the others experimental results.

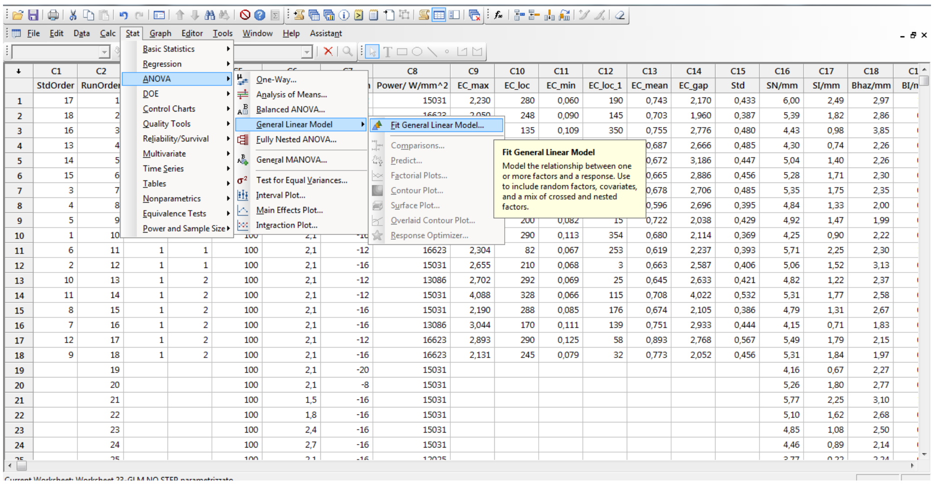

Figure 38: GLM setting

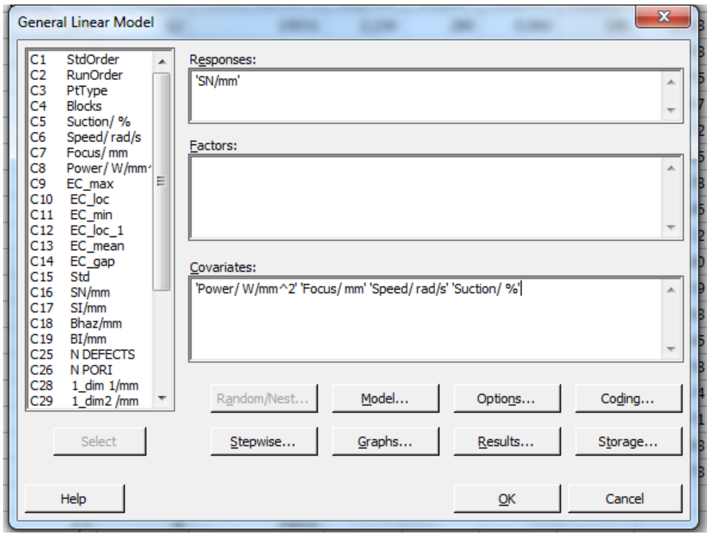

Figure 39: GLM covariates

The GLM is set by considering Power, Focus, Suction and Speed as covariates, while during the previous analysis only power and focus were taking into account being the only two variables. New experiments introduce new variables.

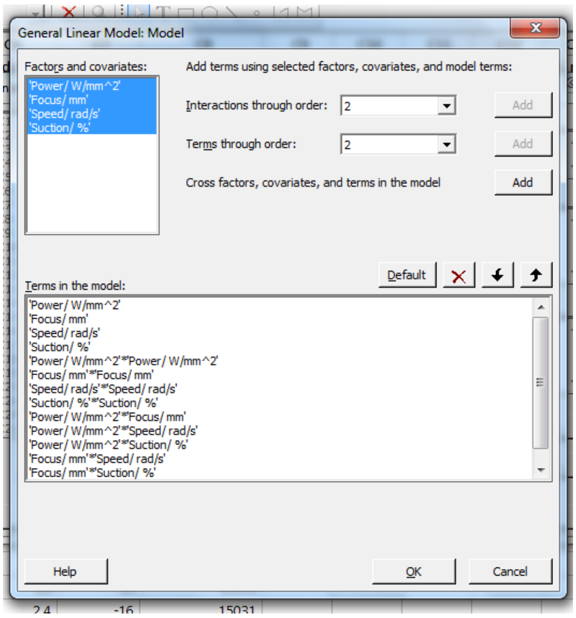

Figure 40: GLM terms in the model

During the analysis is considered not only the effect of all the single process parameters but also its interaction and its own quadratic effect, except for Suction which being expressed in percentage the consideration of its quadratic effect would be needless.

The table below reports the examined outputs by DOE and GLM in order to understand the effect of process parameters on the underlying factors.

$\mathbf{S_n}$	Penetration depth
$\mathbf{S_i}$	Penetration depth from the joining point
$\mathbf{b_{haz}}$	Weld bead length at the interface
$\mathbf{b_i}$	Weld bead length at the joining point
$\mathbf{E_{max}}$	Maximum eddy current peak value
$\mathbf{E_{min}}$	Minimum eddy current peak value
Std	Eddy current Standard Deviation
l/h	Defect dimensions

Table 9: DOE and GLM outputs

3.3 Test development process

The experimental procedure is divided in 3 parts. As any experiment, during the observation procedure and data analysis, the interest increases, and a deeper examination could lead to more satisfied results. Then, in addition to Test 1 developed after DOE planning with production of 18 workpieces, three more tests are carried out. They help to have a larger field of study and more reliable results involving them in statistical examination calling the GLM analysis.

Part 1: Production procedure of Test 2 and Test 3

The experiment starts from the DOE setting described in the previous paragraph producing 18 workpieces in Test 1. Then, the idea is to work in a larger range of parameters and have a broader view of the effect of changes in process parameters. The set DOE keeps the speed constant and make variation only on power and focus. The production of more workpieces is carried out in order to observe effects on weld beads due to suction variation, speed changing and range over power and focus values. The table below shows the parameters used to produce 10 workpieces keeping suction at 100 % and 6 more workpieces using only suction as variable. Power and speed are reported in parameterized values. The total number of produced workpieces in Part 1 is 16.

Test 2

	Speed/rad/s	Power/W/mm^2	Focus/mm	Suction/ %
N1	2,1	15031	-20	100
N2	2,1	15031	-8	100
N3	1,5	15031	-16	100
N4	1,8	15031	-16	100
N5	2,4	15031	-16	100
N6	2,7	15031	-16	100
N7	2,1	12025	-16	100
N8	2,1	17684	-16	100
N9	2,1	15031	-4	100
N10	2,1	15031	0	100

Table 10: Test 2

Test 3

	Speed/rad/s	Power/ W/mm^2	Focus/mm	Suction/ %
A1	2,1	15031	-16	100
A2	2,1	15031	-16	90
A3	2,1	15031	-16	80
A4	2,1	15031	-16	70
A5	2,1	15031	-16	60
A6	2,1	15031	-16	50

Table 11: Test 3

Part 2: Production procedure of Test 4

During the analysis development and by observing the material metallography and differences in geometrical parameters, the interest of studying in deep lead to more research. Using other combinations of the operating parameters, 18 more workpieces are produced ranging over power and focus values. Welding of P1 and P9 did not occur because of the too low operating power conditions.

Test 4

	Speed/rad/s	Power/ W/mm^2	Focus/mm	Suction/ %
P1	2,1	13086	-20	100
P2	2,1	13086	-8	100
P3	2,1	13086	-4	100
P4	2,1	13086	0	100
P5	2,1	16623	-20	100
P6	2,1	16623	-8	100
P7	2,1	16623	-4	100
P8	2,1	16623	0	100
P9	2,1	12025	-20	100
P10	2,1	12025	-12	100
P11	2,1	12025	-8	100
P12	2,1	12025	-4	100
P13	2,1	12025	0	100
P14	2,1	17684	-20	100
P15	2,1	17684	-12	100
P16	2,1	17684	-8	100
P17	2,1	17684	-4	100
P18	2,1	17684	0	100

Table 12: Test 4

Part 3: Production procedure of Test 5

Test 5 involved the production of 7 more components. The aim of the test is to compare the weld bead microstructure producing 3 sample with the material used in the previous tests (NB1,NB2,NBW) and 3 more sample with the same material but in different chemical composition (G1,G2,GW).
All the pieces are tested under the main parameter configuration. Two sample, GW and NBW, are produced in the worst parameter condition. The worst case is the one examined during the previous tests showing the highest number of defects.

Test 5

	Speed/rad/s	Power/ W/mm^2	Focus/mm	Suction/ %
G1	2,1	15031	-16	100
G2	2,1	15031	-16	100
GW	2,1	15031	-12	100
NB1	2,1	15031	-16	100
NB2	2,1	15031	-16	100
NBW	2,1	15031	-12	100

Table 13: Test 5

At the end the total number of produced workpieces is 58.

3.4 Metallographic preparation and inspection methods

3.4.1 Eddy current inspection

Eddy currents were first observed by scientist François Arago during the 1824. At that time, he discovered the possibility to magnetize most conductive material. But was ten years later, during the 1855 that eddy current was definitely discovered by the French physicist Léon Foucault. He observed that the force needed to rotate a copper disk when its rim is placed between the poles of a magnet, such as a horseshoe magnet, increases and the disk is heated by the induced eddy currents [37].

Eddy currents, also known as Foucault's currents, are based on the Faraday's law of induction. According to the subscribed law, eddy currents are loops of electrical current induced within conductors by a variable magnetic field in the conductor. Also, circulating currents or eddy current are induced in bulk pieces of metal moving through a magnetic field. They can be considered as analogous to eddy currents in fluids and it explains the associated name. As the plate enters the field, the changing magnetic flux induces an electric magnetic field in the plate, which in turn causes the free electrons in the plate to move, producing the swirling eddy currents.
According to Lenz's law, the produced magnetic field from eddy currents is opposite in direction respect to the induced magnetic field.

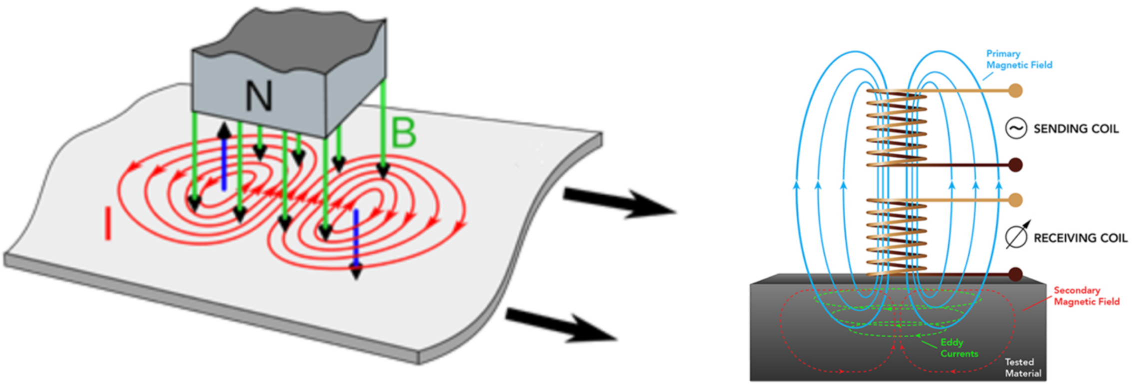

Figure 41: Eddy current phenomenon

Hence, the net effect is a drag. The magnitude of the current in a given loop is proportional to the strength of the magnetic field, the area of the loop and the flux change rate as well, while is inversely proportional to resistivity of the material.

The effect of eddy current can be expressed by the diffusion equation derived from the differential form of Ampère's Law which defines the magnetizing field H surrounding a current density J.

By definition, the magnetic field $\vec{B} = \mu_0(\vec{H} + \vec{M})$, where M is the magnetization of the material and μ_0 is the vacuum permeability. Thus, the diffusion equation is:

$$\nabla^2\vec{H} = \mu_0\sigma\left(\frac{\partial\vec{B}}{\partial t}\right) \quad (10)$$

Eddy current testing

Eddy Current Testing (ECT) is a form of the Electromagnetic Testing (ET) method usually used for the detection of surface or near-surface defects in materials. It is typically used on non-ferromagnetic metals, but it finds application also in inspection of composite materials such as carbon fiber reinforced polymer (CFRP) [38].

Eddy current testing is a non-destructive technique which is widely used in metal industry to check the material quality. The advantage of this technique is the electrical inspection of conductive materials at very high speeds avoids any contact between the test piece and the sensor. Generally non-destructive techniques are chosen in metal industries in order to evaluate possible defects or material properties without causing damage. The most common non-destructive methods are electromagnetic, ultrasonic and liquid penetrant testing. Furthermore, eddy current testing is used for the inspection of conductive materials such as copper, aluminum or steel. It allows detection of cracks in conductive materials, either ferromagnetic or nonferromagnetic [39].

A big advantage of eddy current technique is the possibility to get an instantaneous result instead of other methods such as liquid penetrant or optical inspection which requires more time to have information about a possible presence of defects. In addition, eddy current technique can be used also to distinguish pure materials and alloy compositions to determine the hardness after heat treatments [40].

The principle of eddy current is based on the interaction between a magnetic field source and the material leading to creation of eddy or Foucault's current in the test piece. Once the magnetic field is induced in the workpiece, the process starts with the production of an excitation current by a transmittance amplifier which is driven by a generator. A large magnetoresistance sensors is installed in order to catch from the eddy probe the voltage signal, which is amplified on acceptable values set on the low noise. The receiving coil is connected to voltage meter while the sending coil is connected to a voltage source and a current meter. Then the detected signal is processed to produce an eddy current image of the flow on x and y coordinates. By monitoring the flow, changes in eddy current trend means presence of discontinuities. In particular, the presence of cracks is defined by current drops [41].

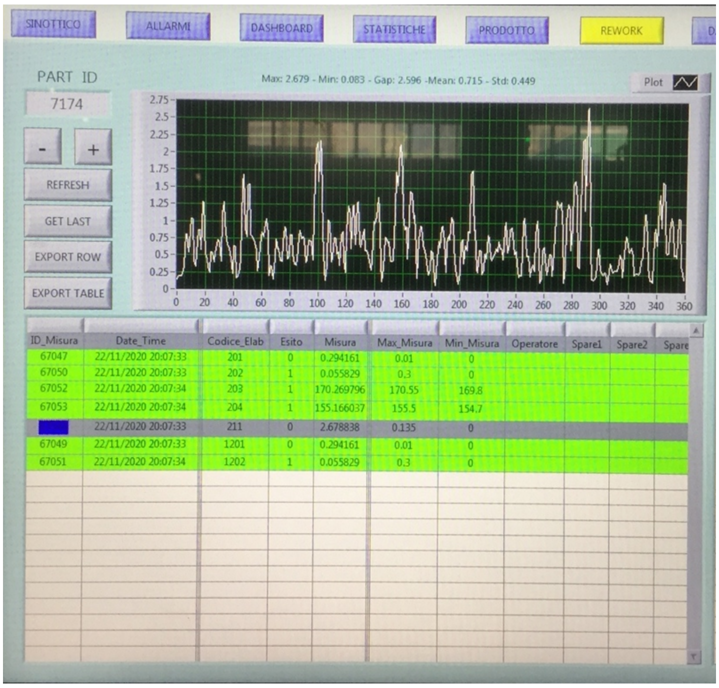

Figure 42: Eddy current machine-user interface

Cracks that cut across the eddy current path are easily detected, although cracks parallel to the current flow can be missed because they do not disturb the eddy currents. Moreover, weld probe with a smaller diameter will produce lower eddy current around the probe, thus reduce the depth subsurface defect inspection ability.

The frequency of the alternating current passing through the eddy current test coil affects the depth of penetration of the eddy current field in the test material. The intensity of the eddy current flow will decrease exponentially with increasing depth into the material. This phenomena are known as skin effect [42].

In the case of study, once all the pieces are welded, the workpieces are subjected to a turning process in order to be inspected by the eddy current NDT. Thanks to the eddy current workstation installed on the process line, a first defect inspection is carried out.

Figure 43: Eddy Current testing

The Elotest-IS belongs to Rohmann GmbH which evaluates the electrical conductivity and the magnetic properties of the material giving information about material structure and defects. It has the maximum amplification equal to 60 dB while the maximum inspection depth is about some tenths from the workpieces surface. Nevertheless, the machine-user interface illustrates what the probe intercepts by showing a location-current graph on it.

3.4.2 Metallographic preparation and inspection

After eddy current testing, metallographic inspection is essential in order to observe the weld bead geometry and the material characteristics. The procedure describing the metallographic preparation process is explain as follows.

All the pieces are cut by using the Abrasive cutting machine Bitech Europe 300 available at LBN laboratory.

Figure 44: Abrasive Cutting Machine Bitech Europe 300

Each workpiece is cut in two sections, one at 180° with respect to the on-off point and one at 270 °. The following figures describe the sequence process in order to produce the small thin sections. The inspection of two sections instead of a single one of each component intensifies the observation and make the analysis more reliable.
Then, all the sections need to be enbedded by using the embedding machine Hitech Europe EP series available at LBN laboratory.

Figure 45: Embedding machine Hitech Europe EP

The sections are incorporeted in Epoglass epoxy thermosetting resin with glass fibers, then by activated the reported machine they are hot compressed producing the final sample test after some minutes.

Figure 46: Sample test

In order to guarantee a clear inspection during the metallographic inspection, the sample surface has to be polished and cleaned. The polisher machine Hitech Europe AP series is used.

Figure 47: Polisher machine Hitech Europe AP

Each sample surface is polished by using abrasive papers in the described sequence. The polishing process starts with the 80 grit paper, moving to the 240 grit paper , then 320, 800 and in conclusion the 1200 grit paper. The polishing time required is set at 9 minutes for the 80 grit abrasive sheet, while it decreases to 7 minutes during the process with the left abrasive papers. After that, the surface is cleaned by using compressed air and ready for the next step. The achivement of a deep polishing implies also the use of diamond liquids. The diamond liquids work on soft paper and the procedure starts using the 6 micron diamond liquid , after that the soft paper needs to be changed in order to procede with the 3 micron diamond liquid and concluding with the 1 micron diamond liquid. The working time for each step is set at 7 minutes. At this point the last step is reaching a clear vision of the weld bead. The weld bead shows up thanks to the application of Nitric Acid on the sample surface and leaving it to act for few seconds. A too long application could attack the metal surface compromising a clean weld bead view.

Then, the sample is ready to be inspected. For each sample, meaning for both section, the inspection aims to research specific geometric measurements by using a metallographic microscope Laborlux 12 ME Leitz, which belong to LBN laboratory. At the same time defect inspection is conducted.

Figure 48: Optical microscope

The weld bead geometry parameters detected are: penetration depth (Sn), penetration depth from the joining point (Si), weld bead length at the interface (Bhaz) and the weld bead length at the joining point (bi). The examination is conducted with an objective lens magnification of abount 5X/ 0,09 and an ocular lens magnification of 10X/18 M.

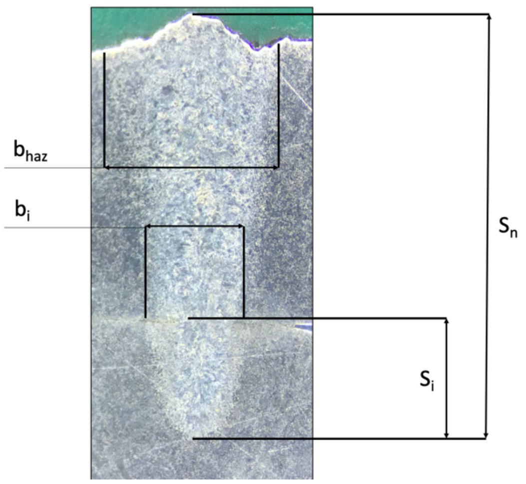

S_n	penetration depth
S_i	penetration depth from the joining point
b_{haz}	weld bead length at the interface
b_i	weld bead length at the joining point

Figure 49: Geometric weld bead measurements detected

In addition, defects can be investigated. During the defect inspection only defects with a dimention higher than 40 micron are taken into account and the metallographic analysis looks for longitudinal and transversal cracks, and pores. The microscope catches defects through an objective lens magnification of about 20 X/0,40. All the measurements are transcribed associating also the relative defect position, reporting as Top the area over the weld joining point, Bottom as the area under the weld joinining point and Middle as the area within 1,50 micron under and over the joining point. For each section all the data are reported, counting the total number of defects as well as the total number of the specific defect type. In addition, the weld bead shape is distinct in overlap, normal or overcutting.

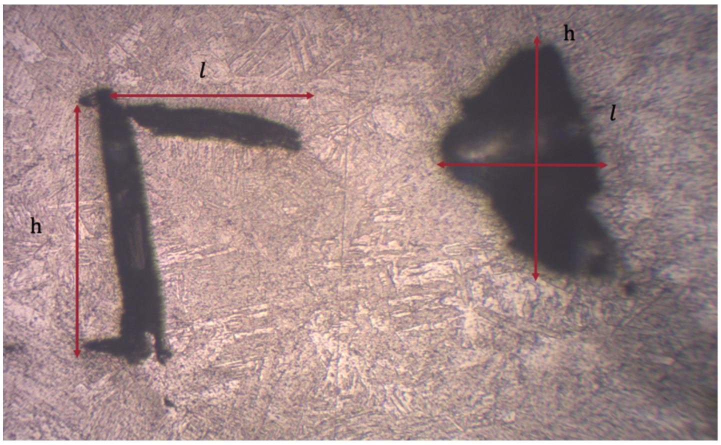

Figure 50: Geometric defect dimensions detected

To sum up all the informations , a final sheet is filled reporting the geometric measurements as the avarage of the two section geometric measuraments of each component while as defect dimention the largest dimention of each defect type for each component.

Besides, the stereo microscope is used to show a magnification on each weld bead in order to have an overview in terms of weld bead differences.

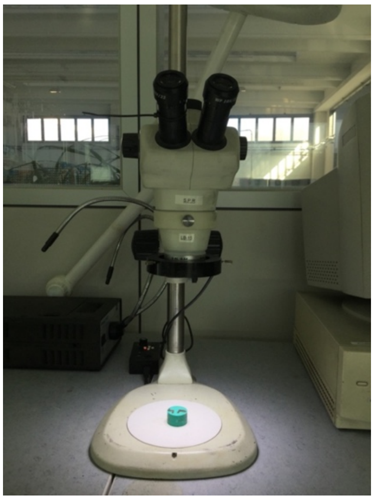

Figure 51: Stereomicroscope

The study is intensified by observations at the profilometer microscope Zygo NewView 9000 available at Politecnico di Torino. The optical surface profiler provides powerful measurements in terms of surface roughness in welded, no welded and transition zone. Moreover, the profiler is able to give information about defect depth trough 2D and 3D images.

Figure 52: Optical surface profiler

CHAPTER 4

Results and discussion

4.1 Power density

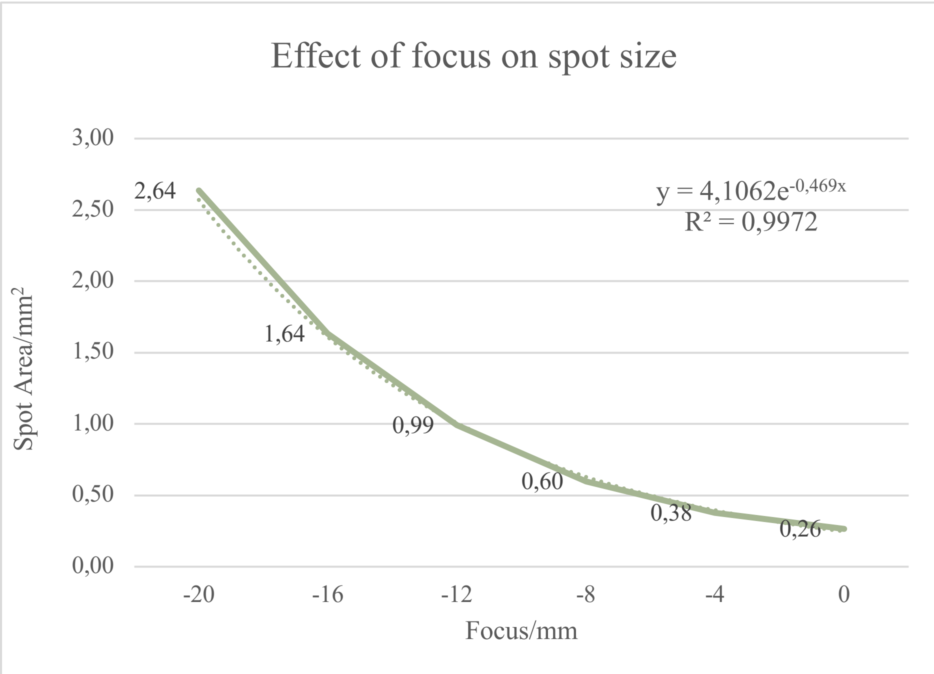

Plot 1: Effect of focus on spot size

The graph shows the effect of focus on the Spot Area. Starting from the radius spot value at focus equal to 0 referred to IPG YLS 5000, it is possible to extrapolate the relative data for all the others focus tested during the experiments. The equation describes numerically the SpotArea-Focus trend. Results show how by increasing the focus and so as much as the focus moves away from the workpiece surface, the projected spot size decreases. The overall effect is notable on the power density.

The power is strongly related to Power density as well as the power density is related to focus, considering that Power density is inversely proportional to the Spot Area. At the same time the Spot Area depends on focus as the graph illustrates.

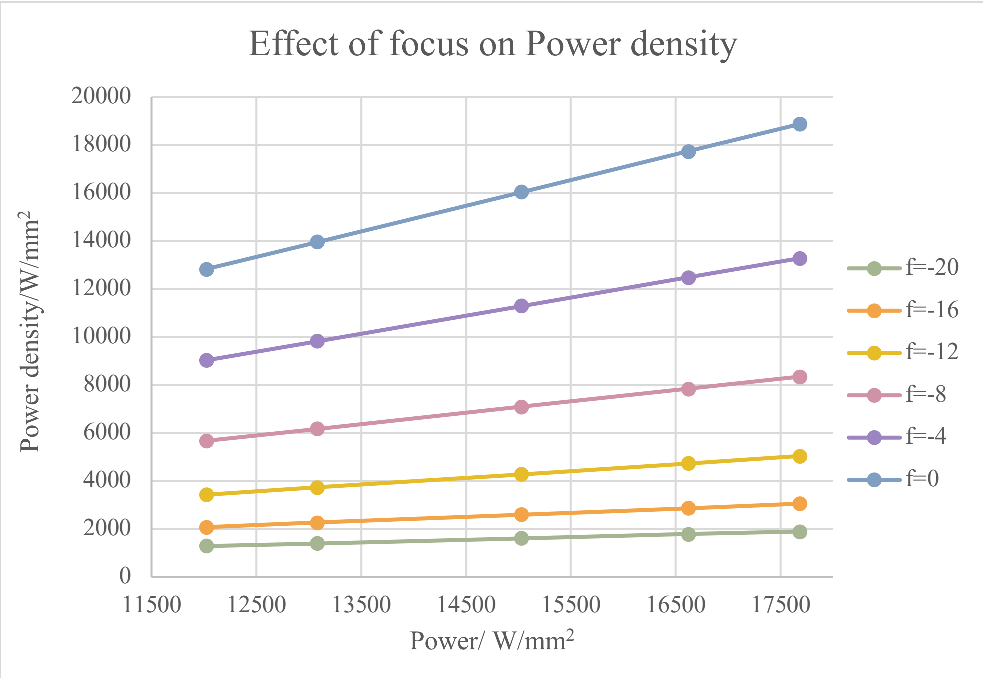

Plot 2: Effect of focus on Power density

As expected by increasing the power, the power density rises as well while the spot area decreases, and the focus increases at the same time. The graph could be explained considering that at parity of power, moving the focus away from the surface, the laser beam converges on the surface increasing the incidence of power density. Thus, by varying the focus, the irradiance changes and for higher power values higher power density values are obtained.

It is possible to observe the effect of power and focus on the weld bead by looking at posters in paragraph 4.3 stating the numerical data.

4.2 DOE and GLM

Results are only related to the analysis conducted on the depth of penetration (S_n), being the only parameter influenced by the working conditions. No significance of process parameters is found on all the others involved outputs.

4.2.1 DOE

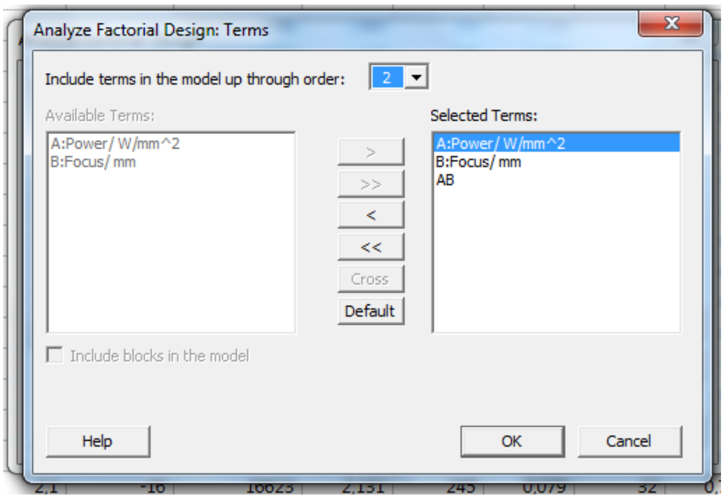

Figure 53: Analyze factorial design: terms

General full factorial selected as DOE and implemented on Minitab includes power and focus as terms and its own interaction. The analysis is conducted with a confidence level of about 95 %.

General Factorial Regression: SN/mm versus Power/ W/mm^2; Focus/ mm

Factor Information

Factor	Levels	Values
Power/ W/mm^2	3	13086; 15031; 16623
Focus/ mm	2	-16; -12

Analysis of Variance

Source	DF	Adj SS	Adj MS	F-Value	P-Value
Model	5	3,67216	0,73443	10,77	0,000
Linear	3	3,61483	1,20494	17,67	0,000
Power/ W/mm^2	2	2,98089	1,49044	21,86	0,000
Focus/ mm	1	0,63394	0,63394	9,30	0,010
2-Way Interactions	2	0,05733	0,02866	0,42	0,666
Power/ W/mm^2*Focus/ mm	2	0,05733	0,02866	0,42	0,666
Error	12	0,81823	0,06819		
Total	17	4,49039			

Model Summary

S	R-sq	R-sq(adj)	R-sq(pred)
0,261124	81,78%	74,19%	59,00%

Figure 54: DOE numerical results

The statistical analysis is reliable with an R-sq(adj) of about 74,19 %. In particular looking at P-value, the model could be considered as linear and the influence of power and focus is relevant being the p-value lower than 5 %.

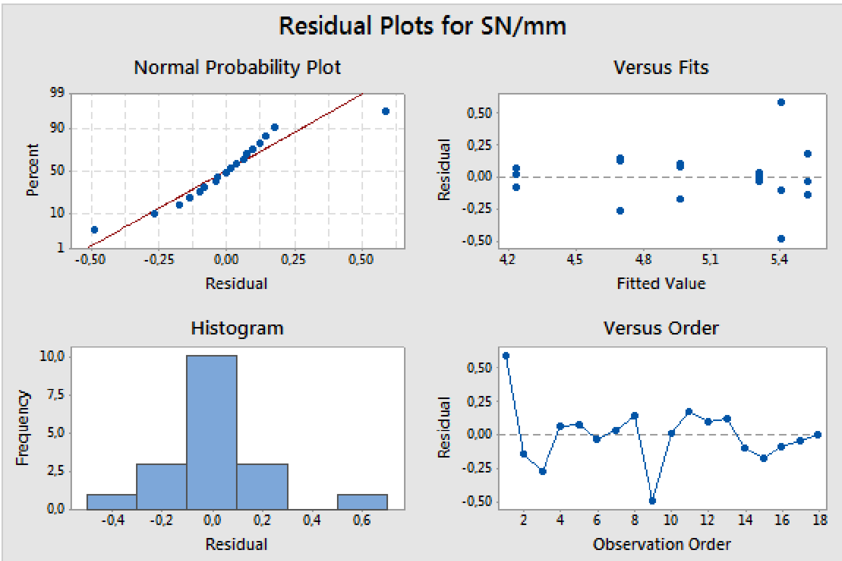

Plot 3: DOE Residual plot for Sn

Residual plots show a histogram almost following the gaussian trend while the Versus Order plot illustrates a non-homogeneous trend of residuals as well as the Versus Fits plot shows hot residuals are not equally distributed. Below is shown the normal probability plot.

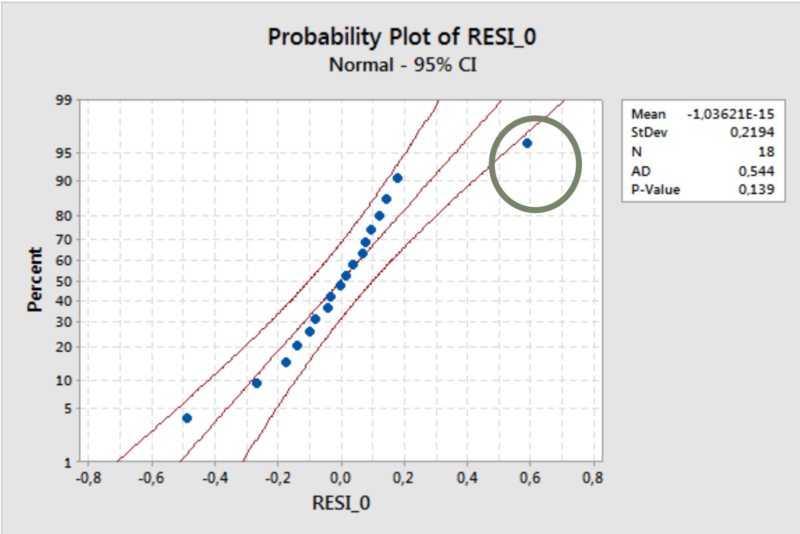

Plot 4: DOE probability plot for Residual and outlier detection

The normal probability plot is a graphical technique for assessing whether or not a data set is approximately normally distributed. As the graph illustrates an outlier is identified being out from the range. The p-value is higher than 5 % concluding on the impossibility to detect systematic deviation from normal distribution with a risk of error of 5 %.

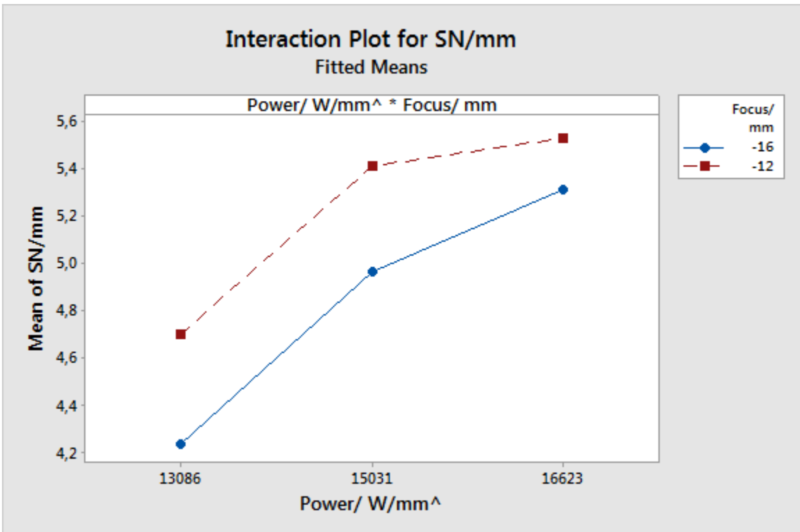

Plot 5: DOE Interaction plot for Sn

It’s interesting to look at the interaction plot and noticing no interaction between focus and power, according to numerical data.

Outlier identification

The outlier refers to row 1 on Minitab reporting an Sn measurement much higher than the others depth of penetration. The outlier management implies the value substitution with the arithmetic average of the others two repeated measurements.

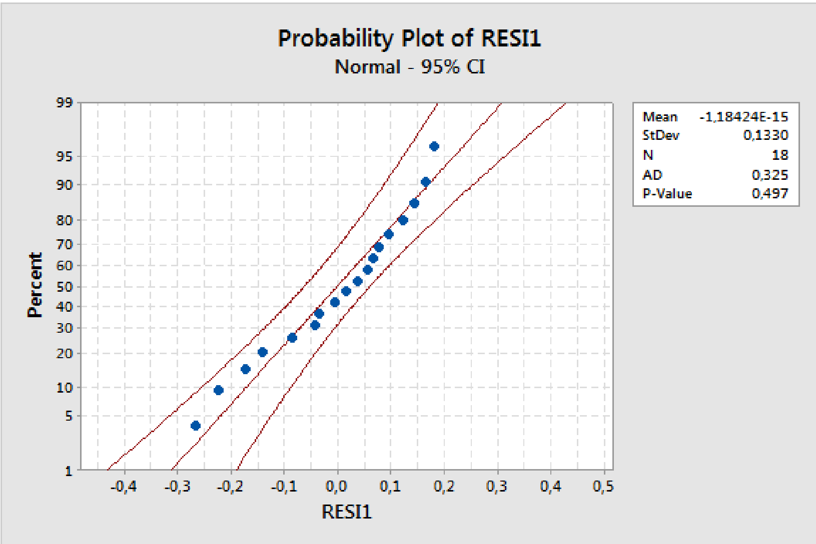

Plot 6: DOE/1 Probability plot for Residuals

By managing the outlier, the result shows how the normal probability plot follows the normal distribution with a p-value higher than 5%. The outlier management allows the residuals to be within the extreme range limits.

General Factorial Regression: SN/mm versus Power/ W/mm^2; Focus/ mm

Factor Information

Factor	Levels	Values
Power/ W/mm^2	3	13086; 15031; 16623
Focus/ mm	2	-16; -12

Analysis of Variance

Source	DF	Adj SS	Adj MS	F-Value	P-Value
Model	5	3,23287	0,64657	25,79	0,000
Linear	3	3,16149	1,05383	42,03	0,000
Power/ W/mm^2	2	2,79227	1,39613	55,68	0,000
Focus/ mm	1	0,36923	0,36923	14,73	0,002
2-Way Interactions	2	0,07137	0,03569	1,42	0,279
Power/ W/mm^2*Focus/ mm	2	0,07137	0,03569	1,42	0,279
Error	12	0,30090	0,02507		
Total	17	3,53376			

Model Summary

S	R-sq	R-sq(adj)	R-sq(pred)
0,158350	91,49%	87,94%	80,84%

Figure 55: DOE/1 numerical results

Different numerical results show the same conclusion. The significance of power and focus is valid with an R-sq(adj) of about 87,94 %. Instead of that, the following graph shows no interaction between the two input factors.

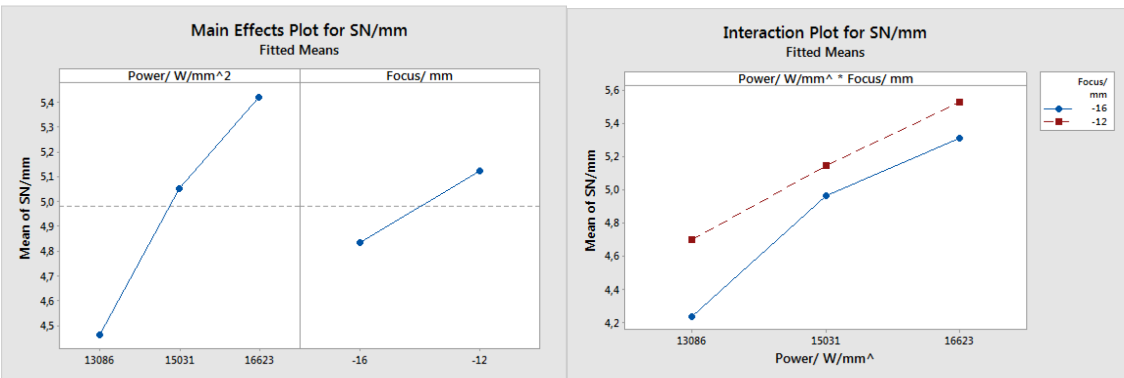

Plot 7: DOE/1 Main effect plot and interaction plot for Sn

The main effect plot explains the most influent parameter. The higher distance from the horizontal line, the higher parameter influence. In the specific case power has higher significance in terms of effect than focus.

Interaction plot highlights no interaction between focus and power according to numerical results.

4.2.2 GLM

As explained previously in order to have a statistical analysis on an unbalanced linear plan General Linear Model is applied.

General Linear Model: SN/mm versus Power/ W/mm^2; Focus/ mm; Speed/ rad/s; Suction/ %

The following terms cannot be estimated and were removed:
Power/ W/mm^2*Suction/ %; Focus/ mm*Suction/ %; Speed/ rad/s*Suction/ %

Analysis of Variance

Source	DF	Adj SS	Adj MS	F-Value	P-Value
Power/ W/mm^2	1	0.4136	0.41364	17.93	0.000
Focus/ mm	1	0.9006	0.90061	39.05	0.000
Speed/ rad/s	1	0.6073	0.60727	26.33	0.000
Suction/ %	1	0.0345	0.03447	1.49	0.228
Power/ W/mm^2*Power/ W/mm^2	1	0.0160	0.01598	0.69	0.410
Focus/ mm*Focus/ mm	1	1.7462	1.74623	75.71	0.000
Speed/ rad/s*Speed/ rad/s	1	0.1012	0.10119	4.39	0.042
Power/ W/mm^2*Focus/ mm	1	0.8683	0.86828	37.64	0.000
Power/ W/mm^2*Speed/ rad/s	1	0.4162	0.41617	18.04	0.000
Focus/ mm*Speed/ rad/s	1	0.8971	0.89715	38.90	0.000
Error	41	0.9457	0.02307		
Lack-of-Fit	28	0.6439	0.02300	0.99	0.531
Pure Error	13	0.3017	0.02321		
Total	51	24.4999			

Model Summary

S	R-sq	R-sq(adj)	R-sq(pred)
0.151872	96.14%	95.20%	*

Figure 56:GLM numerical results

Numerical results give information about factors significance with an R-sq(adj) of about 95 %, which is a good result being the percentage high enough to consider the model as correct.

Looking at the P-value and working at a confidence index of 95 %, the most significant parameters are : Power, Focus , Speed and the interaction between power and focus, power and speed, focus and speed. Moreover, quadratic effect is relevant as well for power, speed and focus.

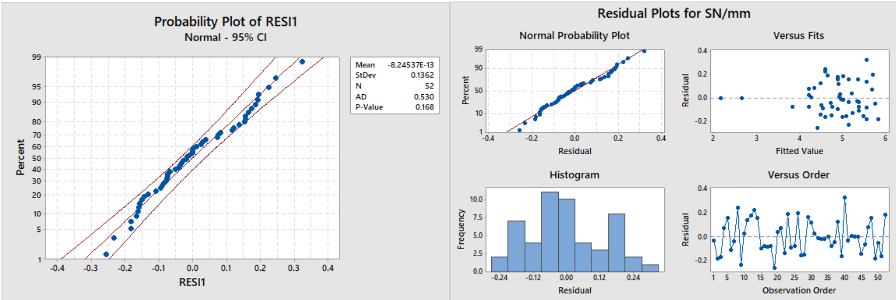

Plot 8: GLM probability plot of residual and residual plot for Sn

The graph shows a normal probability plot with residuals widely aligned along the normal distribution. While the Versus Order graph illustrates an apparent homogenous distribution of residuals, the Versus Fits graph emphasizes the presence of two values detached from the group.

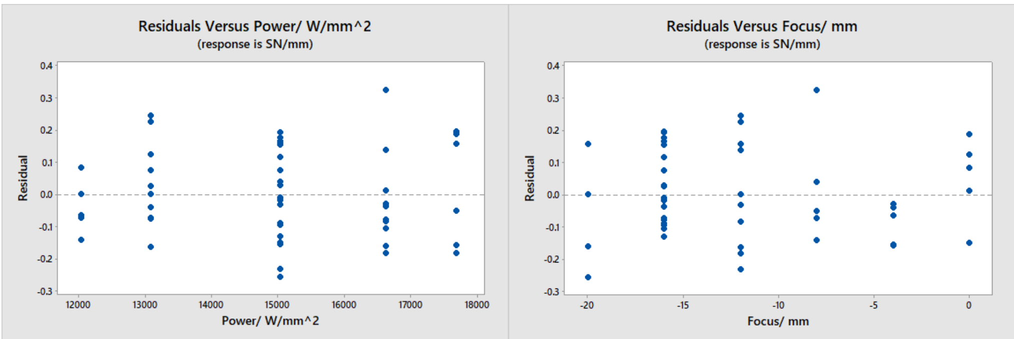

Plot 9: Residuals versus Power and Focus

Focusing on Residuals and looking at their distribution respect to power and focus, the graphs show groups quite concentrated and a homogenous distribution about the zero line.

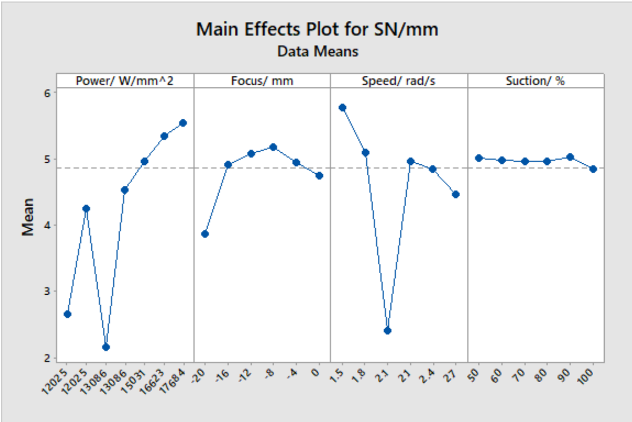

Plot 10: Main Effects plot for Sn

Main effect plots highlight the no significance of suction according to numerical results and an approximate quadratic trend of focus. Speed and Power are enough significant having points enough distant from the horizontal line, but at the same time two terms disturb their linearity.

GLM - Stepwise

In order to elaborate on the results, the analysis is thickened by means of stepwise. In statistics, stepwise regression is a method of fitting regression models in which the choice of predictive variables is carried out by an automatic procedure. In this way, what is not significant is automatically excluded and the maximum risk of error is set to be less than 15 %.

General Linear Model: SN/mm versus Power/ W/mm^2; Focus/ mm; Speed/ rad/s; Suction/ %

Stepwise Selection of Terms

α to enter = 0.15; α to remove = 0.15

Analysis of Variance

Source	DF	Adj SS	Adj MS	F-Value	P-Value
Power/ W/mm^2	1	0.2352	0.23519	3.74	0.059
Power/ W/mm^2*Power/ W/mm^2	1	0.1795	0.17954	2.85	0.098
Focus/ mm*Focus/ mm	1	4.9321	4.93206	78.38	0.000
Power/ W/mm^2*Focus/ mm	1	4.8695	4.86954	77.39	0.000
Focus/ mm*Speed/ rad/s	1	1.2143	1.21428	19.30	0.000
Error	46	2.8944	0.06292		
Lack-of-Fit	33	2.5927	0.07857	3.39	0.011
Pure Error	13	0.3017	0.02321		
Total	51	24.4999			

Model Summary

S	R-sq	R-sq(adj)	R-sq(pred)
0.250843	88.19%	86.90%	82.86%

Figure 57: GLM - stepwise numerical results

Numerical results give a P-value less than 15 % for the interaction between power and focus, focus and speed. A relevant influence is significant for power squared and focus squared. Power squared has a p-value higher than 5 %, but it could be significant because lower than 15 %. The model is correct with a R-sq(adj) of about 86,90%.

Plot 11: GLM - stepwise Residual plot for Sn and probability plot for Sn

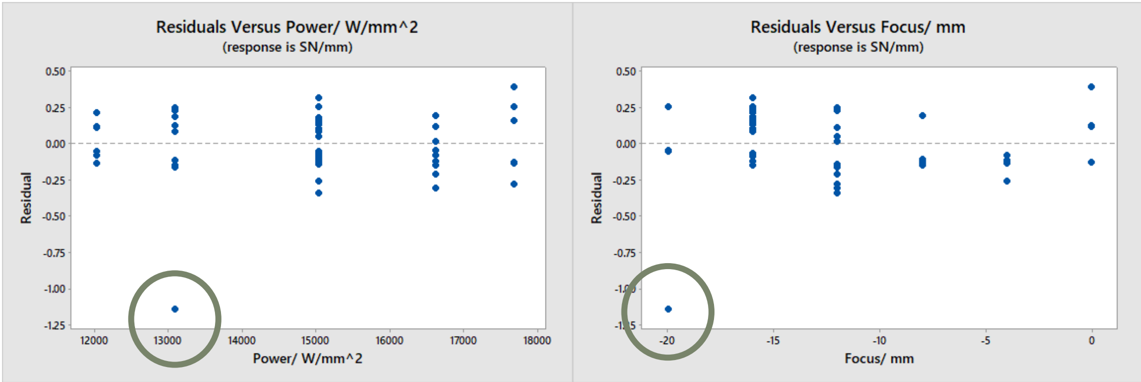

Plot 12: GLM - stepwise Residuals Versus Power and Focus

Plots immediately highlights the presence of an outlier. The outlier is identified being totally distant from the distribution group in all the graphs. In particular, the normal probability plot shows the outlier to be out from the limit range making the plot not normally distributed. The substantial effect is reflected in all the graphs. Examining the histogram plot it looks unimodal with a clear distance of the point in question.

Outlier management

The detected outlier belongs to one of the two not welded workpieces. Probably the model has not enough input values to be able to predict that point, thus the results come with a high estimation error taking to identify the residual as outlier. In particular, it regards to row 35 where being not a repeated measure the only way to manage the outlier is to eliminate the row and proceed with the analysis.

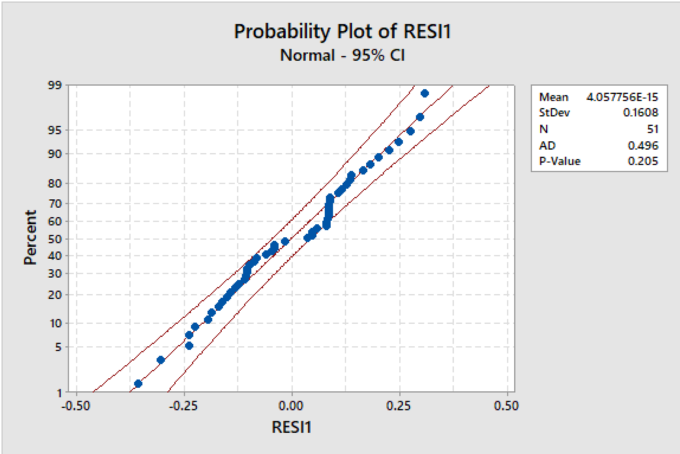

Plot 13: GLM- stepwise probability plot of residuals

By eliminating the outlier, the residual probability plot shows how the residuals follow the normal distribution within the range limits with a P-Value higher than 5 %.

General Linear Model: SN/mm versus Power/ W/mm^2; Focus/ mm; Speed/ rad/s; Suction/ %

```
Stepwise Selection of Terms

α to enter = 0.15; α to remove = 0.15


Analysis of Variance

Source                          DF   Adj SS    Adj MS  F-Value  P-Value
  Power/ W/mm^2                  1   0.2289   0.22891     7.96    0.007
  Power/ W/mm^2*Power/ W/mm^2    1   0.1692   0.16921     5.89    0.019
  Focus/ mm*Focus/ mm            1   2.7697   2.76974    96.37    0.000
  Power/ W/mm^2*Focus/ mm        1   3.5633   3.56328   123.98    0.000
  Focus/ mm*Speed/ rad/s         1   1.1135   1.11346    38.74    0.000
Error                           45   1.2933   0.02874
  Lack-of-Fit                   32   0.9916   0.03099     1.34    0.296
  Pure Error                    13   0.3017   0.02321
Total                           50  17.0322


Model Summary

       S    R-sq  R-sq(adj)  R-sq(pred)
0.169531  92.41%     91.56%      88.56%
```

Figure 58: GLM/1 numerical results

Test is run one more time without the presence of the outlier’s row.
Numerical results come with a determination coefficient of about 91,56 %. The model has higher predictive power than the previous analysis showing the significance of Power, focus squared, Interaction between Power and focus and the interaction between focus and speed.

The regression equation for the final mathematical model is defined as follows:

$$\text{Sn} = -1{,}01 + 0{,}000679\ \text{Power}\ - 0{,}006976\ * \text{Focus\^{}2}\ - 0{,}000016\ \text{Power} * \text{Focus} + 0{,}05784\ \text{Focus} * \text{Speed} \tag{11}$$

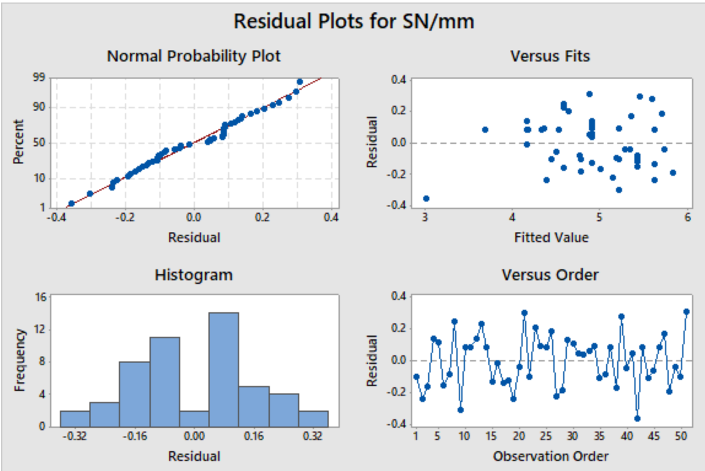

Plot 14: GLM/1 Residual plot for Sn

The histogram looks fairly symmetric and unimodal except for the central point, which may not follow the normal distribution because it's a single measure. Versus Order illustrates centered points and homogeneously distributed. A deeper study can be carried out by observing the trend of the residuals.

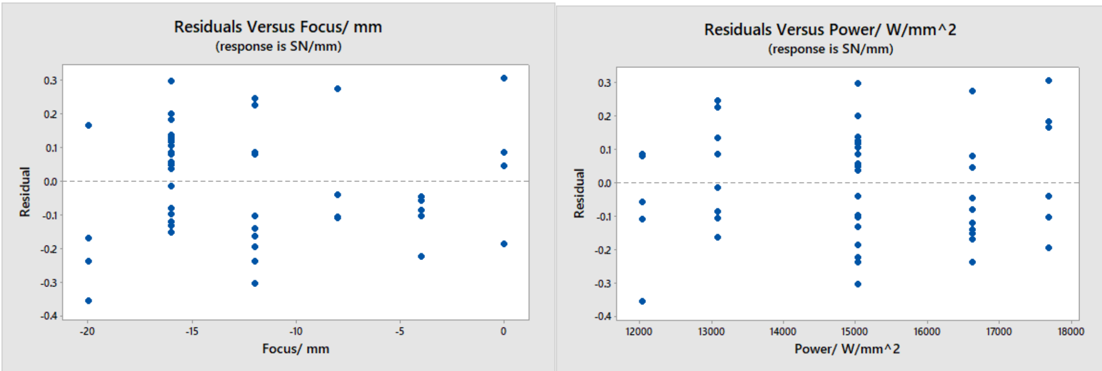

Plot 15: GLM/1 Residual Versus Focus and Power

The both graphs show residuals well distributed and the groups are concentrated and centered respect to the zero line.
Residuals Versus Focus shows lack of information in some points making some groups less dense than others. Overall, the distribution is homogeneous, and the points are centered. These results make the mathematical model correct enough to valid the process parameters significance.

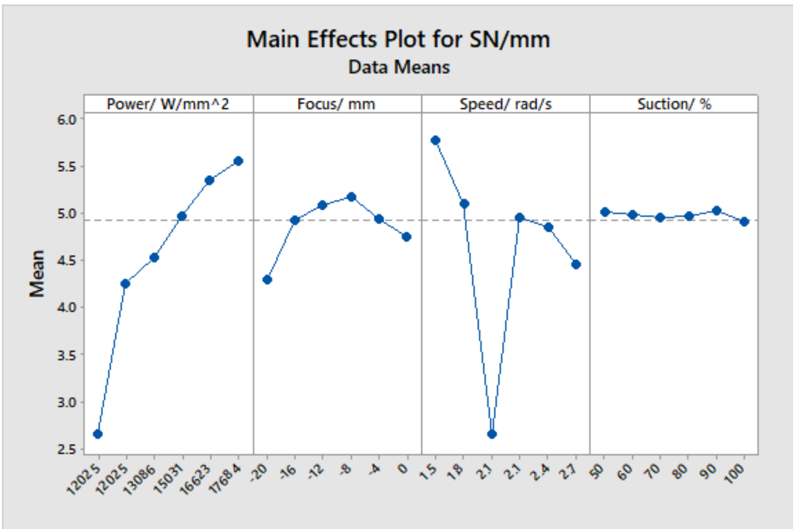

Plot 16: GLM/1 Main effects plot

In particular, the Main Effect Plot gives information about the influence of each process parameter. The effect of power is strongly influencing having points very distant from the horizontal line, as numerical results describe. Moreover, the power trend is linear according with the mathematical model.
The effect of Suction is null having a trend almost following the horizontal line.
Focus effect is almost quadratic, according also with numerical results where the focus quadratic effect is significant with a risk of error lower than 5 %. Nevertheless, focus is not influential as much as power.
If we would not consider the point that totally detaches from the speed trend, the trend could be seen as linear. Probably the most distant point regards to a SN measure very low which moves the relative group average to the bottom.

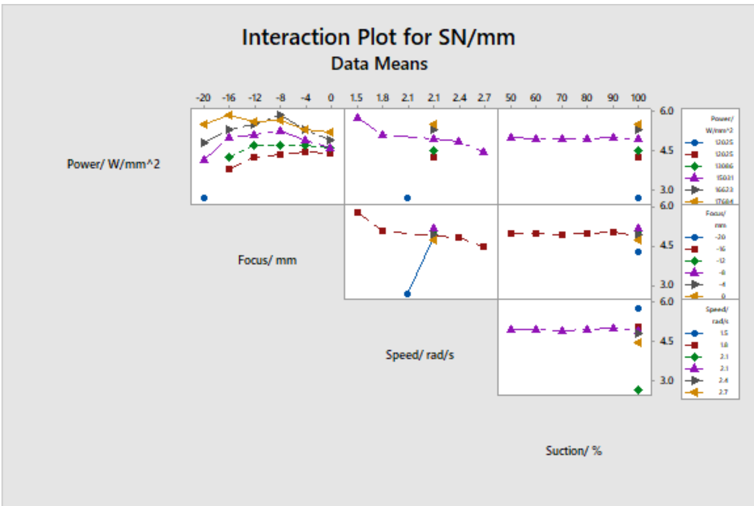

Plot 17: GLM/1 Interaction plot for Sn

The interaction plot makes on evidence, according to numerical results, the interaction effect of power and focus, where the relative lines cross each other showing an interaction. The same interaction could be observed between Focus and Speed.

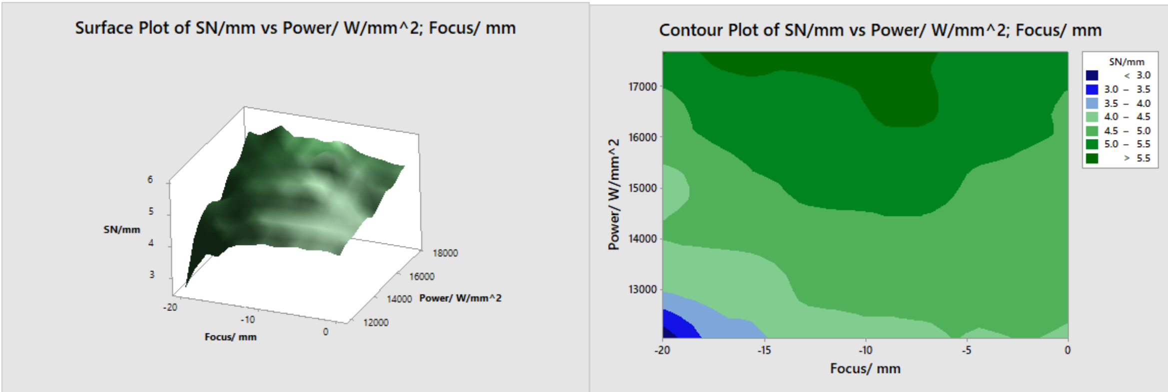

Plot 18: GLM/1 Surface and contour plot

Surface and Contour plot illustrates the general effect of power and focus on SN. There is no doubt that by increasing power, SN reaches higher values. On the other hand, by rising Focus, the depth of penetration increases until a certain value, than it decreases. Contour plot perfectly agrees with the Interaction plot, showing the quadratic effect of focus.

Prediction for SN

In order to verify the correct estimation of the removed outlier is possible to implement a prediction function for the outlier value on Minitab. The result comes out with a prediction interval of about 95% level of confidence.
The outcome indicates that the minimum interval value is higher than the experimental value (about 2,16), thus the model is not enough strong to predict the experienced value. This explain why it is considered as an outlier.

Prediction for SN/mm

```
Regression Equation

SN/mm = 0.000543 Power/ W/mm^2 - 0.007025 Focus/ mm*Focus/ mm - 0.000000 Power/ W/mm^2*Power/
       W/mm^2 + 0.05814 Speed/ rad/s*Focus/ mm - 0.000016 Focus/ mm*Power/ W/mm^2


Variable       Setting
Speed/ rad/s       2.1
Focus/ mm          -20
Power/ W/mm^2    13086


    Fit     SE Fit        95% CI              95% PI
3.56146  0.0799712  (3.40049, 3.72244)  (3.18642, 3.93650)
```

Figure 59: Prediction for Sn

GLM is applied on all outputs extract from metallographic observation, but according to the statistical analysis the significance of the effect of the process parameters can only be considered valid on depth of penetration (Sn).

No significance is found for all the others output and no correlation between process parameters and defects.

Nevertheless, the clarity of statistical analysis, the study is conducted in parallel to metallographic analysis in order to have confirm of statistical conclusions by looking at the study from another point of view.

4.3 Metallography

A visual effect of how the weld bead changes by varying process parameters is summarized in the following figures. In this way, it's possible to easily visually observe the effect of power, focus, speed and suction on the final weld bead.

4.3.1 Visual inspection

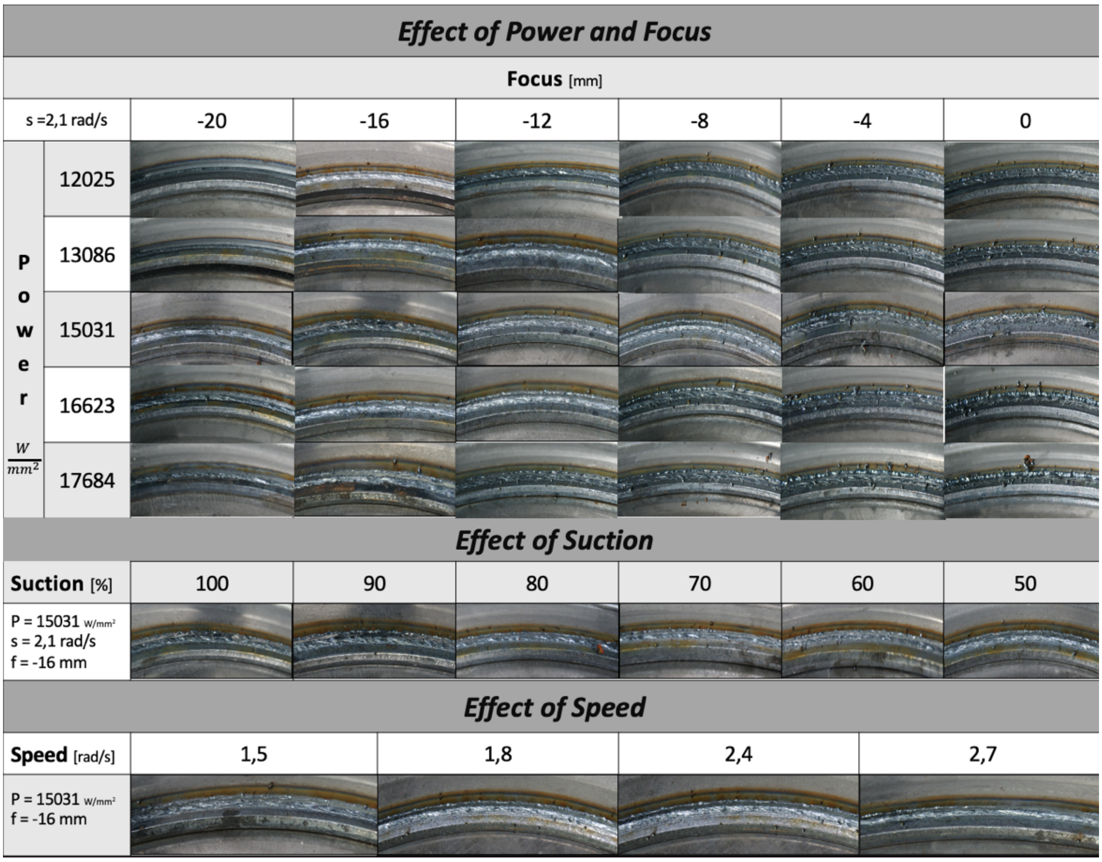

Figure 60: Weld bead visual inspection

The poster includes the weld bead of workpieces produced in Test 1, Test 2, Test 3 and Test 4. The images are taken by using a Nikon Camera. The top section regards the effect of power and focus on the weld bead, keeping speed and suction constant.

At the same power level, by increasing focus the quantity of spatter increases as well. The weld bead surface becomes more polluted with higher amount of material drops. It could be explained by the fact that, as the focus increases the projected spot area on the workpieces decreases, making the laser beam convergent on the surface. By keeping a constant power, the power density increases as well, concentrating the laser beam intensity on a small spot area. A high intensity level melts the material, involving an ejection of melt from the weld pool, disintegrating into droplets on the metal surface.

On the contrary by keeping a constant focus while rising the power level, the weld bead becomes sturdier. It's possible to observe better the phenomena in the following figures.
No great differences on weld bead are cached during this first approach by varying speed and suction.

4.3.2 Stereoscopic overview

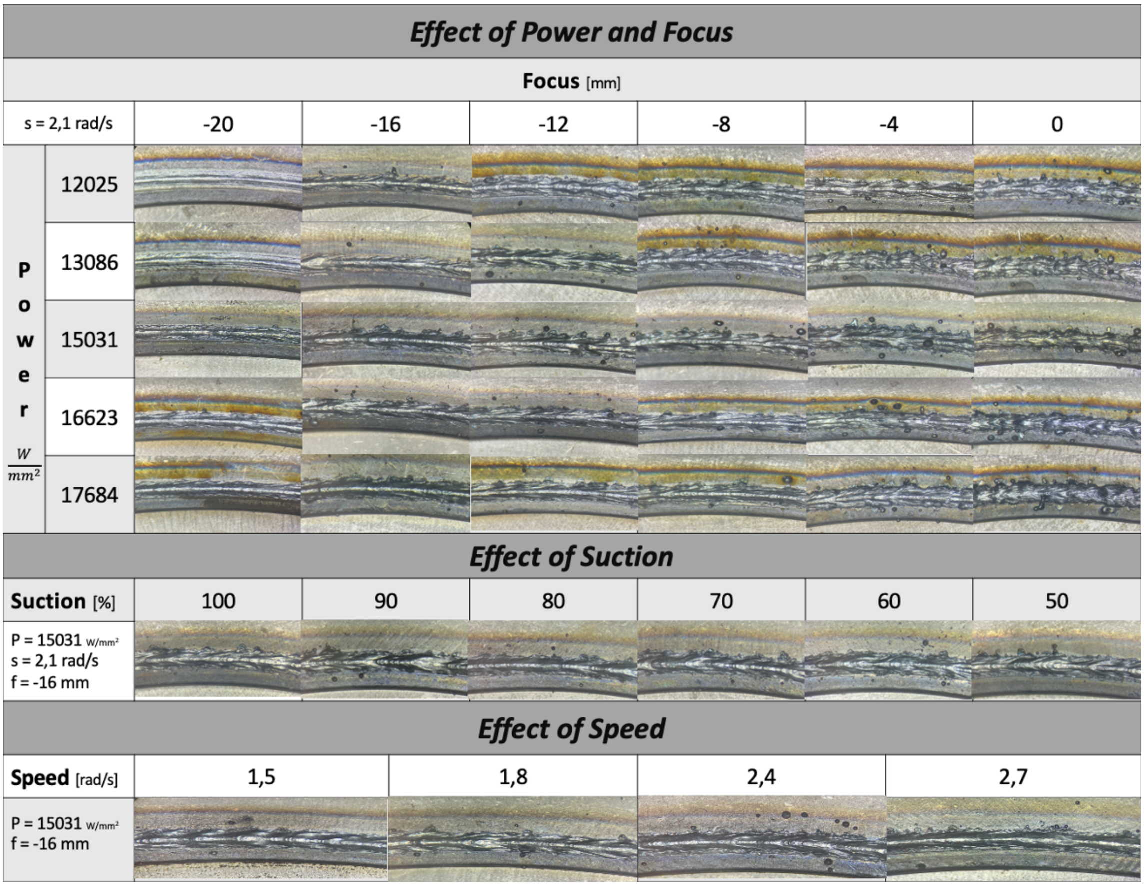

Figure 61: Stereoscopic overview

As mentioned previously, the effect of power is more evident by observing the weld bead frames taken at the stereoscopic microscope. In particular, at low focus and low power, the welding does not occur as shown in the first two images at focus -20. That's due to a too low power density as a result of both power and focus low values. At low focus, although the effect of increased power guarantee welding, it's evident how the weld bead surface is more clean than the one obtained at higher focus level.

At this point, the *Effect of Suction* gives no information about weld bead changes and the *Effect of Speed* as well. The visual results match with the statistical data having not found correlation between effect of suction and speed on depth of penetration.

4.3.3 Metallographical Inspection

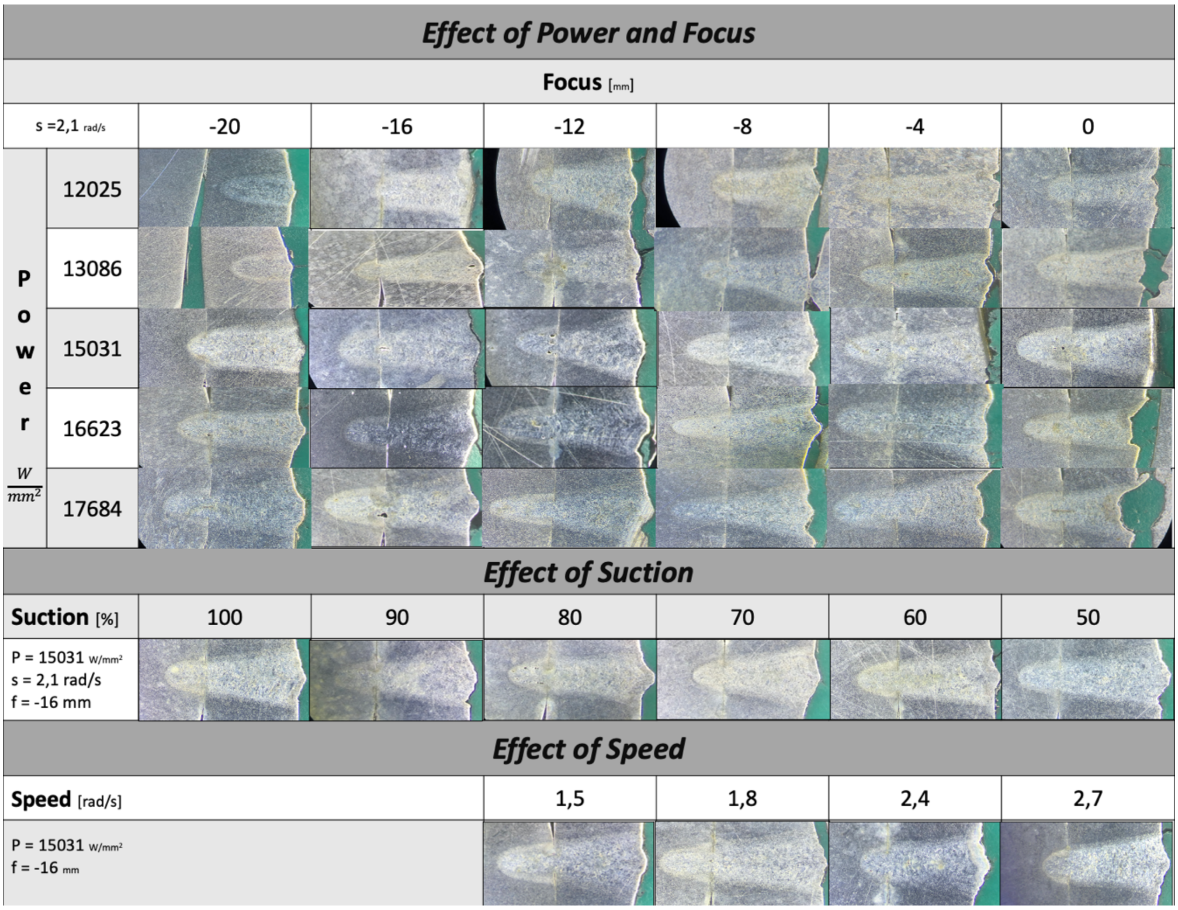

Figure 62: Weld bead metallographic inspection

Moving to an optical microscopic inspection it is possible to go deeper and explore the effect of process parameters on weld bead geometry.
Starting from the first section, the first two images confirm what described previously. At low power and low focus, the amount of power density is not enough to guarantee the welding process. Looking at the weld bead geometry, there is no doubt that as much as the power level increases the depth of penetration increases as well. Moreover, it could be

affirmed that at constant power, by rising up the focus level the depth of penetration increases until a certain point, then it decreases again as shown in the last column. The last would match with statistical results, which lead to think at a quadratic effect of focus. The first row highlights how despite focus changes, the depth of penetration keeps being small at low power. Moreover, it is s noticeable how the process parameters affect the weld bead shape in terms of overlap and undercutting. Most of weld beads show overlap, only at high power and focus level they start showing undercutting. Despite the submitted observation, literature associates the cause to a too high welding speed.
Also, at this point, no *Effect of Suction* is noticed.
Moving to *Effect of Speed*, on the contrary of what observed in the previous posters, at this point there is no doubt that an increment in speed level leave to a decrease in depth of penetration.

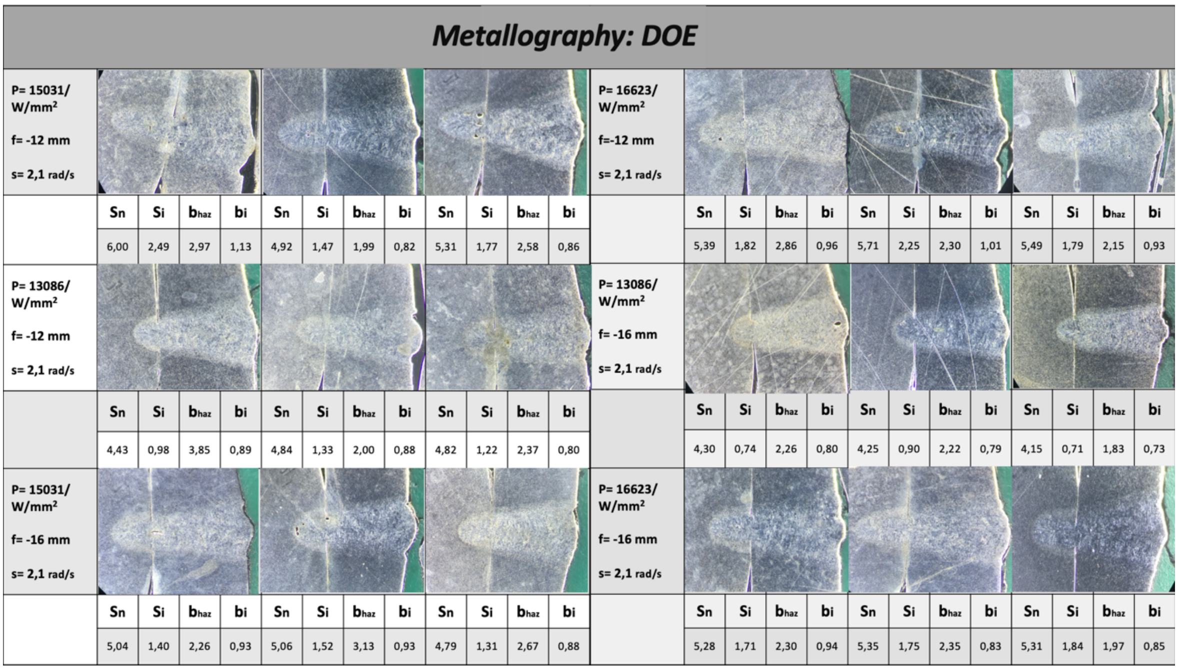

Figure 63: DOE Metallography

The poster make in comparison results coming from the three repetitions performed in DOE. On each repetition the value of all the outputs catched during the optical microscopic inspection are reported. Despite the process parameters do not change, the weld bead geometric mesauraments are never the same, but they vary in each repetition. So even If the working condition does not varies, outputs could be different. Overall, it could be affirmed that no great variations are observed.

4.3.4 Metallography of defects

The type of detected defects during the microscopic inspection are pores and longitudinal and transversal cracks. Most of the observed pores are localized on the weld bead bottom, while a high amount of crack is detected in middle-top area. At each detected defect the relative dimension is reported.
In addition to pores, two type of cracks are observed: residual stresses and solidification cracks. Looking at Figure 64, the first frame on the first row shows solidification crack type while the next frame illustrates crack related to residual stress case. The argument will be discussed in deep in paragraph 4.5.
In general, the presence of defect is verified in most of the conducted tests. It's evident how in Figure 67 - Test 4 the amount of workpieces with no defects detected is higher than all the other tests.

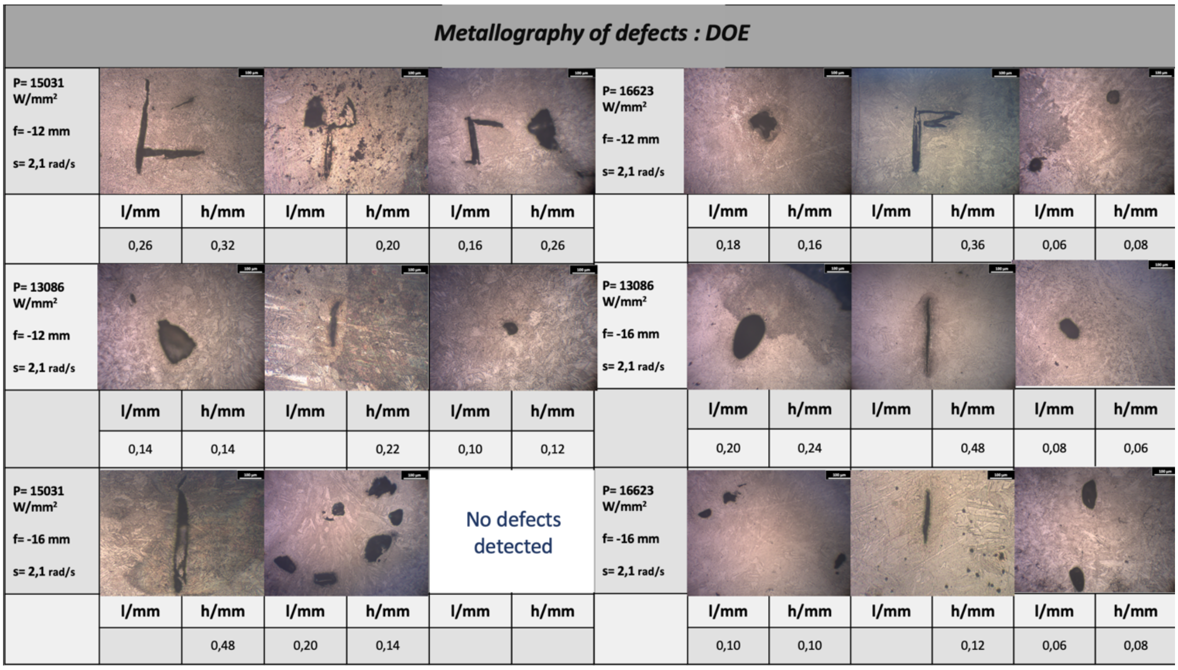

Figure 64: Metallography of defects DOE

Metallography of defects* : *Test 2										
Power/W/mm^2	15031		15031		15031		15031		15031	
Focus/mm	-20		-8		-16		-16		-16	
Speed/ rad/s	2,1		2,1		1,5		1,8		2,4	
	No defects detected		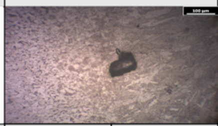		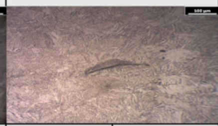					
	l	**h**	**l**	**h**	**l**	**h**	**l**	**h**	**l**	**h**
			0,06	0,08	0,1		0,01	0,08	0,1	0,14
Power/W/mm^2	15031		12025		17684		15031		15031	
Focus/mm	-16		-16		-16		-4		0	
Speed /rad/s	1841		2,1		2,1		2,1		2,1	
	No defects detected		No defects detected		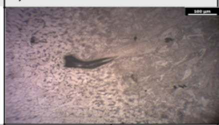		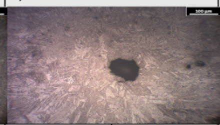			
	l	**h**	**l**	**h**	**l**	**h**	**l**	**h**	**l**	**h**
					0,2		0,16	0,14	0,16	0,18

Figure 65: Metallography of defects Test 2

Metallography of defects* : *Test 3						
	P = 15031 W/mm^2		s = 2,1 rad/s		f = -16 mm	
Suction (%)	**100 %**		**90 %**		**80 %**	
	No defects detected		No defects detected		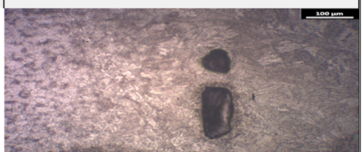	
	l	**h**	**l**	**h**	**l**	**h**
					0,1	0,12
Suction (%)	**70%**		**60%**		**50 %**	
	No defects detected		No defects detected		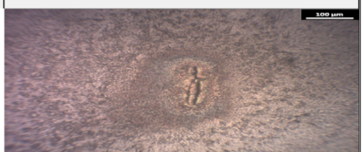	
	l	**h**	**l**	**h**	**l**	**h**
						0,2

Figure 66: Metallography of defects Test 3

Metallography of defects: Test 4												
Power	13086 W/mm²		13086W/mm²		13086/W/mm²		13086/W/mm²		16623/W/mm²		16623/W/mm²	
Focus [mm]	-20		-8		-4		0		-20		-8	
	No defects detected		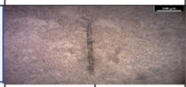		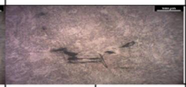		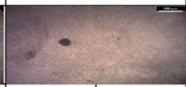		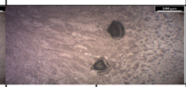			
	l	h	l	h	l	h	l	h	l	h	l	h
				0,2	0,2	0,2	0,10	0,08	0,4	0,08	0,10	0,08
Power	16623/W/mm²		16623/W/mm²		12025/W/mm²		12025/W/mm²		12025/W/mm²		12025/W/mm²	
Focus [mm]	-4		0		-20		-12		-8		-4	
	No defects detected				No defects detected		No defects detected		No defects detected		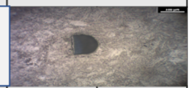	
	l	h	l	h	l	h	l	h	l	h	l	h
				0,4							0,34	0,3
Power	12025/W/mm²		17684/W/mm²		17684/W/mm²		17684/W/mm²		17684/W/mm²		17684/W/mm²	
Focus [mm]	0		-20		-12		-8		-4		0	
	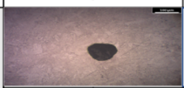		No defects detected		No defects detected		No defects detected		No defects detected			
	l	h	l	h	l	h	l	h	l	h	l	h
	0,16	0,14										0,5

Figure 67: Metallography of defects Test 4

4.4 Eddy current

Eddy current analysis is carried out in order to have a first visual approach in terms of presence of defects. Unfortunately, the probe was not enough effective to give relevant results and catch the presence of defects observed at the microscope. As mentioned previously, the probe used in the case of study is able to detect defects only few millimeters below the workpiece surface. In addition to this, the unturned workpiece surface creates morphologic irregularities along the circular weld bead which could disturb the signal detected by the probe.
Eddy current plots are reported in the posters below. Each peak demonstrates the presence of a discontinuity detected and its own related localization is reported in degree being a circular weld bead. For each eddy current graph, the maximum and the minimum peak value is reported.

The only result founded is that the peak at about 270° matches with the on-off point. The on-off point is where the starting and final weld bead point meet each other. Most of the graphs show a peak about that degree because the NDT detector catches the presence of a discontinuity at that point, which is reasonable.

Eddy Current parameters such as max, min, Standard Deviation and mean values are tested as output during the GLM analysis, but no correlation is found between process parameters and eddy current variables. Furthermore, no matching record found by correlating the recorded current value from NDT and the defect dimensions extrapolated from the metallographic inspection. Even if looking at the same degree of the cut section on the plot, no correlation was found probably because of the inability of the probe to inspect in deep into the material.

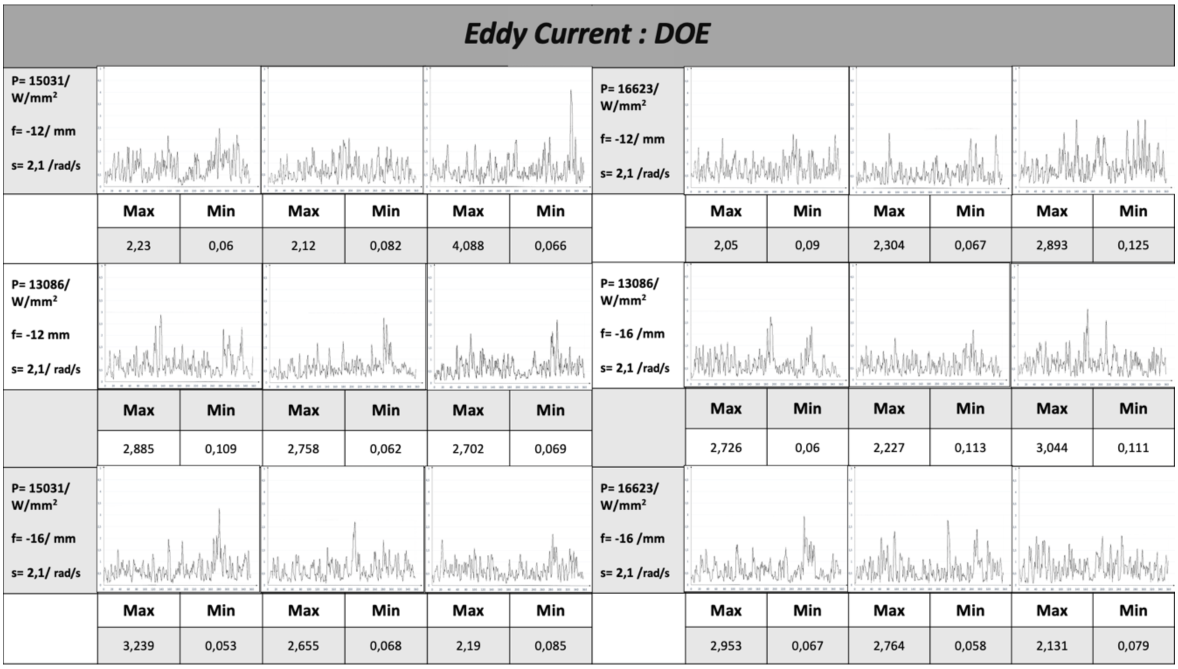

Figure 68:Eddy current DOE

Eddy Current: Test 2										
Power/ W/mm²	15031		15031		15031		15031		15031	
Focus/ mm	-20		-8		-16		-16		-16	
Speed /rad/s	2,1		2,1		1,5		1,8		2,4	
	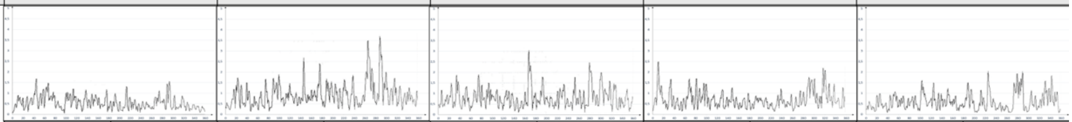									
	Max	Min	Max	Min	Max	Min	Max	Min	Max	Min
	1,69	0,048	3,711	0,096	3,053	0,105	2,531	0,127	2,126	0,08
Power/ W/mm²	15031		12025		17684		15031		15031	
Focus/mm	-16		-16		-16		-4		0	
Speed/rad/s	2,7		2,1		2,1		2,1		2,1	
	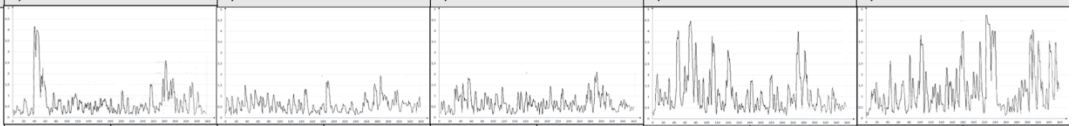									
	Max	Min	Max	Min	Max	Min	Max	Min	Max	Min
	4,148	0,072	1,914	0,079	2,095	0,087	4,512	0,082	4,736	0,064

Figure 69: Eddy current Test 2

Eddy Current: Test 3						
	P = 15031 W/mm^2		s = 2,1 rad/s		f = -16 mm	
Suction (%)	100 %		90 %		80 %	
	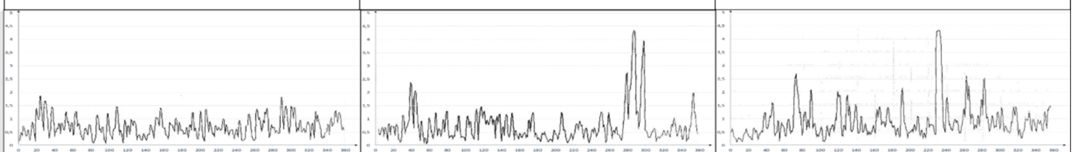					
	Max	Min	Max	Min	Max	Min
	1,909	0,06	4,309	0,081	4,319	0,06
Suction (%)	70%		60%		50 %	
						
	Max	Min	Max	Min	Max	Min
	2,639	0,099	2,679	0,083	2,408	0,073

Figure 70: Eddy current Test 3

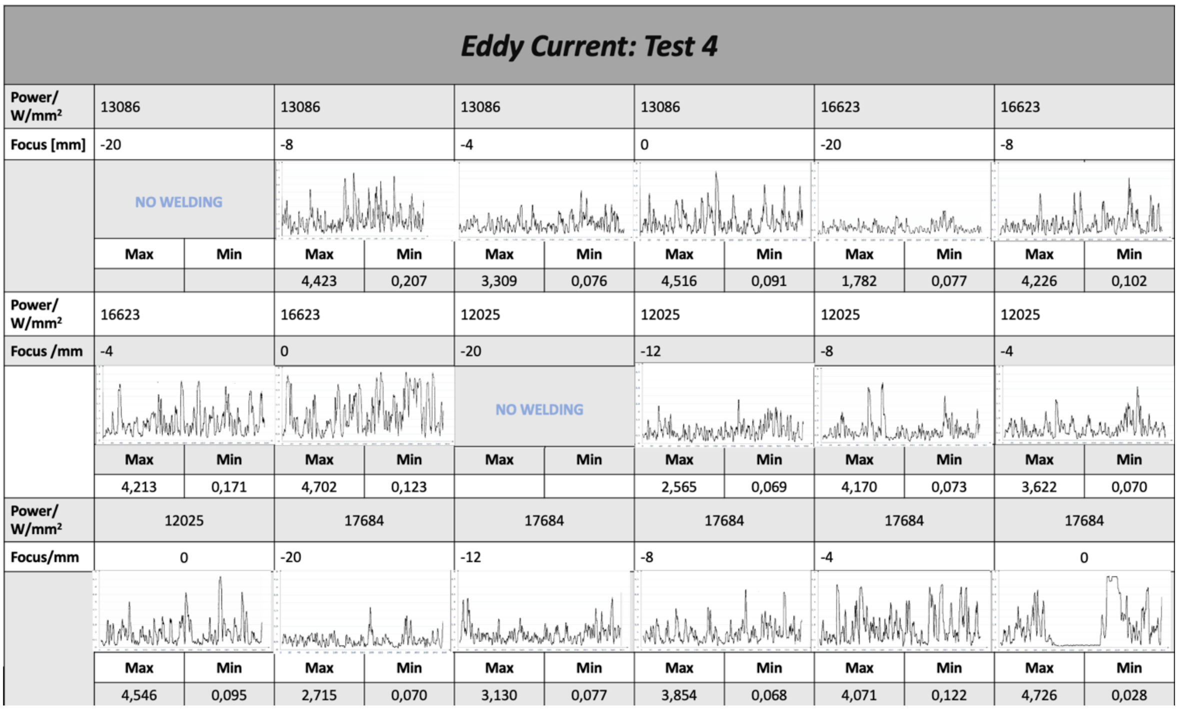

Eddy Current: Test 4												
Power/ W/mm²	13086		13086		13086		13086		16623		16623	
Focus [mm]	-20		-8		-4		0		-20		-8	
	NO WELDING											
	Max	Min	Max	Min	Max	Min	Max	Min	Max	Min	Max	Min
			4,423	0,207	3,309	0,076	4,516	0,091	1,782	0,077	4,226	0,102
Power/ W/mm²	16623		16623		12025		12025		12025		12025	
Focus /mm	-4		0		-20		-12		-8		-4	
					NO WELDING							
	Max	Min	Max	Min	Max	Min	Max	Min	Max	Min	Max	Min
	4,213	0,171	4,702	0,123			2,565	0,069	4,170	0,073	3,622	0,070
Power/ W/mm²	12025		17684		17684		17684		17684		17684	
Focus/mm	0		-20		-12		-8		-4		0	
	Max	Min	Max	Min	Max	Min	Max	Min	Max	Min	Max	Min
	4,546	0,095	2,715	0,070	3,130	0,077	3,854	0,068	4,071	0,122	4,726	0,028

Figure 71: Eddy current Test 4

4.5 Defects and material

Once obtained the observed data, the DOE statistical analysis, followed by a more detailed GLM analysis provided important results: some process parameters have an influence on some geometric parameters, but there is no correlation between process parameters and the presence of defects. At this point the idea is to investigate on a possible influence of material chemistry on the presence of defects.
By analyzing the microstructure at the optical microscope, different type of defects is detected. Types of observed defects could be classified in three different categories:

- Type 1: Residual stresses
- Type 2: Solidification Cracks
- Type 3: Porosity

➢ **Type 1:** Intergranural or transgranular fractures come from residual stresses.

Intergranular fracture occurs when a crack propagates along the grain boundaries of a material, usually when these grain boundaries are weakened. In particular cracks propagates due to austenitic segregation at the grain boundaries. At room temperature, intergranular fracture is commonly associated with segregation of solutes or impurities at the grain boundaries. In fact, the presence of a high amount of low melting material such as sulfur and phosphorus lead to austenitic segregation. At high impurity levels, the likelihood of intergranular fracture is greater. The presence of impurities creates residual stresses during the working process which can degenerate in cracks propagation.

Transgranular fracture is a fracture that follows the edges of lattices in a granular material. High carbon content in the zone of last solidification means presence of bainitic structure, which could generate crack propagation at low temperature.

Regardless If crack propagation is related to transgranular fracture, intergranular fracture or a combination of the two, the crack generally grows as much as the applied load increases, until it reaches a critical size where the surrounding uncracked section of the material can no longer support the applied stress. At that point complete fracture occurs [43].

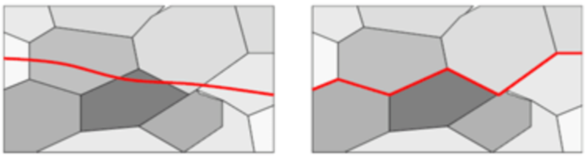

Figure 72: Transgranular and intergranular fracture

➢ **Type 2:** Solidification cracks, which appears in longitudinal and vertical direction are identified as formed at high temperature before the complete weld cooling. In particular If the crack shows the presence of dendritic crystals at the center of the defect the fracture is defined as Solidification Crack. If not, the crack is due to shrinkage phenomena during solidification.

Studies on cracks have been performed by using electronic microscopes in order to make a good distinction between defect of type 1 and type 2. Electron microscopes are versatile instruments that can provide a wide range of information depending on the user's needs. As the name suggests, electron microscopes employ an electron beam for imaging. Different signals are captured from the interaction between electrons and material, carrying useful information about the sample. In the case of a scanning electron microscope (SEM), two types of electrons are typically detected: backscattered electrons (BSEs) and secondary electrons (SEs).

BSEs are reflected back after elastic interactions between the beam and the sample while SEs originate from atoms of the sample by an inelastic interactions between the electron beam and the sample. Moreover, if BSEs come from deeper regions of the sample, SE originate from surface regions. Thus, the two carry different types of information. BSE images appears differently depending on atomic number. In fact, the higher atomic number, the brighter the material providing information about the chemical composition of the steel. SE imaging can provide more detailed morphological information showing a visual distinction between type 1 and type 2 defect.

Type 1 SE Defect :

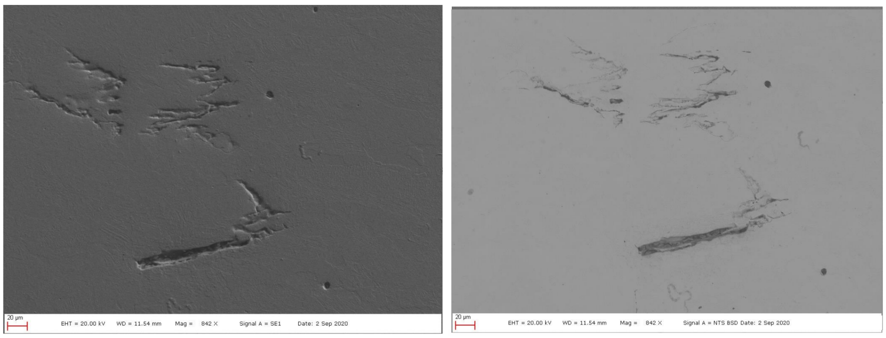

Figure 73: Type 1 SE defect

Type 2 SE Defect:

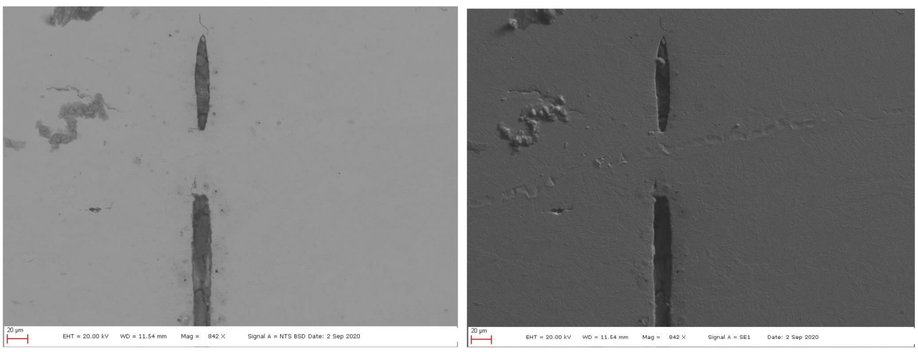

Figure 74: Type 2 SE defect

4.5.1 Material chemistry analysis

Once stated the presence of two different type of cracks, the study wants to know more about the chemistry of material and its possible cause of presence of Type 1 defect.

In order to do so, a DD steel with a different chemical composition is tested. The aim is to observe possible differences in terms of defects after welding by using different chemistry. The material chemical composition is described by the histogram below, which compare the new material chemistry with the one used during the previous tests.

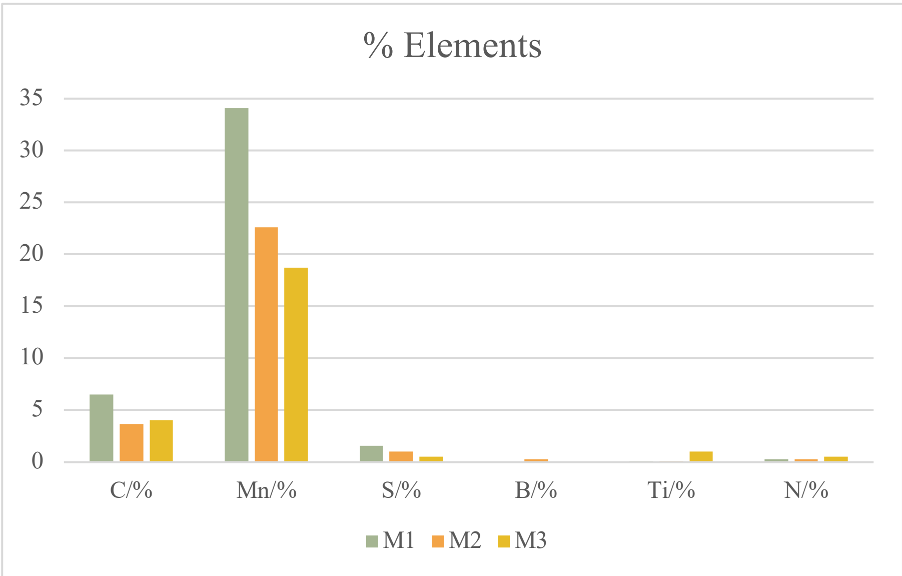

Plot 19: Percentage of chemical elements

The new material is defined as M3, while M1 and M2 are the one used previously related to the workpiece of 6 mm welded with the component of 3,2 mm respectively. M3 is a material provided from a different supplier.

On the basis of the observed percentages, some considerations can be made. It is preferred to keep Carbon and Manganese in a small percentage to reduce the formation of bainite, which as mentioned above, could lead to transgranular fracture formation.

On that basis, the weldability of the 3 implied steels is verified by calculating the carbon equivalent for each material by applying equation (4) and equation (5), giving as result CE 1/% and CE 2/% respectively.

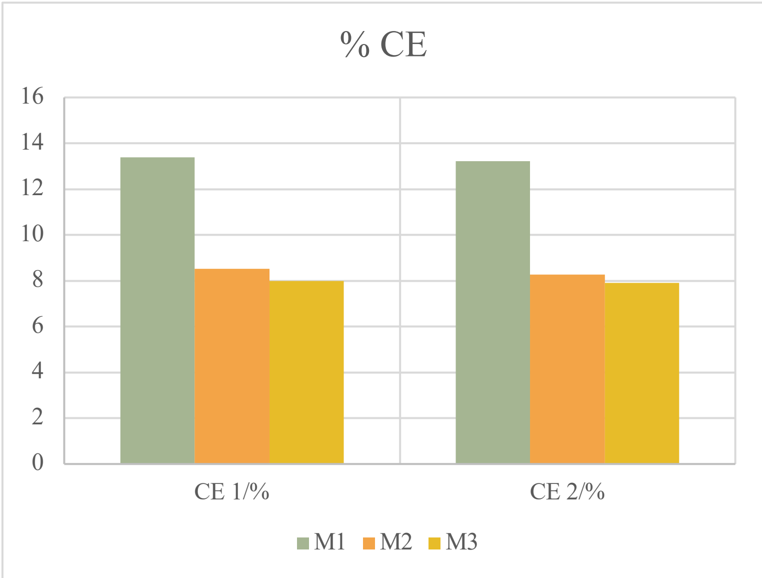

Plot 20: Percentage of carbon equivalent

By according to what described in paragraph 2.6.2 the carbon equivalent should be less than 0,40 for **Errore. L'origine riferimento non è stata trovata.** and less than 0,35 for **Errore. L'origine riferimento non è stata trovata.** by looking at Table 2 in order to affirm an excellent weldability for the material. The histogram shows a Carbon equivalent less than the mentioned percentages stating an excellent weldability for all the material. Despite the flawless numerical result, metallography inspection shown a high amount of defects in M1 and M2 materials.

Apart from that, further attention should be focused on the amount of Manganese and Sulfur in materials. In particular in case of laser welding the equilibrium of %C, %Mn, %S needs to be considered according to EN1011-6 2018. The presence of Mn and S causes the formation of weaking MnS in the solidified zones. The MnS bond leads to microcracks resulting from shrinkage strains as the weld metal is cooling down in the zone of last solidification enriched in carbon and detrimental elements. The welding stresses might be

also too high and the shrinkage strains too by consequence, due to a too high welding speed and cooling rate.
According to standard EN 1011-6:2018, setting the chemical criteria for base materials dedicated to laser welding application, the %Mn and %S need to be adjusted versus %C content limited as indicated here below:

C content	0,06 to 0,11	0,11 to 0,15	0,15 to 0,18
Mn/S ratio	>22	>40	>60

Table 14: %Mn/S VS %C, EN 1011-6:2018

The ratio of Manganese and Sulphur for all the materials and the relative amount of Carbon content is calculated and illustrated in the following histograms. The horizontal line introduces the minimum value of Mn/S ratio and C content to respect the standard.

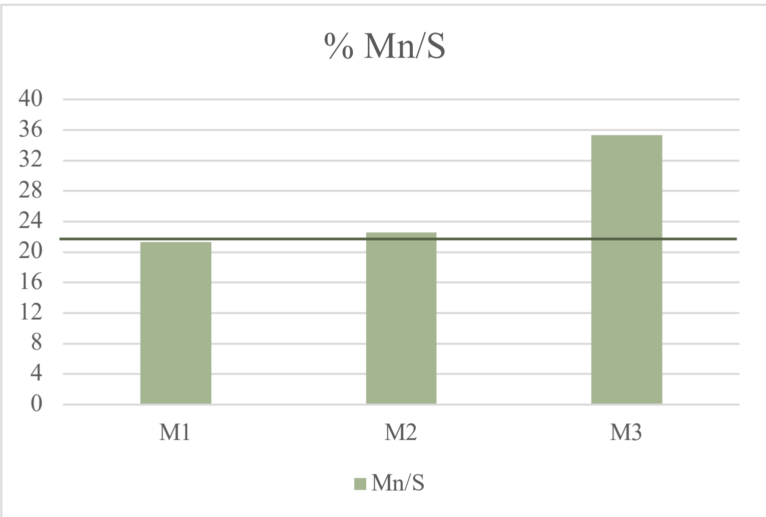

Plot 21: Percentage of manganese and Sulfur ratio

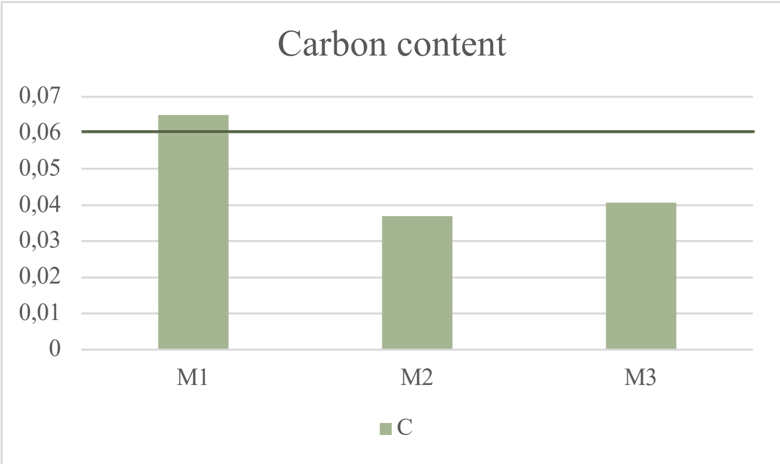

Plot 22: Carbon content

Looking at M1 carbon content it falls within the range 0,06-0,11 but the expected relative Mn / S ratio is too low (about 20 %). M2 shows an amount of carbon lower than the minimum limit set by the standard and Mn / S ratio is slightly higher than the relative 22 % value. M3 similarly shows an amount of carbon content smaller than 0,06 and a Mn / S ratio much higher than the relative 22 %.
In conclusion, none of the chemical considered complies with the norm 1011-6:2028 in terms of % Mn / S and carbon content. Only M3 introduce a % Mn/S ratio higher than 22.

4.5.2 Test 5 analysis

After analyzing the material chemistry of M1, M2, M3 one more test in conducted in order to observe possible differences in terms of defects during the microscopic inspection. Six more workpieces are worked out. Four workpieces are produced in the main parameter configuration while the last two in the worst parameter condition. The worst parameter condition regards the one related to the welded and analyzed workpiece during previous tests which shows the highest number of defects (10 defects). The idea is to observe the behavior of the material M3 in the worst condition, expecting an improvement in weld bead morphology with respect to the previous observed weld beads, due to the different material chemical composition. Three workpieces are worked with M3 material coming from Supplier A, while the last three samples are produced with M1 and M2 materials coming from Supplier B. The numerical parameters conditions are reported below.

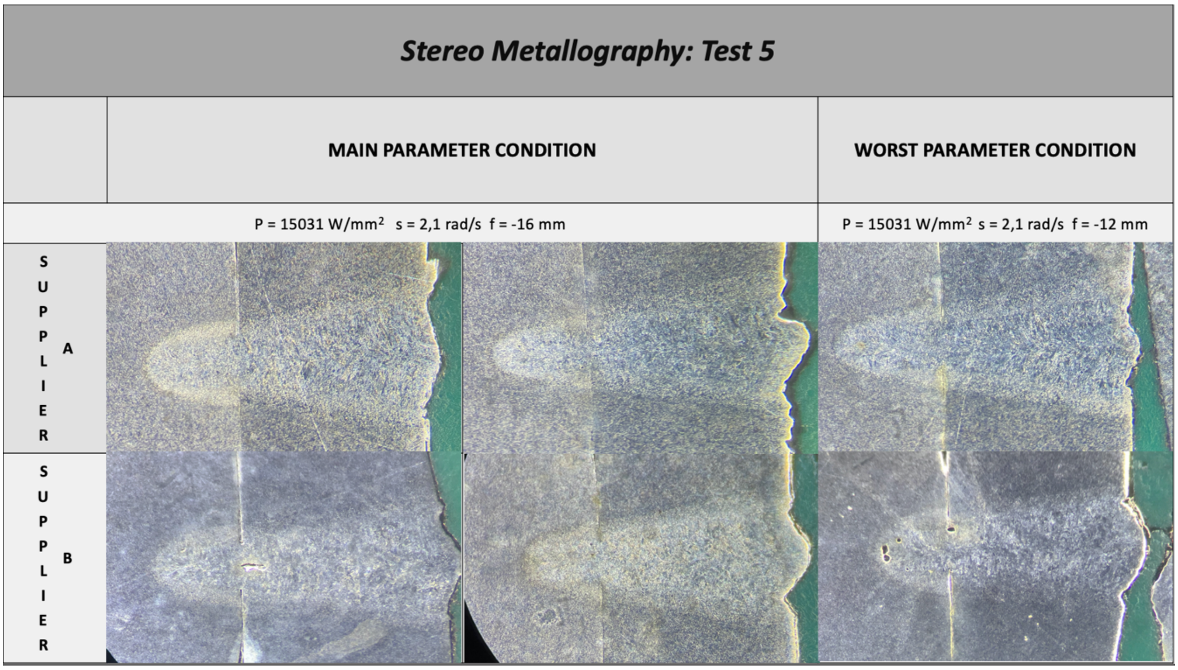

Plot 23: Stereo metallography Test 5

Frames captured at the stereoscope show differences in weld beads by looking at both row Supplier A and row Supplier B. The visual approach gives information by comparing the first two frames in both rows. It noticeable that no defects can be detected in material M3, while a longitudinal crack in the weld bead middle area is evident in the first frame of row Supplier B.
By observing how the weld bead changes in worst parameter condition, the presence of cluster porosity is relevant in case of M1 and M2 materials, while M3 seems to show a clean weld bead.
An analysis in terms of geometric parameters, surely confirm that the depth of penetration tends to be higher in case of Supplier A than in case of Supplier B.
A deeper observation on the presence of defects made at the optical microscope proves what described above.

Metallography of defects: Test 5			
	MAIN PARAMETER CONDITION		WORST PARAMETER CONDITION
P = 15031 W/mm² s = 2,1 rad/s f = -16 mm			P = 15031 W/mm² s = 2,1 rad/s f = -12 mm
SUPPLIER A	No defects detected	No defects detected	No defects detected
SUPPLIER B		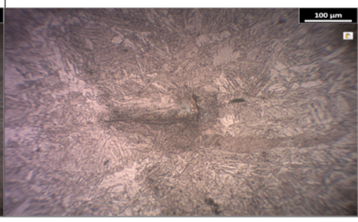	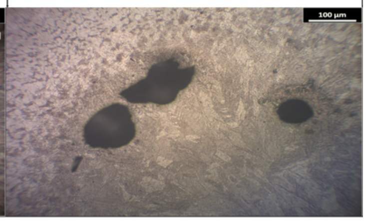

Figure 75:Metallography of defects Test 5

The last poster exhibits the weld beads observed further under the microscope and it is evident how the chemistry of the material affects the presence of defects. No defects are detected in welding of the M3 material, even in the worst conditions, while relevant defects are observed in sections related to M1 and M2 welding materials. In row Supplier b, the microscopic inspection highlights the presence of transversal and longitudinal cracks in the first two frames, adding the existence of cluster porosity in case of the worst conditions, which was evident even at the previous visual inspection.

In conclusion, it could be proved how changes in material chemistry can affect the presence of defects during laser welding. The last study illustrates that by varying some percentage of chemical elements into the material better results could be reached in terms of defects.

4.5.3 DD steel material structure

The DD steel microstructure is scanned at the optical microscope in order to observe possible anomalies. The frames below regard to material microstructure after welding at the *no welded zone*, *welded zone* and *transition zone*. The images are taken at different magnification, one at 500X and one at 200X.

- No welded zone

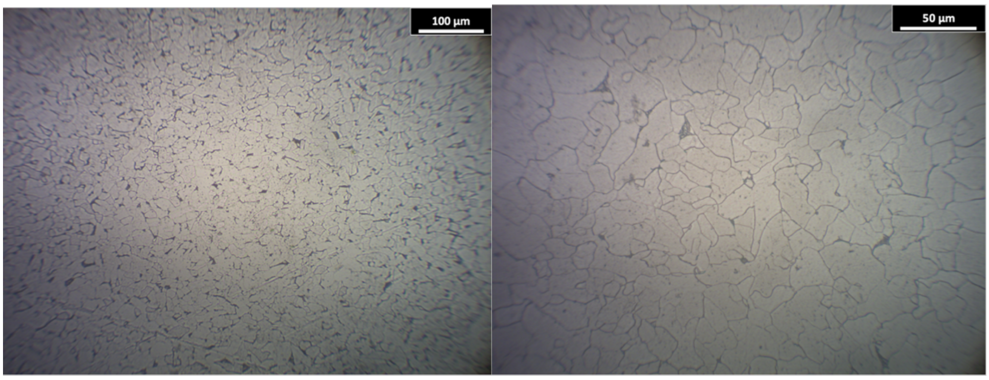

Figure 76: DD steel no welded zone

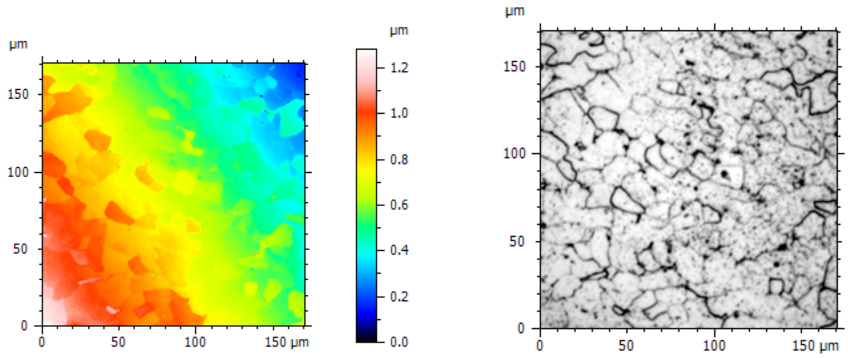

Figure 77: Topography of no welded zone

The microstructure at no welded zone shows the presence of white ferrite with small interstitial grains of perlite. The small back dots are cementite carbides.

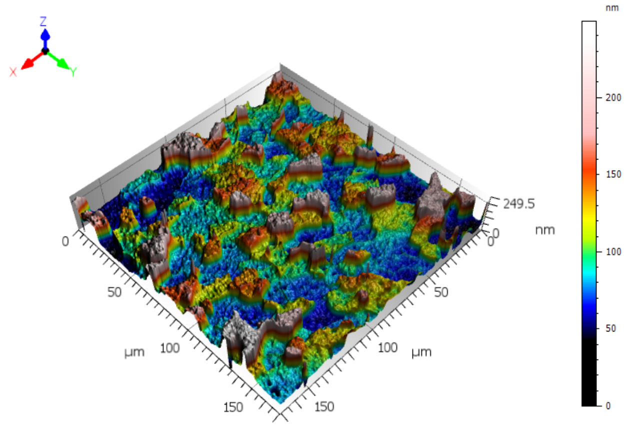

Figure 78: 3D surface of no welded zone

➢ Transition zone

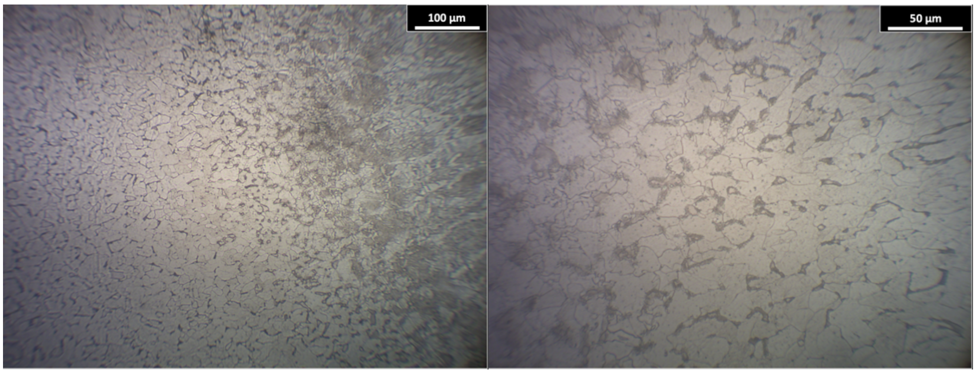

Figure 79: DD steel transition zone

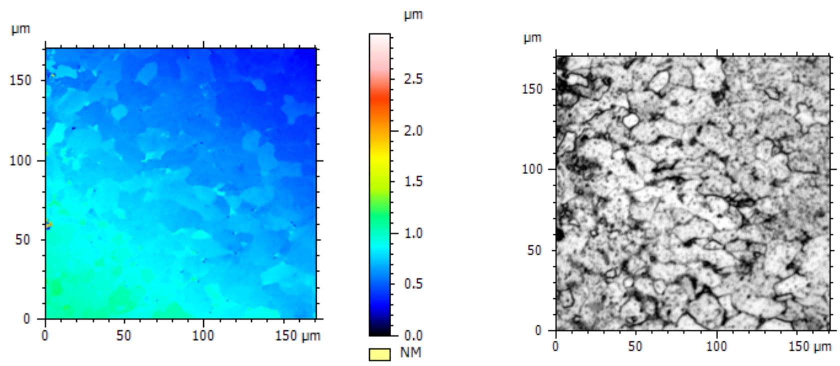

Figure 80: Topography of transition zone

The transition zone is affected by a heat treatment. During the welding process the induced heat by the laser affects the area surrounding the bead. As a result, grains go through a recrystallization process. Nevertheless, the frames show a correct material microstructure exhibiting no martensite formation.

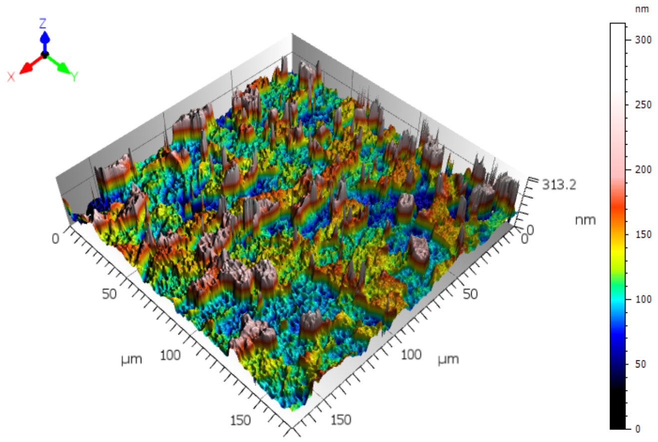

Figure 81: 3D surface of transition zone

- Welded zone

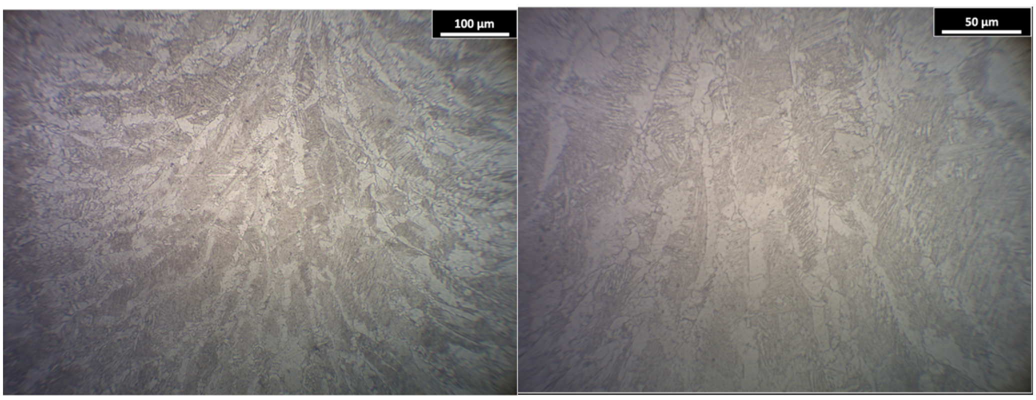

Figure 82: DD steel welded zone

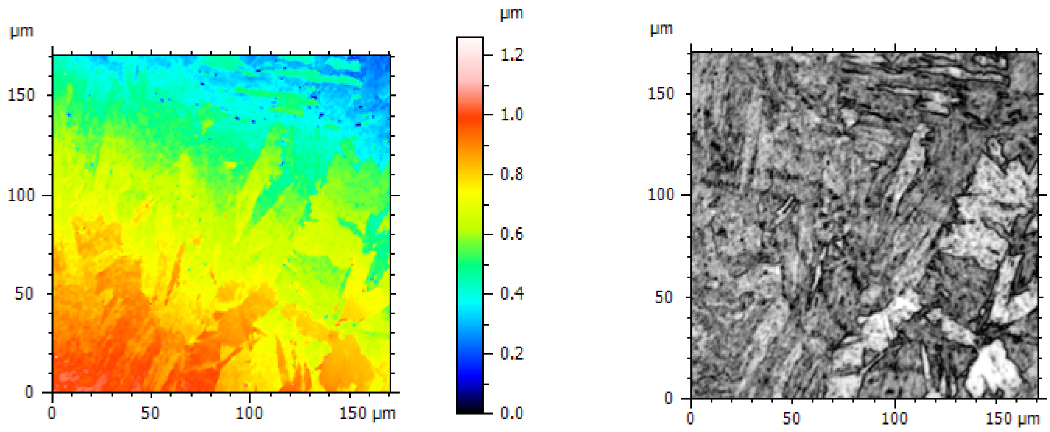

Figure 83: Topography of welded zone

The welded zone is the most heated area which reaches high temperatures. Large white grains highlight the ferrite formation while the black grains show the presence of bainite.

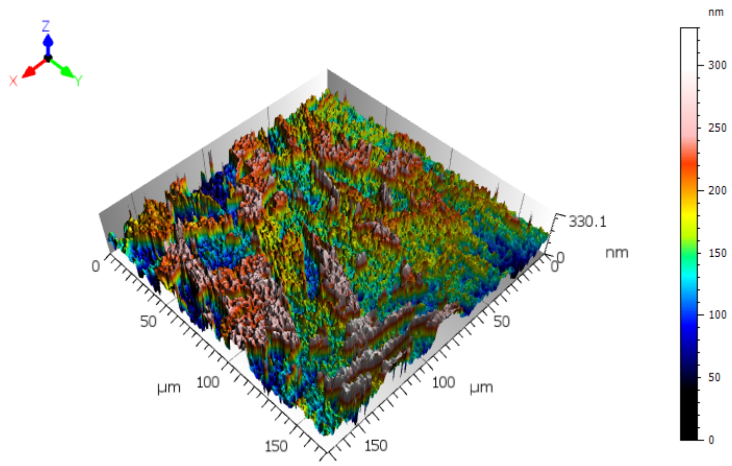

Figure 84: 3D surface of welded zone

4.5.4 Defects profilometry

The worst crack and pore detected during the microscopic inspection are subjected to profile investigation through the optical surface profiler. The images below show a 2D and a 3D topography representation a longitudinal crack and a pore. As expected, the crack and pore middle zones are deeper than the surrounding area. The 3D view explains visually what described in 2D images, giving an idea of defect morphology.

Longitudinal crack

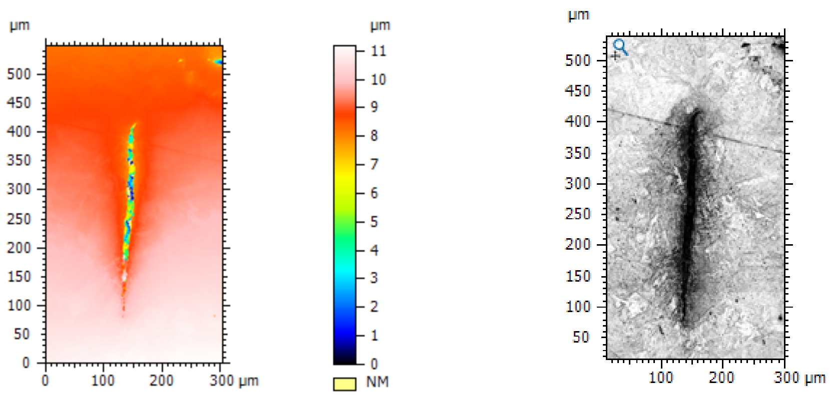

Figure 85: Topography of a longitudinal crack

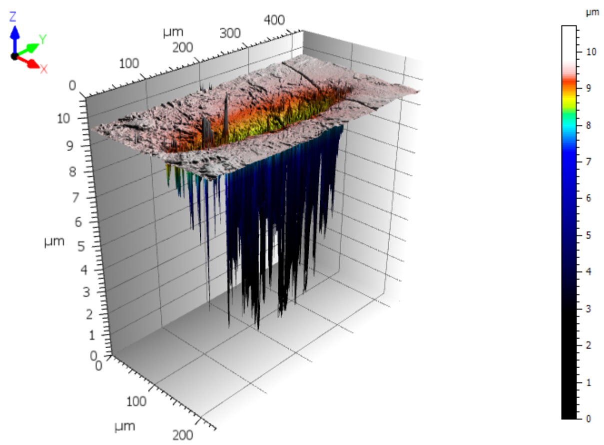

Figure 86: 3D surface of a longitudinal crack

Pore

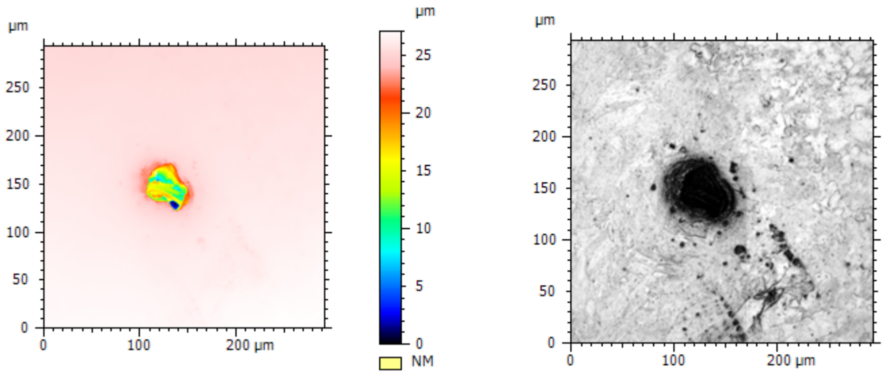

Figure 87: Topography of a pore

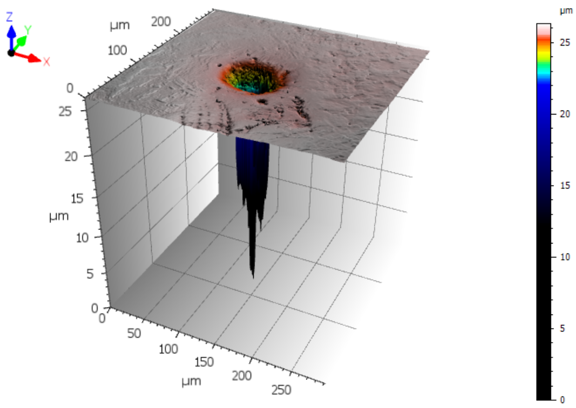

Figure 88: 3D surface of a pore

CHAPTER 5

Conclusions and Future Developments

5.1 Conclusions

A full factorial DOE of 18 runs (2 factors, 3 replicates) was drawn up in order to correlate the most influential parameters of the laser welding process (power and focus) with the experimental results obtainable from metallographic inspection and from NDT (eddy current). Both factors were significant (R-sq (adj) = 88%) for the depth of penetration.
In addition to the experiments envisaged by the DOE, further welds were performed in order to include in the analysis the effect of welding speed and suction using a GLM. In total 52 workpieces were performed.
The GLM model results describe the depth of penetration as a function of the process parameters (R-sq (adj) = 92%). In particular the effect of power and the quadratic effect of focus is highly significant as much as the combined effect of focus with power and speed as well. A detected outlier is probably due to the lack of model to predict that value.
Furthermore, the GLM shows that there is no apparent significant effect on eddy current parameters, the number of defects and defect dimensions, penetration depth from the joining point (Si), weld bead length at the interface (Bhaz) and the weld bead length at the joining point (bi).

These results were also presented in terms of visual and metallographic inspection. The microstructure in the area affected by the welding is essentially composed of bainite and ferrite and therefore is not critical. Although the carbon equivalent value always indicates excellent weldability, numerous defects were found in all weld seams obtained. In particular, in addition to gas porosity, cracks associated with residual stresses/segregations and cracks associated with non-solidification were found in the weld bead.

The introduction of a new chemical composition experienced in Test 5 with a manganese-Sulfur ratio higher than 22 seems to have allowed the elimination of crack defects.

It might be concluded that while geometric parameters could depend on working condition, the presence of defect is related to material chemistry.

The eddy current probe does not appear suitable for identifying surface defects, being able to detect defects only few millimeters below the workpiece surface. However, it shall be mentioned that this result is perhaps related to the fact that the inspection was conducted on unturned weld beads.

5.2 Future developments

In the future, the measurement outputs could be analyzed in terms of Vickers microhardness variations.
The study could be deepened by making more analysis on the new material experienced in terms of fatigue test and at the same time it can be tested under a larger range of parameter conditions. In addition to this, the best parameter condition could be found by matching the costumer request with the working condition in which the component will work once mounted on the VT3 engine. Moreover, in order to have more reliable results from the eddy current testing, a suggestion is to realize the inspection on turned workpieces.
By the statistics side, analysis could be amplified by increasing the number of levels and the factors and including supervised models of machine learning.

Bibliography

[1] "The incredible story of laser welding," *VO+,* 2017.

[2] A. Kornienko, "Benardos Nikolai Nikolaevich and his famous invention," 2006.

[3] Handbook of laser welding technologies, Seiji Katayama, 2013.

[4] J. Oliveura and Z. Zeng, "Laser Welding," *Metals ,* 2019.

[5] "Modeling and Simulation of Laser Welding," in *Laser in Manufacturing*, J. Paulo Davim , 2012 , p. Chapter 6 .

[6] "Laser Welding," in *Laser Material Processing* , Springer , 2010 , p. Chapter 4.

[7] C. Dawes, Laser Welding, Woodhead.

[8] O. K. T. Y. Kitani Yaushi, "Application of Laser Welding Technologies to Automotive Bodies," *JFE technical report,* no. 20, 2015.

[9] "PuchPowerTrain," [Online]. Available: https://www.punchpowertrain.com/en/products/1/vt3.

[10] S. Neil, Mechanism and mechanical devices sourcebook, 2011.

[11] C. C. d. W. H. B. Pietro J. Dolcini, Dry Clutch Control for Automotive Applications, Springer.

[12] M. Holgerson, "Wet Clutch Engagement Characteristics," 1999.

[13] a. J. Svenungsson, I. Choquet and A. F. H. Kaplan, "Laser welding process," *Physics Procedia,* no. 78, pp. 182-191, 2015.

[14] in *Gas lasers*, Masamori Endo ; Robert F. Walter, 2006, pp. 2-3.

[15] S. Katayama, in *Foundamental and details of laser welding*, Carlos P. Bergmann, pp. 1-14.

[16] "Laser Welding," in *Plastic Design Library*, William Andrew, 1997, p. Chapter 13.

[17] D. Paschotta, Power Density, 2020 .

[18] A. Bharti, "Laser Welding," vol. 11, pp. 191-212, 1988.

[19] R. YP, "HEATING OF A GAS BY A POWERFUL LIGHT PULSE," *Soviet physics JETP ,* vol. 21, no. 5, p. 1009, 1965.

[20] K. K. C. d. F. A. W. ,. V. H. Yannis Kinds, "On the influence of laser defocusing in Selective Laser Melting of 316L," *Additive Manufacturing,* vol. 23, pp. 161-169, 2018.

[21] J. Shan, "Laser welding of magnesium alloys," *Focal Position,* 2010.

[22] F. P. D. B. C. B. &. N. E. Antonia Rabl, "Influence of the focus wobbling technique on the integrity and the properties of electron beam welded MarBN steel," *Welding in the world ,* vol. 63, pp. 715-724, 2019.

[23] P. H. Libor Mrna, " Study of laser wobbling welding process through the radiation of plasma plume," *Lasers in Manufacturing Conference,* 2017.

[24] R. Regello, "Weld defects and how to avoid them," *Welders Universe,* 2012.

[25] "Weld discontinuities," *AlcoTec,* 2015.

[26] B. Lucas, "Distortion - types and causes".

[27] P. Berger, "Understanding on humping based on conervation of volume flow," 2011.

[28] I. Samarasekera, "Microstructural phenomena," *Hot Rolling,* 2001.

[29] "Continuously hot rolled low carbon steel sheet and strip for cold forming — Technical delivery conditions," *British Standards 10111-2008.*

[30] M. K. a. K. UETANI, "Laser welding for ultra carbon steels," 1998.

[31] K. U. Muneharu KUTSUNA, "Laser Welding of Ultra Low Carbon Steels," 1998.

[32] A. A. B. A. A. B.S. Yilbas, "Laser welding of low carbon steel and thermal stress analysis," *Optics & Laser Technology,* 2009.

[33] J. Antony, Design of Experiments for Engineers ans Scientists, Elsevier, 2003.

[34] L. Eriksson, Design of Experiments - Principles and Applications, L. Eriksson, 2000.

[35] T. K. B. Prasanta Sahoo, "Full Factorial Design," *Mechatronics and Manufacturing Engineering,* 2012.

[36] D. C. MONTGOMERY, Design and Analysis of Experiments, John Wiley & Sons.

[37] "What is Eddy Current," *Magcraft,* 2015.

[38] Innerspec , "Eddy current technology".

[39] J. G.-G. ,. E. V.-S. Javier García-Martín, "Non-Destructive Techniques Based on Eddy Current Testing," *Advanced Sensing Technology for Nondestructive Evaluation,* 2011.

[40] R. Singh, "Eddy current Testing," *Applied Welding Engineering,* 2012.

[41] A. N. A. N. K. M. A. M. F. Damhuji Rifai, "Subsurface Defects Evaluation using Eddy Current Testing," *Indian Journal of Science and Technology,* 2016.

[42] TWI, "WHAT FACTORS AFFECT EDDY CURRENTS?".

[43] A. P. Mouritz, "Fracture processes," in *Introduction to aereospace materials*, 2012.

[44] M. K. and K. T., "Encyclopedia of Microfluidics and Nanofluidics," Springer, 2008.

[45] Direct Industry, "YLR-HP Series: 1-50kW Ytterbium Fiber Lasers," in *Hish Power Fiber Lasers for industrial applications*.

List of figures

List of plots

List of tables

Acknowledgements

This paragraph has to be intended as excluded from the academic content of the Thesis. To allow reading to people who are unfamiliar with English language, the further text will continue in my mother tongue.

Riporto dei pensieri al termine di un lavoro che ho iniziato anni fa con grande cura e che concludo con tanta soddisfazione. Anni che mi hanno insegnato a gioire, a piangere, a crescere, ad amare e a sbagliare. Anni che mi hanno regalato momenti di conforto e sconforto, di follie e rimpianti, ma soprattutto di amore. L'amore che ho raccolto durante il mio percorso universitario è la base di tutto il mio lavoro. Ho scritto tutto questo con una grande consapevolezza, che oggi so amare ed è grazie a questi anni e a loro:

Mamma e papà, vi dedico tutto questo perché siete la mia vittoria. Grazie per essere il mio punto fisso, irremovibile, unica gioiosa certezza della mia vita.

Vincenzo, sei la vera conclusione di questi anni e soprattutto sei l'inizio di tanti altri. Grazie a te, per avermi insegnato ad amare.

Chiara, la mia complice, specchio della mia persona, essenza di questi anni. Grazie per avermi teso la mano, non la lascio più.

Amedeo, ci siamo ascoltati, consigliati, guardati e capiti. Grazie per le ore di purezza e di rara sincerità, grazie per bussare e trovarti sempre.

Giorgio, sei il mio compagno d'avventura. Abbiamo iniziato e concluso insieme questo fantastico viaggio. Grazie per aver trasformato ogni giorno in una bellissima risata.

Giovanna, amore mio, sei stata il mio luogo sicuro di tutti questi anni. Grazie per essere il mio posto magico dove adoro rifugiarmi.

Nonni, mi avete trasmesso segreti d'amore e di umiltà, grazie perché oggi li custodisco e li vivo in ogni momento della mia vita.

Zie e zii, siete i fiori che colorano la mia vita. Grazie per donarmi gioia e allegria, per avermi sempre risollevato dallo sconforto aiutandomi a riprendere il sorriso.

Elisa, Gianni e la piccola Katy, siete ciò che non ho, i miei fratelli. Grazie per esserci sempre, da sempre e per sempre. Siete fiducia, famiglia, casa.

Ringrazio infine il professor Gianfranco Genta, l'ingegnere Roberto Cagliero e il dottor Giacomo Maculotti per aver reso possibile il lavoro con cui concludo questo percorso con grande soddisfazione. Vi ringrazio per avermi fornito le basi necessarie per lo sviluppo, per avermi affiancato nella cura dei dettagli con interessanti suggerimenti e per essere sempre stati disponibili a garantire un miglioramento continuo e costante del progetto di ricerca.